2007

Investigation of Phospholipid Tubule Morphology for Use in Drug Delivery

Colleen Colson Garrett
Louisiana State University and Agricultural and Mechanical College, ccolso2@lsu.edu

INVESTIGATION OF PHOSPHOLIPID TUBULE MORPHOLOGY FOR USE IN DRUG DELIVERY

A Dissertation

Submitted to the Graduate Faculty of the
Louisiana State University and
Agricultural and Mechanical College
in partial fulfillment of the
requirements for the degree of
Doctor of Philosophy

in

The Department of Chemistry

By
Colleen Colson Garrett
B.S., University of Southern Mississippi, 2002
May 2007

Dedication

This dissertation is dedicated to my niece

Kaitlyn Victoria Tullis

October 30, 1996-December 1, 2005

Her life on this earth was inspirational to many people, including myself. She has directed my career path to the pharmaceutical industry. Since there was no cure for her brain cancer, I am motivated to go to work everyday, in the hopes that one day there will be a cure and another family will be spared the loss of a precious child.

Acknowledgements

First, I would like to thank my mom, Susan Colson, who has always been my number one fan. When I was younger, she used to read me *The Little Engine that Could*, and taught me that I could do anything as long as I put my mind to it. Her belief in me enabled me to believe in myself. She always put me and my brother first, even sacrificing things for herself in order to provide us with a good education, and without that education and her support, I would not be where I am today.

I also want to thank my husband, Gentry Garrett, who has supported and encouraged me throughout my graduate career. I appreciate you following me to Baton Rouge and pursuing your career here. I know at times it was not easy, but your love and confidence in my abilities has kept me going during the difficult days.

I owe a great deal to my advisor, Dr. Britt Thomas, who has guided me in my studies. None of this would be possible without you, and I truly appreciate your support and all you have done for me, including editing this dissertation.

I would also like to thank Dr. Paul Russo, my co-advisor. His vision with the IGERT program is what brought me to LSU. I am grateful for the many opportunities that have been available to me as a result of IGERT. Not only did he play a role in my decision for graduate school, but he also welcomed me into his group during my last year, and I very much appreciate his support.

I greatly appreciate the Russo group members for welcoming me into their group and their lab space with open arms. Derek, Erick, Nadia, and Jiahong, thanks for accepting me as one of your group members. A special thanks to Derek, who is my IGERT team member. Since

sharing lab space in the basement, he has always been there for me, especially when it comes to my many computer problems.

I would like to thank my church family here in Baton Rouge, 1st Church of the Nazarene. Without your prayers and support, I am not sure I could have made it to where I am today. Also, thanks to Becky Brauch, who has been my great friend throughout my graduate career. She beat me out of here, but I am not far behind her, and I still rely on her for strength and advice, long distance.

I must also thank my outside advisors Noel Clark at University of Colorado, Boulder and PJ Persichini at Allegheny College for allowing me to spend time at their universities in their research groups in order to collaborate on projects.

Thanks to Michelle Long and Dave Stroz, my managers during my internship at Abbott, for teaching me so much during my short time there. I look forward to working with both of them in the future.

Special thanks must be given to Dr. C. Allan Guymon, my undergraduate research advisor. He took me into his research group during my freshman year. I was allowed to work on my own project by my sophomore year, present my research at conferences, and publish. Without this undergraduate research experience, I doubt that I would have been interested in pursuing an advanced degree.

Table of Contents

Dedication ii

Acknowledgements iii

List of Tables viii

List of Figures ix

List of Schemes xiii

List of Abbreviations xiv

Abstract xvi

Chapter 1 Background, Overview, and Research Synopsis 1
1.1 Background 1
1.1.1 Discovery of Tubules 1
1.1.2 Chiral Sub-structure 2
1.1.3 Tubule Formation 4
1.1.4 Theoretical Challenges 10
1.2 Overview 11
1.2.1 Phosphonates 11
1.2.2 Phospholipid/Protein Cones 14
1.2.3 Tubules with Tunable Diameters 15
1.2.4 Positioning and Alignment 18
1.2.5 Bending and Radial Deformation of Tubules on SAM 18
1.2.6 Templated Synthesis 19
1.3 Research Synopsis 20
1.4 References 20

Chapter 2 Materials and Methods 24
2.1 Materials 24
2.2 Methodologies 25
2.2.1 Tubule Stock Solution Preparation 25
2.2.2 Protein-Modulated Tubules 25
2.2.3 Addition of Chemotherapy Agents 25
2.2.4 Addition of DOPE and Cholesterol 26
2.3 Instrumentation and Theory 27
2.3.1 Optical Microscopy 27
2.3.2 Theory of Nomarski DIC 27
2.3.3 Atomic Force Microscopy (AFM) 30
2.3.4 Theory of AFM 30
2.3.5 Scanning Electron Microscopy (SEM) 31
2.3.6 Theory of SEM 31

2.3.7 Energy Dispersive Spectroscopy (EDS) 32
2.3.8 Theory of EDS 32
2.4 References 33

Chapter 3 A New Tubule Formation Intermediate: The Tubelet 34
3.1 Introduction 34
3.2 Deposition Bed 38
3.3 Tubelets 39
3.3.1 Cylindrically Wound Tubelets 40
3.3.2 Axially Twisted Tubelets 41
3.3.3 Flat Tubelets 41
Other Regions 42
3.4 Tubelets as a Precursor 43
3.5 Conclusions 47
3.6 References 48

Chapter 4 Encapsulation Studies with Chemotherapy Agents 50
4.1 Introduction 50
4.2 Methotrexate Studies 52
4.3 Mitoxantrone Studies 57
4.4 Carboplatin Studies 60
4.5 Conclusions 65
4.6 References 66

Chapter 5 Optimization of Phospholipid Tubule Morphology 68
5.1 Introduction 68
5.2 DOPE Studies 69
5.3 Cholesterol Studies 71
5.4 Conclusions 77
5.5 References 77

Chapter 6 Modifying DC(8,9)PC to Create New Tubule-forming Molecules 79
6.1 Introduction 79
6.2 Synthetic Steps 80
6.2.1 Acetonide Protection of Glycerol 80
6.2.2 Addition of Diethylchlorophosphate 82
6.2.3 Deprotection 82
6.2.4 Addition of Fatty Acid Tails 82
6.3 Equipment 83
6.4 Synthesis 83
6.4.1 Acetonide Protection 83
6.4.2 Addition of Diethylchlorophosphate 83
6.4.3 Deprotection 84
6.4.4 Addition of Fatty Acid Tails 84
6.5 Results 86

6.6 Conclusions....89
6.7 References....90

Chapter 7 Conclusions and Future Work....92
7.1 Conclusions....92
7.1.1 New Tubule Formation Intermediate: The Tubelet....92
7.1.2 Encapsulation Studies with Chemotherapy Agents....93
7.1.3 Optimization of Phospholipid Tubule Morphology....95
7.1.4 Modifying DC(8,9)PC to Create New Tubule-forming Molecules....96
7.2 Future Work....97
7.3 References....98

Appendix A: Supplemental NMR Data....100

Appendix B: Permission to Reprint....105

Vita....106

List of Tables

Table 1.1 Tubule diameters as a result of acyl chain length……..17

List of Figures

Figure 1.1 Chemical structure of 1,2-bis(10,12-tricosadiynoyl)*sn*-glycero-3-phosphocholine [DC(8,9)PC]…….1

Figure 1.2 Chemical structure of achiral DC(8,9)PC isomer, "β–TFL"……...4

Figure 1.3 A. L_{α} chain melted phase, B. $L_{\beta'}$ chain-frozen phase……....5

Figure 1.4 Nomarski DIC micrograph of DC(8,9)PC tubule array formed by the edgewise separation and helical winding of 1 μm-width ribbons from a large (300 μm x 100 μm), surface-bound parallelogram phospholipid multi-layer sheet.....10

Figure 1.5 Chemical structures of A. *S*-"C4" DC(8,9)PC phosphonate derivative and B. R-"C3" DC(8,9)PC phosphonate derivative.....11

Figure 2.1 Tubule preparation…….26

Figure 2.2 Nomarski differential interference contrast microscopy; showing light path (adapted from McCrone)……29

Figure 2.3 Schematic of atomic force microscopy……..31

Figure 3.1 A low magnification scanning electron micrograph of an air-dried deposition bed of DC(8,9)PC-lysozyme specimen subjected to the tubule/cone formation process, showing extensive cracking of the deposition bed……..……35

Figure 3.2 Scanning electron micrograph of a protein-bearing deposition bed crack discontinuity. Cones are evident on the unbroken bed face, but tubelets are only resolvable when they emerge at the crack discontinuity……...36

Figure 3.3 Cross-section of proposed tubelet structure. Note that it has a height of two bilayers, twice that of a simple bilayer……..37

Figure 3.4 Scanning electron micrograph "edge-on" view of a protein/tubule deposition bed crack, showing stratification and broken ribbon-like structures projecting into free space……..…….39

Figure 3.5 Scanning electron micrograph view of a crack face discontinuity from which structures possessing types of "A" and "B" windings are seen to project…….41

Figure 3.6 Scanning electron micrograph of unwound tubelets at a narrow crack interface……..42

Figure 3.7 Scanning electron micrographs. (Top): A tubelet that emerges from a crack face with a right-handed type "B" winding, changes to flat configuration at its center, and resumes a right-handed type "B" winding before emerging at the opposing crack face discontinuity, (Bottom): A tubelet that undergoes a continuous transition from a type "A" winding at its left, to a type "B" winding at its center, and finally to a flat state as it enters the crack discontinuity…….....43

Figure 3.8 Scanning electron micrograph of an axially-twisted (type "B") tubelet, with characteristic 3 μm twist periodicity and a 90 degree kink where axial twist handedness sometimes, but not always, changes chiral sense. (This structure's left-handed twist does not change chiral sense at this junction.) (Inset): Magnification of the hollow tubelet's right end…….44

Figure 3.9 The formation of type "B" and "A" curvature structures appears to begin with the formation of the cylindrical tubelet (left), which spontaneously flattens (center). The tubelet occasionally remains flattened but far more likely assumes a type "B" curvature conformation (top right) or a cylindrical "A" curvature (bottom right). The inset drawing indicates the bilayer orientation of the amphiphilic molecules……...……45

Figure 4.1 Chemical structure of methotrexate…….……..53

Figure 4.2 100 μm x 100 μm contact mode atomic force micrograph of DC(8,9)PC doped with 28% methotrexate……..…54

Figure 4.3 50 μm x 50 μm contact mode atomic force micrograph of DC(8,9)PC doped with 28% methotrexate…….…….55

Figure 4.4 100 μm x 100 μm contact mode atomic force micrographs of A. DC(8,9)PC tubules (shown for comparison) and B. DC(8,9)PC tubules doped with 8% methotrexate……..…….56

Figure 4.5 10 μm x 10 μm contact mode atomic force micrographs of A. DC(8,9)PC tubules (shown for comparison) and B. DC(8,9)PC tubules doped with 8% methotrexate……...……56

Figure 4.6 Chemical structure of mitoxantrone……...……57

Figure 4.7 100 μm x 100 μm contact mode atomic force micrograph of DC(8,9)PC doped with 28% mitoxantrone……..58

Figure 4.8 100 μm x 100 μm atomic force micrographs of A. DC(8,9)PC tubules (shown for comparison) and B. DC(8,9)PC tubules doped with 8% mitoxantrone…….59

Figure 4.9 10 μm x 10 μm atomic force micrographs of A. DC(8,9)PC tubules (shown for comparison) and B. DC(8,9)PC tubules doped with 8% mitoxantrone…….59

Figure 4.10 Chemical structure of carboplatin……..60

Figure 4.11 15 μm x 15 μm atomic force micrograph of DC(8,9)PC tubules doped with 28% carboplatin. This seems to be cone-shaped…….…..61

Figure 4.12 100 μm x 100 μm contact mode atomic force micrographs of A. DC(8,9)PC tubules (shown for comparison) and B. DC(8,9)PC tubules doped with 8% carboplatin……..…62

Figure 4.13 10 μm x 10 μm contact mode atomic force micrographs of A. DC(8,9)PC tubules (shown for comparison) and B. DC(8,9)PC tubules doped with 8% carboplatin……..62

Figure 4.14 Energy dispersive spectroscopy results of the tubule itself……..….64

Figure 4.15 Energy dispersive spectroscopy results at the perimeter of the tubule……..64

Figure 4.16 Energy dispersive spectroscopy results of the substrate area without tubules present……65

Figure 5.1 Structure of 1,2-dioleoyl-*sn*-glycero-3-phosphoethanolamine, (DOPE)……..….69

Figure 5.2 100 μm x 100 μm contact mode atomic force micrograph of A. DC(8,9)PC tubules (shown for comparison) and B. DOPE:DC(8,9)PC [1:1] tubules, showing an increase in diameter……...70

Figure 5.3 100 μm x 100 μm contact mode atomic force micrograph of A. DC(8,9)PC tubules (shown for comparison) and B. DOPE:DC(8,9)PC [2:1] tubules, showing an increase in diameter…….……..71

Figure 5.4 Chemical structure of cholesterol……..72

Figure 5.5 Scanning electron micrograph of DC(8,9)PC tubules with 11 mole% cholesterol, showing tubule morphology is consistent with that of pure DC(8,9)PC.....73

Figure 5.6 100 μm x 100 μm contact mode atomic force micrograph: A. DC(8,9)PC tubules (shown for comparison) and B. DC(8,9)PC tubules with 40 mole% cholesterol, showing a change in tubule morphology……...74

Figure 5.7 50 μm x 50 μm contact mode atomic force micrograph: A. DC(8,9)PC tubules with 30 mole% cholesterol and B. DC(8,9)PC tubules with 40 mole% cholesterol.....74

Figure 5.8 Atomic force microscopy section analysis yielding DC(8,9)PC tubule height profile. Tubule height ~100 nm……75

Figure 5.9 Atomic force microscopy section analysis yielding DC(8,9)PC tubules with 30 mole% cholesterol tubule height profile. Tubule height ~200 nm……...76

Figure 5.10 Atomic force microscopy section analysis yielding DC(8,9)PC tubules with 40 mole% cholesterol tubule height profile. Tubule height ~300 nm……...76

Figure 6.1 Represents the tails of the phospholipid rotating about the diyne to enter the "bow" confirmation…….…..79

Figure 6.2 Structures of A. oleic acid, B. linoleic acid, and C. γ-linolenic acid……...…..81

Figure 6.3 100 μm x 100 μm atomic force micrograph of new tubule-forming compound, showing that some tubules are present……...87

Figure 6.4 100 μm x 100 μm atomic force micrograph of new tubule-forming compound, showing rigid, sheet-like structures……...87

Figure 6.5 A. and B. 100 μm x 100 μm atomic force micrograph of new tubule-forming molecule, arrows are pointing to sheets…….89

Figure A.1 ^{1}H-NMR of 6.4.4.1.....100

Figure A.2 ^{13}C-NMR of 6.4.4.1 101

Figure A.3 ^{1}H-NMR of 6.4.4.2.....102

Figure A.4 ^{13}C-NMR of 6.4.4.2 103

Figure A.5 ^{1}H-NMR of 6.4.4.3.....104

List of Schemes

Scheme 6.1 Acetonide protection of glycerol 81

Scheme 6.2 Addition of diethylchlorophosphate 82

Scheme 6.3 Deprotection of glycerol backbone.....82

Scheme 6.4 Addition of fatty acid tails 83

List of Abbreviations

d	Diameter
g	Gram
μm	Micron
mg	Milligram
mHz	Megahertz
nm	Nanometer
μl	Microliter
v	Velocity
ξ	Correlation length
B-TFL	B-tubule forming lecithin
$CDCl_3$	Deuterated chloroform
DC(8,9)PC	1,2-bis(10,12-tricosadiynoyl)-*sn*-glycero-3-phosphocholine
DCC	Dicyclohexylcarbodiimide
DDT	1-dodecanethiol
DMAP	Diethylaminopyridine
DNPC	1,2-bis(dinonanoyl)-*sn*-glycero-3-phosphocholine
DOPE	1,2-dioleoyl-*sn*-glycero-3-phosphoethanolamine
MTX	Methotrexate
Na_2SO_4	Sodium sulfate
PEG	Polyethylene glycol
PEO	Polyethylene oxide
PDMS	Polydimethylsiloxane

Ppy	Polypyrrole
p-TsOH	Para-toluenesulfonic acid
AFM	Atomic force microscopy
DIC	Differential interference contrast
EDS	Energy dispersive spectroscopy
SAXS	Small angle x-ray scattering
SEM	Scanning electron microscopy
TEM	Transmission electron microscopy
IV	Intravenous
MS	Multiple Sclerosis
PICC	Peripherally inserted central catheter

Abstract

Spherical vesicles consisting of phosphatidylcholines in which diacetylene groups have been inserted in the hydrocarbon tail centers give rise to hollow cylindrical tubes, known as "tubules". The study of tubules has become an area of intense interest in recent years due to their unusual morphology, which raises several profound theoretical issues and suggests their use in a variety of applications. Tubule hollowness suggests medical and industrial encapsulations as well as filtration and purification applications. These potential uses, e.g., for drug and gene delivery, requires optimization of their morphology for the application. Tubules have many technologically desirable properties, such as a very narrow distribution in diameter and length. The ability of the hydrocarbon tails' diacetylene groups to be polymerized suggests post-assembly modifications may be possible. Tubules are also susceptible to alignment with electric and magnetic fields, and being able to manipulate tubules in these ways can lead to a variety of new and innovative applications.

Our main area of study will be the exploration of tubule formation mechanisms via interactions with other molecules. The phospholipid, DC(8,9)PC (1,2-bis(10,12-tricosadiynoyl)*sn*-glycero-3-phosphocholine), is the most heavily-studied, and therefore serves as the standard to which comparisons can be made when the tubule-forming molecule is altered or when other components are added to the system. These morphological changes are critical to one of our primary technological motivations, the encapsulation and delivery of drugs. It is hoped changes of tubule size and shape resulting from either: a) the changes we make to the tubule-forming molecule; or b) the actions of the added molecule will yield; information about tubule internal structure. For example, intrinsic curvatures, bending moduli and correlation lengths, physical properties that must play important roles in determining tubule morphology,

can be measured directly in these perturbed systems and compared to pure DC(8,9)PC tubules' moduli. Studying the effects that certain molecules have on tubule formation can give us a better idea about the structural morphology and, most importantly, may allow optimization of that morphology for a particular application.

Chapter 1

Background, Overview, and Research Synopsis

1.1 Background

1.1.1 Discovery of Tubules

In 1989, Yager and co-workers discovered that phospholipids modified by the insertion of diacetylene groups spontaneously formed tubules, hollow cylinders of diameter 0.5 μm and lengths up to 200 μm.[1-4] The prototypical diynoic lipid is the diynoic phosphatidylcholine 1,2-bis(10,12-tricosadiynoyl)-*sn*-glycero-3-phosphocholine, DC(8,9)PC, (shown in Figure 1.1). Studies involving diynoic derivatives show that these molecules self-assemble to form microscopic hollow cylinders, with a helical trace evident on the exterior, creating a chiral object whose structure is similar to a paper drinking straw. DC(8,9)PC and many of its derivatives are the simplest tubule-forming molecules (a growing number of compounds that form tubules are appearing in the literature), and this simplicity makes them the best candidates for studying the relationship between the molecule's structure and its self-assembly behavior.

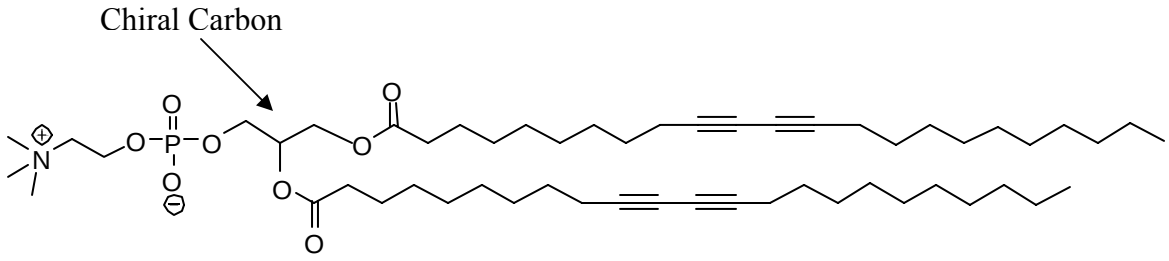

Figure 1.1 Chemical structure of 1,2-bis(10,12-tricosadiynoyl)*sn*-glycero-3-phosphocholine [DC(8,9)PC].

A number of non-diynoic compounds, including peptides,[5-7] gemini surfactants,[8-12] multiple "-ene-"-containing compounds and others[13,14] are currently being added to the group of

tubule-forming compounds that spontaneously form cylindrical structures; typically all these compounds produce cylinders of diameter $\approx 0.1 \leq d \leq \approx 1 \mu m$, with lengths ranging from a few to several hundred μm. Some of these structures are hollow, some are essentially solid, and some are cochlear.[15] One is hard-pressed to identify what molecular features enable self-assembly behavior, and which features (if any) are shared within this class of molecules.

In addition to its structural simplicity, DC(8,9)PC presents an excellent opportunity for self-assembly study because it forms relatively large (and hence easy-to-study microscopically) cylinders. An important facet of DC(8,9)PC's simplicity is that it differs from a manifold of natural and synthetic phosphatidylcholines that do *not* form tubules only by virtue of the diynes in its hydrocarbon tails' mid-sections. Clearly, these diynes are an "enabling" feature for tubule formation: saturated and semi-saturated DC(8,9)PC analogs do not form tubules.

1.1.2 Chiral Sub-structure

A simple cylinder is an achiral object, but DC(8,9)PC cylinders possess a chiral sub-structure. It is apparent that tubules form as a result of a flat ribbon winding helically (and hence chirally), resulting in the tubule "drinking straw" structure. Since the energetics of phospholipid bilayer membrane self-assembly is driven largely by the shielding of hydrophobic hydrocarbon tails from the aqueous environment, one should expect bilayer sheets to be discs. Circles are the minimum perimeter-per-area structure because they minimize the exposed hydrophobic tail at the bilayer's edge. At a non-zero temperature thermal effects cause the flat membrane to undulate; given sufficient membrane size and fluctuation, one should ultimately expect opposing edges of the sheet to encounter each other and fuse. (Indeed, one should ultimately expect these energetically-expensive edges to vanish completely as the sheet bends to form a spherical vesicle.) Justifying the energetics of the approximately 200:1 aspect-ratio ribbon that

subsequently winds to form a tubule is a significant theoretical challenge.[8] Four apparently independent pathways to tubule formation are known, and no one has devised a way to isolate any single process. Thermal analysis has proven to be problematic because of the inability to control the pathways by which tubules form.

R-DC(8,9)PC tubule exteriors are always right-handed helices, while the mirror-image *S*-DC(8,9)PC enantiomer always yields tubules possessing left-handed helical sub-structure.[16] The remarkable correspondence between helical handedness (hereafter, "helicity") and the molecule's chirality suggests powerfully that tubule formation is directed by molecular chirality.[17-19] The so-called "chiral packing" theory develops the idea that DC(8,9)PC's chiral shape causes the "directors" -- molecules' long axes -- of adjacent molecules in the tightly-packed bilayer membrane to be tilted slightly with respect to each other, and this tilt is uniform in a given direction along the length of the membrane. The propagation of this offset angle leads the membrane molecules to twist helically in a manner that ultimately winds to form closed cylinders, tubules.

A competing, but less accepted, "chiral symmetry-breaking" theory asserts that the membrane ribbon chiralizes (that is, selects its helicity) randomly.[20,21] To resolve which theory's assumptions are correct, an *achiral* DC(8,9)PC isomer β–TFL was made by interchanging one of the ester-linked hydrocarbon tails attached to the glycerol backbone's central carbon atom with the phosphocholine head group, forming a symmetric β-tubule-forming lecithin (β-TFL) that lacks a chiral center (see Figure 1.2).[22] This compound formed tubules at the same yield and under the same conditions as DC(8,9)PC, proving that tubule formation is *not* dependent on molecular chirality, and that the process appears to be better-described by the more general chiral symmetry-breaking theory. β-TFL produces an equal number of right and left-handed tubules.[22]

These results reveal that the chiral packing theory alone is not adequate to explain the tubule structure, and yet the chiral symmetry-breaking theory alone does not explain the remarkable helicity: chirality correspondence found with enantiopure *R*- or *S*-DC(8,9)PC.

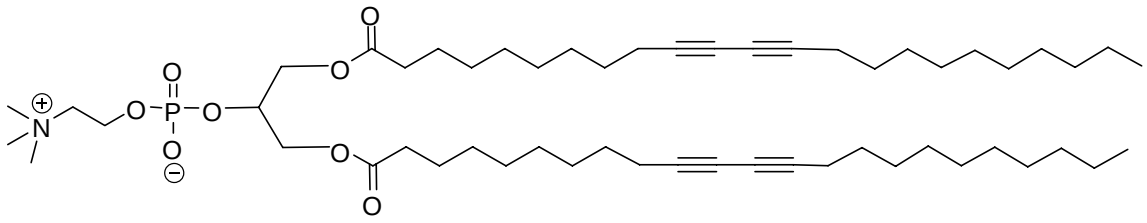

Figure 1.2 Chemical structure of achiral DC(8,9)PC isomer, "β–TFL".

1.1.3 Tubule Formation

Additional theoretical challenges in explaining tubule structure and formation result from the distinct, rather disparate physical processes by which tubules are seen to form: we have observed three distinct phospholipid tubule formation mechanisms. All three occur in ethanolic DC(8,9)PC solutions heated above 50°C that are cooled slowly (approximately 5°C/hour) to room temperature. These solutions become turbid upon cooling to ~40°C; small angle x-ray scattering (SAXS) shows this turbidity to be a consequence of multilamellar vesicles; optical microscopy shows these vesicles to be of the usual spherical symmetry. When the solution reaches room temperature, tubules form. Approximately 90% of the lipid found as tubules ultimately precipitates as tubules, while the balance remains in clear solution at room temperature; no other self-assembly products are found. Tubule self-assembly persists over a wide range of pH, solvent composition, and ionic strength.

Tubules may also be prepared in an isothermal process, where dilute DC(8,9)PC lipid in pure ethanol is slowly titrated with water, in which the phospholipid is less soluble. This solution also becomes turbid and tubules eventually precipitate. An alternative to direct titration

involves putting the pure ethanol/DC(8,9)PC solution into a dialysis bag and placing this bag in a large water reservoir.

The thermal process is experimentally more accessible because temperature is easier to control on a microscopic scale than is solvent composition, e.g., via a hot stage-equipped microscope or a SAXS experiment conducted upon a sufficiently thin sample that is under computer-mediated temperature control. For these technical reasons, the isothermal process' kinetics have not been studied as thoroughly as those of the thermal process, and this process will not be discussed further, other than to say it produces the same product with about the same yield.

In contrast, the thermal process has been extensively characterized by *in situ* Nomarski differential interference phase contrast microscopy (DIC) and SAXS probes, and its products by atomic force microscopy (AFM) and electron microscopy. DIC has been particularly powerful in resolving the three tubule formation mechanisms, which we now summarize.

1.1.3.1 Emergence from Vesicles

Under conditions of ultra-slow cooling ($dT/dt \approx 0.1$ °C/hr), DIC reveals the dominant tubule self-assembly mechanism to be the rapid (≈1.0 μm/s) growth of helices from spherical multilamellar vesicles.[23] SAXS shows the spherical vesicles to be in the chain-melted, disordered L_α phase, while the product tubules are in the chain-frozen, highly-ordered tilted $L_{\beta'}$ phase as shown in Figure 1.3.[24]

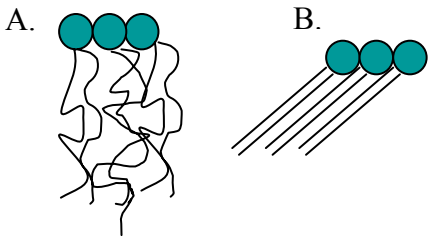

Figure 1.3 A. L_α chain melted phase, B. $L_{\beta'}$ chain-frozen phase.

As mentioned above, DC(8,9)PC tubule size permits direct DIC microscopy observation of the process. As the vesicle is cooled from the L_α phase, nodules appear on the surface of the vesicle; under conditions of ultra-slow cooling these nodules can persist for tens of minutes. Helical ribbons then abruptly begin to nucleate and grow from these nodules, and a typically a tangled "nest" of tubules form as all the material in the spherical vesicle converted to tilted $L_{\beta'}$ phase tubules over the course of tens of seconds. These ribbon-like structures emerge and lengthen from the spherical vesicles as helices. A second growth process is occurring simultaneously: As the ribbons grow in length they also widen slowly, until the ribbon's opposing long edges meet, thereby forming a continuous cylinder. While this meeting of the edges seemingly abolishes ribbon edge exposure to the aqueous environment and the associated energetics expense, the perseverance of the helical ridge makes evident these edges do not fuse. While this may be an effect of the tubule's non-fluid, chain-frozen $L_{\beta'}$ phase, several examples are known where the helically-would ribbon's opposing edges do not meet. For example, a considerable portion of DC(8,9)PC microstructures made in solutions where ethanol is replaced with isopropanol are found as "open" helices,[17] and approximately 10% DC(8,9)PC phosphonate tubules are also found in this state under conditions where all DC(8,9)PC microstructures are closed cylinders.[25,26] Also, a number of unrelated tubule-forming systems have exhibited open helical structures.[27,28] As amphiphilic structure formation is driven initially by reducing the hydrocarbon tail/water interaction, the widespread exposed hydrocarbon tail along the extended ribbon edge remains a difficulty when explaining the stability of these open helices. (Later, the "tubelet", a structure discovered in this lab, will be discussed, that explains the stability of the long ribbon and the persistence of the helical trace upon the tubule exterior.)

SAXS shows that DC(8,9)PC tubules formed in ethanolic solutions are multilamellar, i.e., they are composed of coaxially nested cylinders (shown in Figure 2.1);[24] DIC permits the direct observation of the outer tubule layers' formation and shows that these outer cylinders form from a very different mechanism than do the tubules' innermost cylinder, involving material transport between the solution and the condensed phase, in contrast to the inner cylinder's growth from a large reservoir of super-cooled L_α phase spherical vesicles.[23]

DIC shows that several minutes after all L_α phase DC(8,9)PC spherical vesicles have been converted to $L_{\beta'}$ phase tubules, a growth front propagates along the now continuous-walled cylinder's axis. It is apparent that the $L_{\beta'}$ phase cylinders formed from the spherical L_α phase vesicles now serve as nucleation sites for dissolved phospholipid in the still-cooling saturated solution. At $v \approx 0.1\mu m$ / sec, this outer cylinder's growth is an order of magnitude slower than that of the core's growth.

The sphere-to-tubule transition is thermally reversible, but substantial thermal hysteresis is observed. In the spherical, L_α phase to helical $L_{\beta'}$ phase conversion, under ultra-slow cooling, tubule nucleation and growth typically occurs two or three degrees Celsius below the tubule melting temperature. This means that the rapidly formed tubule cores form from *super-cooled* L_α phase spherical vesicles, while the much slower outer layer growth appears to be quasistatic in nature.

The discrepancy of outer and inner cylinders growth rates is reflected most surprisingly in their chiral sub-structure: AFM probes of the quickly-formed tubule core's helicity shows that they are almost equally divided between left and right-handed helicities, in marked contrast to the absolute uniformity of the slowly-formed outer cylinders' helicity, which corresponds to the chirality of the DC(8,9)PC used.[23] This experiment was done by preparing a glass slide whose

entire surface was covered with air-dried tubule suspension. This glass slide was then slowly dipped over the course of about 5 seconds into a 90% ethanol/water solution. The slide was then quickly withdrawn and swirled in a 4 liter beaker containing pure water. The 90% ethanol solution dissolves tubules at room temperature, but the slow lengthwise dipping of the glass slide into the ethanolic solution beaker created an "exposure gradient" – the bottom of the slide endured 10 seconds of exposure to this solution, while the top part of the slide endured only about ½ a second. It was found that the portion of the slide that endured the most exposure to the solution was wiped clean of tubules and residue, while the portion of the slide that endured the briefest exposure showed no real signs of the solvent's effects. Lying between these two extremes were regions where the solvent had sufficient time to strip away tubule exteriors, revealing the core. While the counting statistics are poor, it was clearly evident that while *R*-DC(8,9)PC tubule exteriors always possess right-handed helicity and the *S*-DC(8,9)PC enantiomer always produces left-handed helicity, the inner cylinder helicities are apparently random, hence determined *kinetically* during the rapid conversion of the super-cooled spherical vesicle to cylinder.

A variation of this experiment was to use water-immersion Nomarski optics and add tiny amounts of pure ethanol to the droplet being examined. Once again, the counting statistics are poor, but there is clear evidence of violations of the chirality/helicity correspondence required of the chiral-packing class of theories.

The presumed absolute correspondence between molecular chirality and cylinder helicity, as seen on the tubule exterior essentially required a "chiral-packing" theory, in which the mesoscopic scale (≈1 μm) helical winding is ultimately traceable to the molecule's chirality. The observation of enantiopure tubule cores possessing the "wrong" helical sense of handedness

breaches this association, and the robust formation with the achiral DC(8,9)PC isomer (Figure 1.2) shows that the chiral packing theory must be re-evaluated. "Re-evaluated" rather than discarded, because as mentioned above, the chiral symmetry-breaking theory alone is insufficient to describe the dramatic influence of molecular chirality upon the tubule exterior.

1.1.3.2 Growth from Solution

The second tubule formation mechanism is growth directly from solution, *i.e.*, in cooling saturated DC(8,9)PC solution, as in the previous mechanism, but in regions where spherical vesicles are absent. This mechanism has been observed only a few times and is therefore presumably a minor contributor to the product. The tubules forming under this mechanism appear to grow at both ends, at apparently the same $v \approx 0.1 \mu m$ speed as the ensheathment of the tubules described in the previous mechanism, and concurrently with tubule ensheathment. Because these tubules appear to grow at the same time and same rate as the multilamellar tubules' outer layers, one can tentatively conclude that this mechanism is essentially the same first-order phase transition of solvated molecules to the $L_{\beta'}$ phase that occurs during the formation of multilamellar tubules' outer layers.

1.1.3.3 Detachment from Sheets

The final tubule formation mechanism appears to be a minor contributor to tubule formation, as in the case of tubule growth from solution. Indeed, it is possible this mechanism does not occur at all in the bulk solution in which tubules are prepared, and only under ultraslow cooling of lipid solutions undergoing optical microscopy. This third process begins with the formation of large parallelogram-shaped phospholipid multilayer sheets, on the order of 300 μm x 100 μm, on the surface of the glass microscope slide. As seen in Figure 1.4, these sheets contain striations parallel to their long edges, and in time (typically about a second) five to

fifteen parallel phospholipid tubules form through the edgewise detachment from these striations, with the resulting ribbon winding helically, growing in length, and traveling perpendicular to it's long axis, as if tethered to the large surface-bound sheet. This process happens over the course of ~1 s. While this mechanism appears to be a minor contributor to the overall product, it is important because it is very similar to one proposed in 1996 by Selinger and coworkers for tubule formation in bulk solution from large spherical vesicles or flat sheets.[18] Consequently, the possibility that this mechanism is more dominant in bulk than our infrequent observations of it would suggest cannot be dismissed.

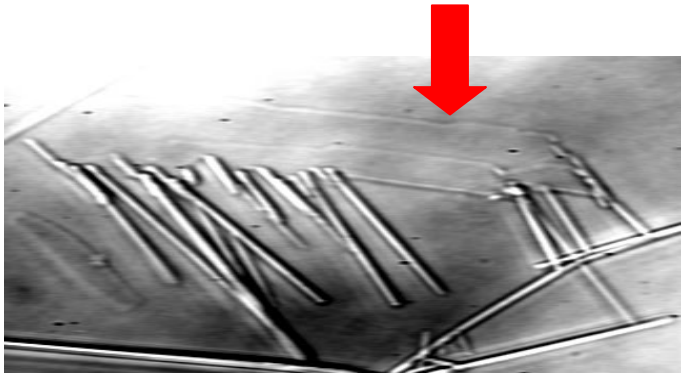

Figure 1.4 Nomarski DIC micrograph of DC(8,9)PC tubule array formed by the edgewise separation and helical winding of 1 μm-width ribbons from a large (300 μm x 100 μm), surface-bound parallelogram phospholipid multi-layer sheet (marked by the arrow). Note the faint line running along the sheet's long axis.

1.1.4 Theoretical Challenges

Tubules are thus seen to form through at least three very different mechanisms: 1) emergence from spherical L_α phase multilamellar vesicles cooled below the $L_{\beta'}$ phase melting temperature; 2) as "free-standing" structures formed through the first-order crystallization of lipid from the cooling saturated lipid solution; and, 3) the edgewise separation and helical winding of ribbons from large, surface-stabilized multilamellar sheets that form as saturated lipid

solutions cool. All mechanisms involve the helical winding of ribbon-like structures and "barber-pole" windings are evident on tubules formed by these mechanisms.

An adequate theoretical model does not exist for explaining the different tubule structures or their formation through the diverse mechanisms. Among the questions a satisfactory theory must address for all tubule formation mechanisms include how a ribbon having a 200:1 aspect ration spontaneously forms, particularly in view of the highly unfavorable energetics of the extended exposed hydrophobic edge, and how this ribbon chiralizes and winds to form a closed cylinder. In Chapter 3 a structure discovered in this laboratory,[29] the "tubelet", will be described, that resolves many of the theoretical problems in tubule formation theory, and that has profound technological consequences, especially for the central topic of this dissertation, drug encapsulation.

1.2 Overview

1.2.1 Phosphonates

Having described the known tubule formation processes, we now consider tubules made from the different molecules of Figure 1.5 which all share the apparently necessary (for phosphatidylcholines, at least) diynoic tails, but differ in their hydrophilic headgroups.

A.

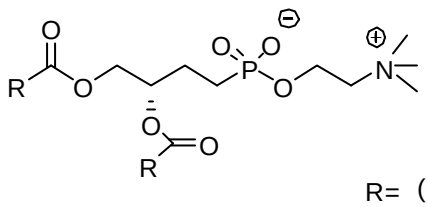

B.

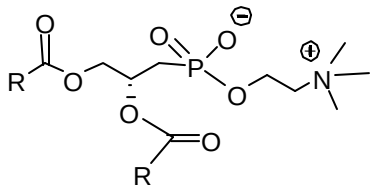

R= $(CH_2)_8-C\equiv C-C\equiv C-(CH_2)_9CH_3$

Figure 1.5 Chemical structure of A. *S*-"C4" DC(8,9)PC phosphonate derivative and B. R-"C3" DC(8,9)PC phosphonate derivative.

1.2.1.1 C4-phosphonate

As the glycerol backbone has a definite influence on tubule morphology (*R*-DC(8,9)PC forms right-handed tubules, while *S*-DC(8,9)PC forms left-handed tubules),[16] it is important to study modifications made to this portion of the molecule to see how tubule morphology is altered. The outcome of replacing the oxygen linkage to the phosphate group with a methylene group (-CH_2-) created a new tubule-forming phospholipid, "C4-phosphonate".[25] The phosphonate was selected because many phosphonate analogues of phosphorylated natural products function as inhibitors for enzymes for which the natural product is a substrate.[30,31] Given enzymes' well-known substrate specificity, and their acceptance of phosphonate analogs as substrate, the (-CH_2-)/O substitution seemed like a change that could be sufficiently small that tubule-forming ability would be conserved, and would be small enough that any observed change could be considered significant.

It was found that the C4-phosphonate fashions tubules in the same manner as DC(8,9)PC: 1) the ethanol/water ratios for optimal yields are alike; 2) tubule yields are 90%; and, 3) the tubule-forming temperatures for the compounds are within 1^{o}C of each other. Also, tubule lengths are very comparable; DC(8,9)PC and C4-phosphonate have tubule lengths of ~26 μm and ~23 μm respectively. Despite the similarities, there are some remarkable differences: 1) C4-phosphonate tubules have diameters of ~1 μm, twice that of DC(8,9)PC; 2; they have a greater propensity to flatten when placed upon a substrate – that is, they seem to be less rigid than DC(8,9)PC tubules; and most consistent with this change, 3) while the phosphonate tubule diameter doubled, there is a decrease in the number of coaxially nested cylinders; that is, phosphonate tubule wall thickness is half that of DC(8,9)PC tubules.

1.2.1.2 C3-phosphonate

Another phosphate analogue was synthesized, since the substitution of the phosphoryl oxygen by a methylene group was successful in altering tubule morphology. The new molecule was made by removing the phosphonate oxygen atom. Since this analogue has a 3-carbon glycerol backbone, it is referred to as "C3-phosponate".[26]

Tubule formation occurs in the same manner as DC(8,9)PC and the "C4" phosphonate, where the solvent ratios, tubule yields, and tubule-forming temperatures are similar. As with the "C4" phosphonate, there was also a 2-fold increase in tubule diameter, yielding tubules with ~1 μm diameters but with shorter lengths of ~16 μm.

1.2.1.3 Conservation of Interlamellar Spacing

These phosphonate molecules reveal a most interesting phosphatidylcholine tubule property, namely, that interlamellar spacing, as determined by SAXS, is a tightly conserved quantity. DC(8,9)PC tubule interlamellar spacing is 64.7 Ångstroms, while the two DC(8,9)PC phosphonate derivatives (whose diameters are twice that of DC(8,9)PC) have interlamellar spacings of 65.3 and 62.6 Ångstroms.[25,26] These measurements are consistent with a long-axis (director) tilt of 32^{o} from the membrane normal for completely expanded, all-trans methylene molecular configurations as projected by Caffrey et al.[32] The few Ångstroms' variation between different molecules' tubules interlamellar spacings are small in comparison to the two-fold changes in tubule diameter. The SAXS correlation lengths ξ, which is a measure of tubule wall thicknesses, are nearly halved from the DC(8,9)PC 430 Ångstroms to 210 Ångstroms as the tubule diameters doubled.[26]

Tubules made from the phosphonates of Figure 1.5 deposited onto glass substrates sometimes partly unravel at their ends, permitting direct measurement of membrane thickness by

AFM. Investigation of these tubules on flat substrates shows that the flat, unraveled portions have heights approximately twice that expected of a single bilayer at the known long-axis tilt of 32^{o} (Thomas, unpublished result). Accordingly, these tubule walls must consist of two bilayers (that is, four monolayers). Since phosphonate tubule wall SAXS correlation lengths are half that of DC(8,9)PC, we conclude DC(8,9)PC tubule walls are four bilayers thick. AFM measurements provide confirmation of SAXS results.

1.2.2 Phospholipid/Protein Cones

DC(8,9)PC tubule-forming solutions where a protein, lysozyme, has been added exhibits the same strict conservation of bilayer spacing and tubule wall thickness. The DC(8,9)PC/lysozyme mixture's prevailing products are that of a gently tapered cone instead of the expected hollow cylindrical tube.[33] Although, some undistorted tubules are present, the majority in this protein-containing solution are conical. Like DC(8,9)PC tubules, these cones have helical ridges, but they are more distinct. DIC video microscopy shows cone formation to be very similar to protein-free tubule formation, the principal difference being that cones emanate from proteinaceous nodules that precipitate early in the cooling cycle, rather from the L_{α} phase spherical vesicles of the protein-free system. While DC(8,9)PC tubule cycle reverses back to spherical vesicles when reheated, DC(8,9)PC/lysozyme systems do not convert back to vesicles upon heating. When cones are subjected to reheating they seem to dissolve back into solution, suggesting spherical vesicles do not form; however, cones do re-appear when the solution is cooled again. Also, cone formation occurs ~10^{o}C higher than that of DC(8,9)PC tubule solutions free of protein.

Spatially-resolved energy dispersive x-ray spectroscopy (EDS) tuned to the protein's sulfur-bearing cysteine residues shows the protein is disseminated uniformly along the cone

length, but is not found elsewhere on the electron microscopy substrate, indicating that lysozyme is associated with the lipid.[33] SAXS results confirm that cones also consist of four bilayers spaced at 66.2 Ångstroms, very close to the interlamellar spacing of 64.7 Ångstroms for protein-free tubules. The addition of protein disrupts normal tubule formation and causes cones to form instead of cylinders, suggesting that tubule morphology may be optimized for a specific application through the addition of such agents, or common polymers such as polyethylene oxide (PEO) or polyethylene glycol (PEG).

1.2.3 Tubules with Tunable Diameters

Diacetylenic lipids produce 0.5 μm diameter tubules no matter what the length of the acyl chain or the placement of the diacetylene groups; however, a recent study using a mixed lipid system composed of short-chain saturated phospholipid "spacers" and diacetylenic phospholipids demonstrates another approach that could avoid the need to resort to costly and time-consuming syntheses to control tubule diameter.[34] A decrease in tubule diameter leads to higher-aspect ratio structures.

Control of tubule diameter will have a major impact on technologies that may use tubules for their aspect ratios. Two examples spring to mind: 1) the release of encapsulated materials from a tubule will undoubtedly depend upon the tubule diameter; and 2) as discussed below, the somewhat surprisingly sole determinant of tubules' effective aerodynamic diameter is the tubule's diameter - - tubule length plays almost no role in tubule aerodynamic behavior.

Mixtures of diacetylenic phospholipids DC(m,n)PCs and saturated lipids DC(m`)PCs, reveal a connection between the n segments of the acyl chains in the diacetylenic phosphocholines and the diameter of tubules produced from these lipid mixtures.[34]

1.2.3.1 Result of Acyl Chain Length of Saturated Spacer Lipids

Singh et al. studied lipid mixtures prepared with DC(8,9)PC and DC(m`)PC ranging from 8-12 carbon long acyl chains in order to determine the effects that the chain length would have on tubule diameter.[34] Tubule diameters were measured immediately after tubule formation was complete (4°C), after annealing for 105 days (4°C), and after 120 hours at room temperature. Both DC(6)PC and DC(8)PC are unable to conceal the functionality of the diacetylene groups in DC(8,9)PC from interacting with neighboring diacetylene groups, and tubules with smaller diameters resulted from secondary interference effects. After annealing, the diameters remain unchanged, within error, but after storing at room temperature, DC(6)PC-doped specimens formed helical ribbons and DC(8)PC-doped solutions' mean tubule diameter increased. DC(9)PC and DC(10)PC hydrocarbon tails, however, are long enough to interact with the diacetylenes, or perhaps interfere with diyne/diyne interactions present in the tubule phospholipid bilayers, and tubules with much larger diameters form. Upon room-temperature annealing, however, these larger diameters decrease to approximately the usual DC(8,9)PC diameter after annealing, making these tubules technologically appealing. The DC(9)PC spacer tubule morphology equilibrates at room temperature, while the DC(10)PC forms vesicles. The measurements for these diameters are shown in Table 1.1, showing that tubule diameter can be controlled by the length of the acyl chain in the spacers and annealing can lead to desirable properties.

1.2.3.2 Result of Diacetylenic Acyl Chain Length

Using the saturated spacer lipid, DC(7)PC, which equals the m segment (m = 8) of DC(m,n)PC, the effect of the n segment was determined.[34] For n = 9, 11, and 13, diameter sizes were approximately 55, 63, and 108 nm respectively. The results reveal that as the n segment

Table 1.1 Tubule diameters as a result of acyl chain length.[34]

DC(n)PC	Tubule Diameter (nm) Immediately (4^oC)	Tubule Diameter (nm) 105 Days (4^oC)	Tubule Diameter (nm) 120 h (25^oC)
DC(6)PC	~57	~58	~30 Helical Ribbons
DC(8)PC	~52	~52	~89
DC(9)PC	~124	~63	~75
DC(10)PC	~93	~55	~167 Vesicle

increases so does the tubule diameter. Similar studies where the m and m` segments were increased by two display the same results: diameter increases as the n segment increases. Both studies also prove that the diameter size is independent of the total diacetylenic acyl chain length. For instance, DC(8,11)PC and DC(10,9)PC have the same amount of carbons in their acyl chains and have approximately the same diameters of their tubules (~70 and ~69 nm) after annealing.

1.2.3.3 DNPC

A mixture of DC(8,9)PC and the short chain saturated lipid 1,2-bis(dinonanoyl)-*sn*-glycero-3-phosphocholine, DNPC, yields tubules with diameters ranging from 50-60 nm.[35] The addition of DNPC also increases the efficiency of polymerization, which can be important in mechanical as well as encapsulation (especially subcutaneous injection) applications. Suspensions of DNPC/DC(8,9)PC held at room temperature for longer period of time show that tubules convert to a network of entangled ribbons.

The annealing that occurs in these multi-component lipid membranes underscores the metastable nature of the initial tubule formation. In other words, tubule formation is clearly

kinetically-driven, and the subsequent annealing is presumably a tendency towards the thermodynamically-stable product.

1.2.4 Positioning and Alignment

The assembly of tubules into patterns on substrates is key in cultivating some of their potential applications. Zhao et al. discovered that by combining dewetting and microfluidic networks, DC(8,9)PC can be aligned into two-dimensional ordered arrays onto glass substrates.[36] The capillary force induces a flow that pulls tubules into the microfluidic network and aligns them in the channels. A patterned gold (Au) substrate with alternating 1-dodecanethiol (DDT) monolayer and Au stripes was made using a polydimethylsiloxane (PDMS) stamp. The alternating hydrophilic and hydrophobic stripes allow for selective positioning of the tubules; the tubules adsorb on the hydrophilic Au stripes in the stripe direction as a result of the phosphocholine group, which is hydrophilic. The resulting tubules remain consistent with normal tubule's morphology, suggesting aligned tubules are not deformed in the process. Some of the factors effecting tubule alignment include withdrawal rate, moving contact line, and adsorption time. As the withdrawal rate increases, the angular distribution becomes restricted. The aligned tubules are perpendicular to the contact line because of surface tension. The quantity of aligned tubules also increases as the adsorption time increases. The ability to align tubules in large amounts onto substrates will enhance their use for a number of applications.

1.2.5 Bending and Radial Deformation of Tubules on SAM

Droplets of DC(8,9)PC tubule solution air dried on hydrophobic DDT self-assembled monolayers undergo an interesting morphology change from a straight cylinder to a cylinder bent into a circular arc and can form a near spherical configuration.[37] These tubules typically have persistence lengths of ~41 μm. Several tubules so bent can be positioned to fashion an annular

structure. In contrast, when DC(8,9)PC tubule solution droplets are dried on a hydrophilic Au surface, they quickly wet the surface and do not form curved tubules. A shrinking contact line as the droplet desiccates is what causes this curve in the tubules, and it is a gradual process since the exterior remains smooth, with no apparent cracking. Being able to understand the mechanical properties of tubules is vital for application development.

1.2.6 Templated Synthesis

The narrow distribution in diameter and length of tubules could lead to their use as templates for growth of inorganic salts, organic crystals, and polymers. Templated synthesis can provide a means to control the resulting crystalline material or polymer structure and morphology. Block copolymers,[38] lipids,[39] and liquid crystals[40] have been used as templated media due to their highly organized structures, making DC(8,9)PC tubules also a great candidate for templated synthesis. The templated synthesis of the conducting polymer, polypyrrole (Ppy), from a solution of DC(8,9)PC lipid tubules has been reported.[41] The Ppy strand morphology progression occurs along the edges or seams of the tubule and not on the tubule surface. The width of the Ppy strand is dependent on polymerization times, illustrating the ability to control resulting properties of this templated synthesis. Tubules that have not completely formed (twisted ribbon-like structures or open tubules) have two parallel edges where the Ppy strands grow and trace each other. Fully formed tubules have one Ppy strand that aligns on the surface in a helical fashion, along the barber-pole winding. Ppy rings are often found at the end of the tubule, even on tubules where Ppy strands have not formed along the edges or seams. Since the reaction could transpire either along the edges or on the surface, what causes Ppy strands to selectively grow along the edges? According to the twisted bilayer ribbon theory, the edges consist of exposed hydrophilic regions; therefore, the acetylene groups may contribute to the

adsorption of Ppy onto the edges. It may also be the favored site because of the high surface energy related to the curved edges. Whatever the circumstances, the edge is the preferred location for the polymerization of pyrrole using tubules as a template.

1.3 Research Synopsis

The potential for technological applications is apparent immediately, and suggested tubule uses include: a substrate for the helical crystallization of proteins, templated synthesis of inorganic salts, organic crystals, and drug encapsulation. This dissertation will focus primarily on two things: Probing the relationship between the DC(8,9)PC molecular structure and the morphology of its self-assembly products, and in a practical vein, how such modifications might lead to their optimization for the application of drugs. We describe a previously unobserved structure, the "tubelet", in Chapter 3, encapsulation of several drugs (Chapter 4), addition of co-surfactants (Chapter 5), and chemical modifications made to DC(8,9)PC (Chapter 6).

1.4 References

1. Schoen, P. E.; Yager, P.; Priest, R. G. Spectroscopic studies of a diacetylenic surfactant. *NATO ASI Series, Series E: Applied Sciences* **1985,** *102* (Polydiacetylenes), 223-232.

2. Schoen, P. E.; Yager, P. Spectroscopic studies of polymerized surfactants: 1,2-bis(10,12-tricosadiynoyl)-sn-glycero-3-phosphocholine. *Journal of Polymer Science, Polymer Physics Edition* **1985,** *23* (10), 2203-2216.

3. Yager, P.; Schoen, P. E. Formation of tubules by a polymerizable surfactant. *Molecular Crystals and Liquid Crystals* **1984,** *106* (3-4), 371-381.

4. Yager, P.; Schoen, P. E.; Davies, C.; Price, R.; Singh, A. Structure of lipid tubules formed from a polymerizable lecithin. *Biophysical Journal* **1985,** *48* (6), 899-906.

5. Aggeli, A.; Bell, M.; Boden, N.; Keen, J. N.; Knowles, P. F.; McLeish, T. C.; Pitkeathly, M.; Radford, S. E. Responsive gels formed by the spontaneous self-assembly of peptides into polymeric beta-sheet tapes. *Nature* **1997,** *386* (6622), 259-262.

6. Aggeli, A.; Bell, M.; Boden, N.; Keen, J. N.; Mcleish, T. C. B.; Nyrkova, I.; Radford, S. E.; Semenov, A. Engineering of peptide b-sheet nanotapes. *Journal of Materials Chemistry* **1997,** *7* (7), 1135-1145.

7. Zhang, S.; Holmes, T.; Lockshin, C.; Rich, A. Spontaneous assembly of a self-complementary oligopeptide to form a stable macroscopic membrane. *Proceedings of the National Academy of Sciences of the United States of America* **1993,** *90* (8), 3334-3338.

8. Oda, R.; Huc, I.; Schmutz, M.; Candau, S. J.; MacKintosh, F. C. Tuning bilayer twist using chiral counterions. *Nature* **1999,** *399* (6736), 566-569.

9. Jaeger, D. A.; Wang, Y.; Pennington, R. L. Pyrophosphate-Based Gemini Surfactants. *Langmuir* **2002,** *18* (24), 9259-9266.

10. Menger, F. M.; Mbadugha, B. N. A. Gemini Surfactants with a Disaccharide Spacer. *Journal of the American Chemical Society* **2001,** *123* (5), 875-885.

11. Peresypkin, A. V.; Menger, F. M. Zwitterionic Geminis. Coacervate Formation from a Single Organic Compound. *Organic Letters* **1999,** *1* (9), 1347-1350.

12. Oda, R.; Candau, S. J.; Oda, R.; Huc, I. Gemini surfactants, the effect of hydrophobic chain length and dissymmetry. *Chemical Communications (Cambridge)* **1997,** (21), 2105-2106.

13. Kulkarni, V. S.; Boggs, J. M.; Brown, R. E. Modulation of nanotube formation by structural modifications of sphingolipids. *Biophysical Journal* **1999,** *77* (1), 319-330.

14. Hui, S. W.; Boni, L. T.; Stewart, T. P.; Isac, T. Identification of phosphatidylserine and phosphatidylcholine in calcium-induced phase separated domains. *Biochemistry* **1983,** *22* (14), 3511-3516.

15. Papahadjopoulos, D.; Vail, W. J.; Jacobson, K.; Poste, G. Cochleate lipid cylinders. Formation by fusion of unilamellar lipid vesicles. *Biochimica et Biophysica Acta, Biomembranes* **1975,** *394* (3), 483-491.

16. Singh, A.; Burke, T. G.; Calvert, J. M.; Georger, J. H.; Herendeen, B.; Price, R. R.; Schoen, P. E.; Yager, P. Lateral phase separation based on chirality in a polymerizable lipid and its influence on formation of tubular microstructures. *Chemistry and Physics of Lipids* **1988,** *47* (2), 135-148.

17. Georger, J. H.; Singh, A.; Price, R. R.; Schnur, J. M.; Yager, P.; Schoen, P. E. Helical and tubular microstructures formed by polymerizable phosphatidylcholines. *Journal of the American Chemical Society* **1987,** *109* (20), 6169-6175.

18. Selinger, J. V.; MacKintosh, F. C.; Schnur, J. M. Theory of cylindrical tubules and helical ribbons of chiral lipid membranes. *Physical Review E: Statistical Physics, Plasmas, Fluids, and Related Interdisciplinary Topics* **1996,** *53* (4-B), 3804-3818.

19. Selinger, J. V.; Spector, M. S.; Schnur, J. M. Theory of Self-Assembled Tubules and Helical Ribbons. *Journal of Physical Chemistry B* **2001,** *105* (30), 7157-7169.

20. Lindsell, W. E.; Preston, P. N.; Seddon, J. M.; Rosair, G. M.; Woodman, T. A. J. Macroscopic Helical and Cylindrical Morphologies from Achiral 1,3-Diynes. *Chemistry of Materials* **2000,** *12* (6), 1572-1576.

21. Seifert, U.; Shillcock, J.; Nelson, P. Role of bilayer tilt difference in equilibrium membrane shapes. *Physical Review Letters* **1996,** *77* (26), 5237-5240.

22. Pakhomov, S.; Hammer, R. P.; Mishra, B. K.; Thomas, B. N. Chiral tubule self-assembly from an achiral diynoic lipid. *Proc Natl Acad Sci U S A* **2003,** *100* (6), 3040-3042.

23. Thomas, B. N.; Lindemann, C. M.; Clark, N. A. Left- and right-handed helical tubule intermediates from a pure chiral phospholipid. *Physical Review E: Statistical Physics, Plasmas, Fluids, and Related Interdisciplinary Topics* **1999,** *59* (3-A), 3040-3047.

24. Thomas, B. N.; Safinya, C. R.; Plano, R. J.; Clark, N. A. Lipid tubule self-assembly: length dependence on cooling rate through a first-order phase transition. *Science (Washington, D. C.)* **1995,** *267* (5204), 1635-1638.

25. Thomas, B. N.; Corcoran, R. C.; Cotant, C. L.; Lindemann, C. M.; Kirsch, J. E.; Persichini, P. J. Phosphonate Lipid Tubules. 1. *Journal of the American Chemical Society* **1998,** *120* (47), 12178-12186.

26. Thomas, B. N.; Lindemann, C. M.; Corcoran, R. C.; Cotant, C. L.; Kirsch, J. E.; Persichini, P. J. Phosphonate Lipid Tubules II. *Journal of the American Chemical Society* **2002,** *124* (7), 1227-1233.

27. Blanzat, M.; Massip, S.; Speziale, V.; Perez, E.; Rico-Lattes, I. First Example of Helices and Tubules in Aqueous Solution of a New Fluorescent Catanionic Sugar Surfactant. *Langmuir* **2001,** *17* (11), 3512-3514.

28. Zastavker, Y., V; Asherie, N.; Lomakin, A.; Pande, J.; Donovan, J. M.; Schnur, J. M.; Benedek, G. B. Self-assembly of helical ribbons. *Proc Natl Acad Sci U S A* **1999,** *96* (14), 7883-7887.

29. Mishra, B. K.; Garrett, C. C.; Thomas, B. N. Phospholipid Tubelets. *Journal of the American Chemical Society* **2005,** *127* (12), 4254-4259.

30. McClard, R. W. A facile route to methylenephosphonate sugars substituted at the anomeric carbon. *Tetrahedron Letters* **1983,** *24* (26), 2631-2634.

31. Yount, R. G. ATP analogs. *Adv Enzymol Relat Areas Mol Biol* **1975,** *43*, 1-56.

32. Caffrey, M.; Hogan, J.; Rudolph, A. S. Diacetylenic lipid microstructures: structural characterization by X-ray diffraction and comparison with the saturated phosphatidylcholine analogue. *Biochemistry* **1991,** *30* (8), 2134-2146.

33. Mishra, B. K.; Thomas, B. N. Phospholipid/Protein Cones. *Journal of the American Chemical Society* **2002,** *124* (24), 6866-6871.

34. Singh, A.; Wong, E. M.; Schnur, J. M. Toward the rational control of nanoscale structures using chiral self-assembly: Diacetylenic phosphocholines. *Langmuir* **2003,** *19* (5), 1888-1898.

35. Svenson, S.; Messersmith, P. B. Formation of Polymerizable Phospholipid Nanotubules and Their Transformation into a Network Gel. *Langmuir* **1999,** *15* (13), 4464-4471.

36. Zhao, Y.; Fang, J. Positioning and Alignment of Lipid Tubules on Patterned Au Substrates. *Langmuir* **2006,** *22* (4), 1891-1895.

37. Zhao, Y.; Mahajan, N.; Fang, J. Bending and Radial Deformation of Lipid Tubules on Self-Assembled Thiol Monolayers. *Journal of Physical Chemistry B* **2006,** *110* (44), 22060-22063.

38. Huang, Z.; Wang, P. C.; MacDiarmid, A. G.; Xia, Y.; Whitesides, G. Selective Deposition of Conducting Polymers on Hydroxyl-Terminated Surfaces with Printed Monolayers of Alkylsiloxanes as Templates. *Langmuir* **1997,** *13* (24), 6480-6484.

39. Burkett, S. L.; Mann, S. Spatial organization and patterning of gold nanoparticles on self-assembled biolipid tubular templates. *Chemical Communications (Cambridge)* **1996,** (3), 321-322.

40. Torres, W.; Fox, M. A. Electrosynthesis of polypyrrole in a nematic liquid crystal. *Chemistry of Materials* **1992,** *4* (3), 583-588.

41. Goren, M.; Qi, Z.; Lennox, R. B. Selective Templated Growth of Polypyrrole Strands on Lipid Tubule Edges. *Chemistry of Materials* **2000,** *12* (5), 1222-1228.

Chapter 2

Materials and Methods

2.1 Materials

1,2-bis(10,12-tricosadiynoyl)*sn*-glycero-3-phosphocholine (DC(8,9)PC) [Catalog # 870016, Avanti Polar Lipids, Inc.], absolute ethanol [AAPER Alcohol and Chemical Company], distilled water, 1,2-dioleoyl-*sn*-glycero-3-phosphoethanolamine (DOPE) [Catalog # 850725, Avanti Polar Lipids, Inc.], lysozyme (from chicken egg white) [CAS # 12650-88-3, Sigma], and cholesterol [CAS # 57-88-5, Aldrich, 99%], were used as received.

Chemotherapy agents, carboplatin, methotrexate, and mitoxantrone, were fresh, surplus clinical materials supplied by Drs. Neal Mauldin & David Hunley of the LSU Veterinary School. These clinical materials were aqueous solutions; pure crystalline carboplatin was provided by Spectrum Pharmaceuticals, Irvine, CA.

Materials used in syntheses (described in Chapter 6) include glycerol [CAS # 56-81-5, Sigma, 99%], acetone [CAS # 67-64-1, Aldrich, 99%], p-TsOH [CAS # 9192-52-5, Aldrich 98.5%], diethylchlorophosphate [CAS # 814-49-3, Aldrich, 97%], ethyl ether [CAS # 60-29-7, Aldrich 99.7%], pyridine [CAS # 110-86-1, Aldrich 99.8%], oleic acid [CAS # 112-80-1, Sigma-Aldrich, 99%], linoleic acid [CAS # 60-33-3, Sigma, 99%], γ-linolenic acid [CAS # 506-26-3, Sigma, 99%], sodium bicarbonate [CAS # 144-55-8, Aldrich 99.5%], chloroform [CAS # 67-66-3, Aldrich 99%], potassium carbonate [CAS # 584-087, Aldrich 99.99%], sodium sulfate [CAS # 7757-82-6, Aldrich 99%], and 1,3-dicyclohexylcarbodiimide [CAS # 36049-771, Aldrich 99%], were used without further purification. Methylene chloride [CAS # 75-09-2, Aldrich 99.5%] was distilled over calcium hydride. Ethyl acetate [CAS # 141-78-6, Aldrich 99.8%] and hexane [CAS # 110-54-3, Aldrich 95%] were distilled over sodium metal.

2.2 Methodologies

2.2.1 Tubule Stock Solution Preparation

A stock solution of tubules was prepared by adding DC(8,9)PC lipid to a mixture of ethanol and water (at various ratios) at a concentration of 1mg of lipid/ml of solvent. The lipid was dissolved by heating to 50^{o}C while vigorously stirring until the solution became clear. The solution was slowly cooled back to room temperature. It first becomes turbid as it enters the high temperature spherical vesicle phase, where the phospholipid is in the L_{α} phase, or chain-melted phase. Upon cooling further, the low temperature $L_{\beta'}$ phase is entered, which is the time when a white precipitate of tubules form from a now-clearing solution. This so-called "thermal" tubule formation process is shown schematically in Figure 2.1.

2.2.2 Protein-Modulated Tubules

Lysozyme in the amount of 1 mg was added to 1ml of stock solution of DC(8,9)PC (with an ethanol to water ratio of 90:10 v:v). This mixture was then taken through the standard thermal tubule formation cycle. As before, upon cooling the solution became turbid, and clarifies upon further cooling as tubules precipitate.

2.2.3 Addition of Chemotherapy Agents

The chemotherapy agents (methotrexate, mitoxantrone, and carboplatin) were added to the stock solution of DC(8,9)PC (with an ethanol to water ratio of 75:25 v:v) at the supplied clinical concentrations. Once a drug was added to the stock solution, it was subjected to the standard thermal cycle, heating to clarity and cooling back to room temperature. Turbidity indicates the formation of light-scattering structures, e.g., the spherical vesicles, but tubule formation is certain only when a precipitate has formed and it is microscopically examined for the presence of tubules.

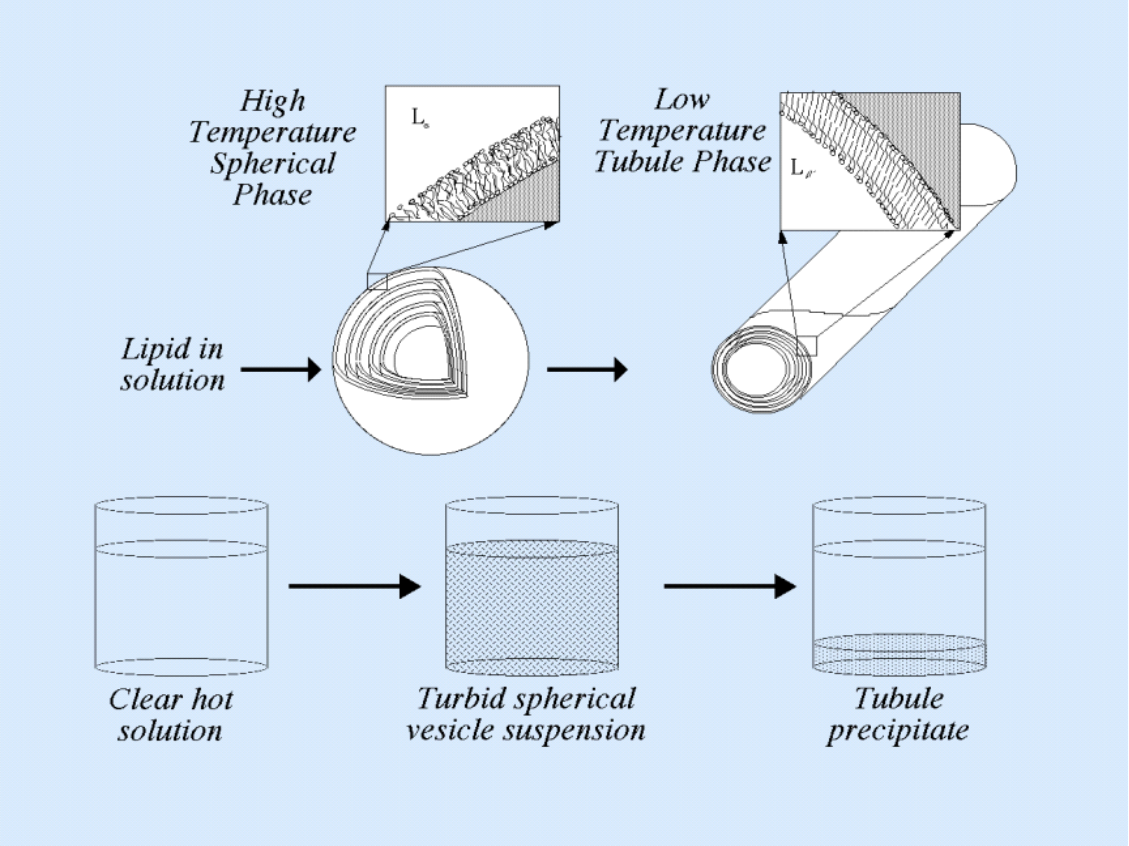

Figure 2.1 Tubule preparation.

2.2.4 Addition of DOPE and Cholesterol

1,2-dioleoyl-*sn*-glycero-3-phosphoethanolamine (DOPE) and cholesterol were added to the stock solution of DC(8,9)PC (with an ethanol to water ratio of 75:25 v:v) at various concentrations. Once DOPE and cholesterol were added to the stock solution, it was heated to clarity and cooled back to room temperature. Again, all turbidity indicates is the formation of light-scattering structures, e.g., the spherical vesicles or similarly-sized structures, but tubule formation is certain only when a precipitate has formed and it is microscopically examined for the presence of tubules.

2.3 Instrumentation and Theory

2.3.1 Optical Microscopy

Differential interference contrast microscopy (DIC) was conducted with a Nikon Diaphot 300 inverted microscope equipped with 60x and 100x Nomarski objectives. A small amount of the sample was placed on a glass microscope slide, air dried and viewed or covered with a glass coverslip and mounted upon the oil-immersion microscope stage for viewing.

2.3.2 Theory of Nomarski DIC

Nomarski DIC is a type of interference microscopy; interference microscopy is generally used in samples that have low optical density (i.e., refractive index) changes at interfaces, such as at a membrane/solution interface, making these edges difficult to see.[1] Interference effects are used to enhance the contrast of materials being viewed.

Interference occurs when a single optical beam is split and the two beams recombine after traveling along paths of optical lengths that differ by any length not happening to be an integral multiple of the light's wavelength. This path difference can be "real" – that is, physical distance, or a consequence of the two beams encountering media of different indices of refraction.

In the practice of interference microscopy, a doubly-refractive crystal plate underneath the sample specimen splits the beam into two spatially-resolved beams that differ in phase, typically ¼ a wavelength.[1] Typically these beams are recombined just before the eyepiece, with an additional ¼ wavelength retardation introduced. Combining two beams differing by ½ wavelength should of course result in cancellation, i.e., a dark field of view. But, variations of the specimen's index of refraction contained within its structure, introduces additional phase differences between the two spatially-resolved beams. That is, in any part of the sample in which neighboring regions vary in refractive index, the two beams are slowed down or refracted

by different amounts (light travels slower in areas with a higher refractive index). When these two beams are reunited after exiting the specimen, differences in brightness occur that correspond to the differences in refractive index (or thickness) of the sample can now be seen, except for the (highly unlikely) possibility that the sample has introduced exactly ½ wavelength between the two beams.

The splitting and recombination of light beams is usually done in two ways: 1) by using reflective surfaces; or 2) birefringent crystals.[2] In the first, the light can take two different paths by reflection from a series of reflecting surfaces, and the second, the light is split into two beams and recombined by using birefringent crystals (as in the case of Nomarski DIC).

Similar to phase contrast microscopy, interference microscopy allows viewing of otherwise transparent objects having even slightly different indices of refraction.[2] This is accomplished by translating the phase changes in light traveling through the specimen's different optical densities into changes of amplitude of the recombined wave. In phase contrast microscopy, the contrast enhancement is attained by a single beam of light, and the diffraction is caused by the sample in order to produce destructive or constructive interference. In interference microscopy, the image is obtained from two beams of light passing separately through the sample in different regions with different refractive indexes.

Nomarski DIC was developed in the 1950s. It is distinguished by a noticeable relief effect giving a three-dimensional appearance, and shallow field depth. The characteristic three-dimensional image appears due to the shearing effect of the Nomarski prisms (see Figure 2.2 for DIC light path). Light first passes through a polarizer, which selects light whose electric field is aligned along a particular direction. This plane polarized light passes through a Nomarski modified Wollaston prism that is positioned 45^{o} with respect to the polarized light beam. The

prism consists of two quartz wedges that are cemented together along their hypotenuse. The shear takes place at the quartz-air interface of the lower prism. Refraction at this interface causes the sheared wave fronts to converge outside the prism. (In the Wollaston prism, shear takes place at the cement boundary.) The 45^{o} prism orientation splits the incident plane-polarized beam into two perpendicular, equal constituents. As the components travel through the condenser, they exit parallel to each other and continue through the sample specimen and objective. A second Nomarski modified Wollaston prism located behind the objective causes the recombination of the two constituents. The analyzer assembles the vibrational directions parallel in order for the light rays to interfere at the intermediate image plane.

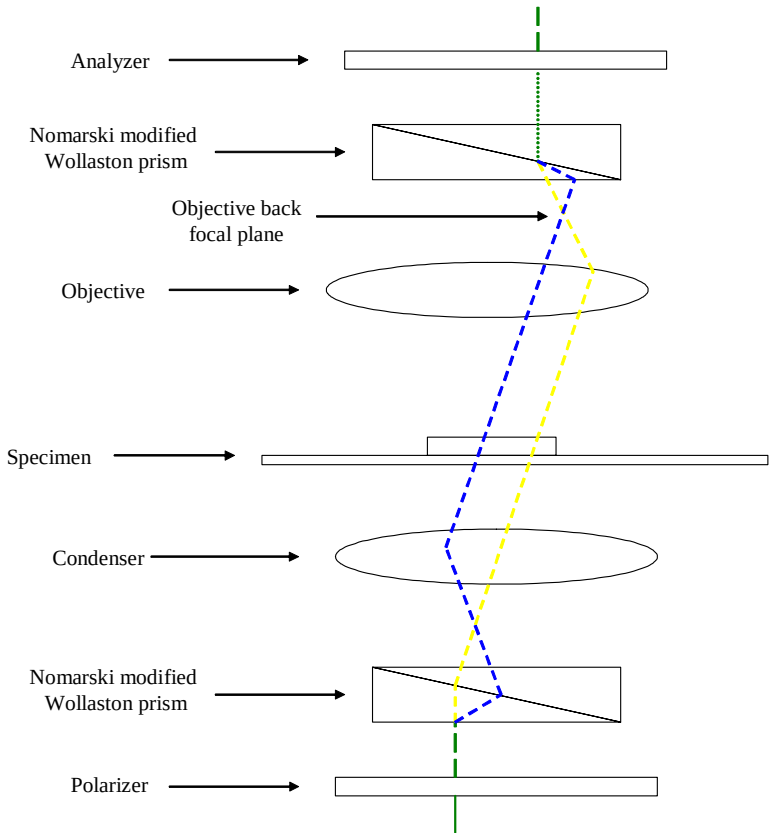

Figure 2.2 Nomarski differential interference contrast microscopy; showing light path (adapted from McCrone).

2.3.3 Atomic Force Microscopy (AFM)

Contact-mode atomic force microscopy (AFM) probes of samples were obtained with a Digital Instruments BioScope, equipped with silicon nitride NanoProbe SPM tips. The sample was prepared in the same fashion as the optical microscopy samples, air dried on a glass slide. Images shown are representative of the entire sample. After acquiring the images, an image flatten method was performed. In the micrographs shown the brightest regions of the scan are the tallest features.

2.3.4 Theory of AFM

The atomic force microscope, also referred to as, scanning probe microscope, was developed by G. Binnig, et al. in 1986.[3,4] AFM gives significant information about surface features. AFM images are created by measuring the interaction of forces between the tip, which is attached to the end of a cantilever, and the surface. As the cantilever is scanned across a surface by a piezoelectric tube, the z-axis, or vertical component, is measured in order to gain information about differences in height.[5] This difference in height is recorded as the laser beam that is positioned on the cantilever is reflected onto a photodiode (see schematic in Figure 2.3). The height is calculated from the z displacement of the cantilever and the spring constant of the cantilever.

In this dissertation, contact mode AFM was employed. In this mode, the tip is brought in contact with the surface and the cantilever deflection remains steady throughout scanning.[6] This is done by using a feedback loop, where a constant force is maintained between the cantilever and the specimen by moving the scanner vertically, so the force between the tip and the specimen remains balanced. This vertical distance is then measured by the photodiode.

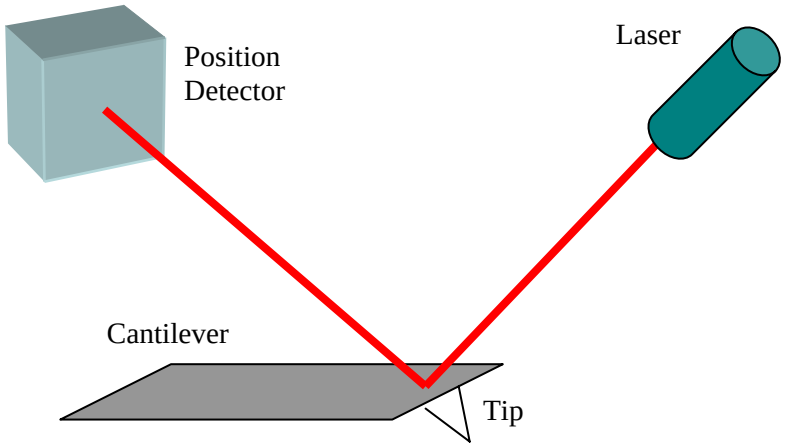

Figure 2.3 Schematic of atomic force microscopy.

2.3.5 Scanning Electron Microscopy (SEM)

A drop of the sample was placed upon a conductive carbon substrate (12mm diameter Carbon Adhesive Tabs from Electron Microscopy Sciences) on top of an aluminum stub and air dried. The air dried samples were then sputter coated with a gold/palladium mixture under vacuum in an Edwards S150 sputter coater before viewing. The specimen was examined on a Cambridge Steroscan 260 Scanning Electron microscope.

2.3.6 Theory of SEM

Scanning electron microscopy was developed in the early 1950s. It uses electrons, instead of light (in the case of optical microscopy), to create an image, and it provides a greater depth of focus as a result.[7] It also is able to create 3-dimensional images, unlike optical microscopy and transmission electron microscopy. SEM has an electron gun at the top of the microscope that produces an electron beam, usually a Tungsten hairpin filament. This filament is a loop of Tungsten that functions as a cathode as it releases electrons towards the anode when sufficient electrical bias is supplied. The electron beam travels vertically down the column of the

microscope as it passes through an anode, which speeds up the electrons, and a series of electromagnetic lenses that focus and define the beam as it approaches the sample. When the electrons hit the sample, backscattered and secondary electrons are produced. Backscattered electrons are a result of the electron beam interacting with the nucleus of the atom. These electrons will circle the nucleus, where they pick up speed due to the positive charge in the nucleus, and head back out of the sample. These electrons are collected in a detector. Secondary electrons, on the other hand, are produced as a result of the electron beam interacting with electrons in the atom. Since the electrons in the atom have a negative charge, the electrons that have entered the specimen are slowed down as it repels the specimen electrons. The electrons in the specimen are forced out of the atom and exit the sample. Since they are moving slowly, the detector collecting secondary electrons must have a positive charge. The detectors collect both backscattered and secondary electrons and translate them into a signal that can be viewed as an image.

2.3.7 Energy Dispersive Spectroscopy (EDS)

A drop of the sample was placed on a copper planchette and air dried. The sample was them viewed with a JEOL 2010 High-resolution Transmission Electron Microscope (HRTEM) attached with an EDAX EDS x-ray analysis for composition analysis.

2.3.8 Theory of EDS

Energy dispersive spectroscopy is a non-destructive analytical tool. It is able to give quantitative composition information without the introduction of standards into the specimen because x-ray fluorescence wavelengths and fluorescence yields from the calibrated electron beam are well-known.[8] EDS allows scans as small as 0.5 microns in size and has minimum detection limits varying from 0.1 weight % to a few weight %. Elements with atomic numbers

ranging from Boron (Z=5) to Uranium (Z=92) can be detected using this technique. When an electron beam interacts with the sample, if the electrons are of sufficiently high energy to ionize are at least promote an atom's *K* electron to an *L*, *M*, *N* edge, or and *L* electron to an *M*, *N*, edge, and so forth, x-rays are produced as the higher-shell electrons cascade down towards the vacancy. The x-rays are collected by a high-resolution detector, usually a SiLi crystal (a Silicon crystal doped with small amounts of Lithium). X-rays that are emitted from the sample atoms are characteristic in energy and hence wavelength to the element of that atom and also give information on which shells lost electrons and which shell has replaced them.

2.4 References

1. McCrone, W. C.; McCrone, L. B.; Delly, J. G. *Polarized Light Microscopy;* McCrone Research Institute: Chicago, 1984.

2. Ross, K. F. A. *Phase Contrast and Interference Microscopy for Cell Biologists;* St. Martin's Press: New York, 1967.

3. Binnig, G.; Gerber, C.; Stoll, E.; Albrecht, T. R.; Quate, C. F. Atomic resolution with atomic force microscope. *Europhysics Letters* **1987,** *3* (12), 1281-1286.

4. Binnig, G.; Quate, C. F.; Gerber, C. Atomic force microscope. *Physical Review Letters* **1986,** *56*, 930-933.

5. Ricci, D.; Braga, P. C. How the Atomic Force Microscope Works. In *Methods in Molecular Biology*, Humana Press Inc.: Totowa, New Jersey, 2004; pp 3-12.

6. Ricci, D.; Braga, P. C. Imaging Methods in Atomic Force MIcroscopy. In *Methods in Molecular Biology*, Ricci, D., Braga, P. C., Eds.; Humana Press Inc.: Totowa, New Jersey, 2004; pp 13-23.

7. Black, T. J. The Scanninge Electron Microscope: Operating Principles. In *Principles and Techniques of Scanning Electron Microscopy*, Hyat, M. A., Ed.; Van Nostrand Reinhold Company: New York, New York, 1974; pp 1-43.

8. Russ, J. C. *Fundamentals of energy dispersive x-ray analysis;* Butterworths: Boston, 1984.

Chapter 3

A New Tubule Formation Intermediate: The Tubelet*

3.1 Introduction

Optical microscopy presents some powerful advantages: 1) temperature control is easily done; 2) the specimen need not be desiccated; and, 3) the microscope observation can be videotaped, enabling "real-time" studies of tubule formation. But, tubule sizes are not ideal for optical microscopy studies. Even with a 100× objective and a 10× eyepiece, the highest power elements available, the tubules' helical substructure is generally very difficult to resolve. Also, at these high magnifications, the focal plane (i.e., depth of view) is very narrow (≈0.1 μm), making observation of the whole tubule difficult. Because optical microscopy, as practiced here, is a transmission-mode probe, the specimen must be sufficiently transparent, e.g., thin enough for light to be transmitted through it; and in our particular case, the tubule suspension must be sufficiently dilute so that isolated tubules can be observed. So, while optical microscopy has provided some of our most dramatic observations – most especially "real-time" tubule formation -- optical microscopy was in fact generally limited to confirming the presence of tubules and cones in DC(8,9)PC/lysozyme mixtures in specimens destined for AFM or electron microscopy study, because the features of interest require these higher magnifications to characterize.

We are going to focus our attention now on the protein-containing specimens described in section 1.2.2.[1] As droplets of the protein-containing suspension deposited on electron microscopy carbon substrates air dried over a period of a few hours, a waxy deposition bed formed as the saturated solution containing the tubules evaporated.[2] Upon further drying, this

---

waxy deposition bed cracked, forming a pattern reminiscent of a desiccated lakebed. We surmise that the mixture of tubules, cones, tubelet ribbons and protein (undoubtedly a random coil at our ethanol concentrations) initially form a gel, which, as drying continues, fractures, creating the surface seen in Figure 3.1. Under identical conditions, protein-free specimens, which are known to be free of cones and ribbons, stay completely smooth and do not crack upon drying.

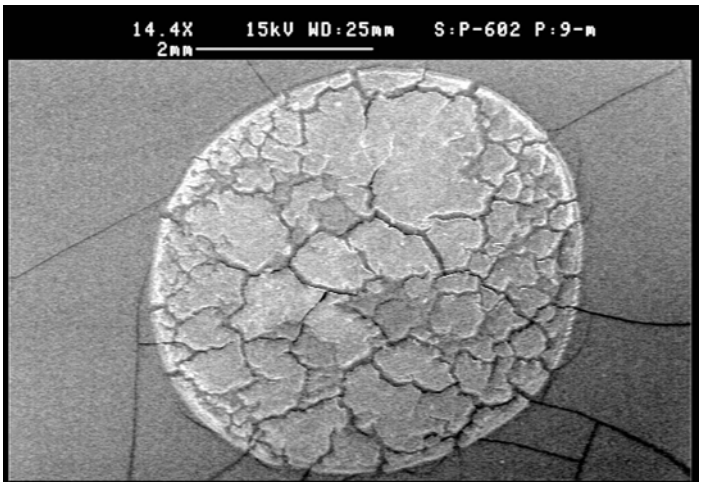

Figure 3.1 A low-magnification scanning electron micrograph of an air-dried deposition bed of DC(8,9)PC-lysozyme specimen subjected to the tubule/cone formation process, showing extensive cracking of the deposition bed. The scale bar is 2mm. Reprinted with permission from reference 2, Copyright (2005) *American Chemical Society.*

The vertical surfaces exposed in these cracks are, in many ways, similar to those revealed by freeze-fracture processes, except that this process is gentler, and because the exposed crack faces are vertical (or nearly so), they present the great benefit of conserving orientational information with respect to the bulk specimen. That is, the interior exposed by this process is *not* randomly selected, as it would be with conventional freeze-fracture techniques, but rather, it

allows us to examine assembly products as a function of depth from the deposition bed surface. This remarkable, wholly unexpected behavior enables examination, in detail, far greater than conventional freeze-fracture allows, a previously-unknown structure that we call the "tubelet". The extent of detail that can be observed is seen clearly in Figure 3.2, in which tubelets are seen to extend from the deposition bed into free space, freeing the object from interfering background, e.g., overlapping nearby structures and dried bulk solution. Since the object projects into space, the electron microscopy stage can be rotated and/or translated in order to obtain very high-contrast images from a single tubelet from several viewpoints.

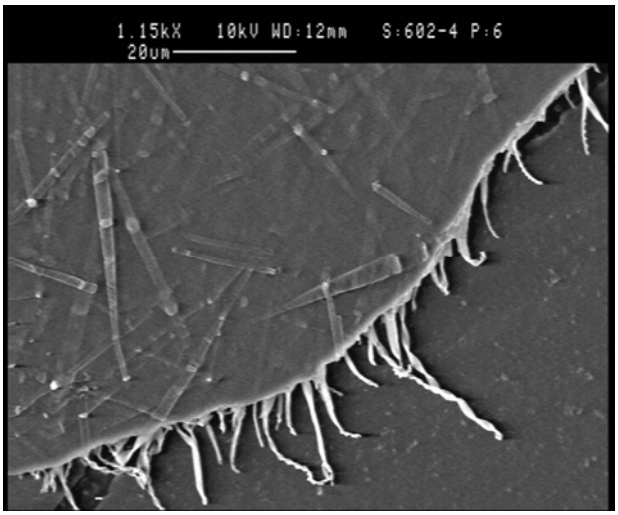

Figure 3.2 Scanning electron micrograph of a protein-bearing deposition bed crack discontinuity. Cones are evident on the unbroken bed face, but tubelets are only resolvable when they emerge at the crack discontinuity. Reprinted with permission from reference 2, Copyright (2005) *American Chemical Society.*

Figure 3.2 shows tubelets to be structures similar to a flattened fire hose that can twist about its long axis, wind helically about this axis, or remain flattened. The topological differences between a phospholipid bilayer ribbon and the nearly edge-free tubelet are

immediately recognizable: The "fire hose" tubelet structure addresses the solvation energetics problems that exist with the flat bilayer ribbon by virtue of nearly eliminating ribbon edge-associated energy costs, except of course, at the flattened tubes' ends. (Of course, the membrane bending energy at the flattened ribbon's edges cannot be ignored, but as will be discussed later, these sharply-curved features may be a consequence of membrane chiralization, and actually represent a lower energy state than the unflattened cylinder.) Tubelet structure also explains the conservation of interlamellar spacing observed over a wide range of tubule compositions and diameters - - no matter how you twist or wind a tubelet, its intrinsic interlamellar spacing will be detected by x-ray diffraction.[1,3,4] Indeed, SAXS and AFM results show that without exception tubule walls have thicknesses that are multiples of two DC(8,9)PC bilayers, which is most easily interpreted as a consequence of tubelet structure, as suggested in Figure 3.3.

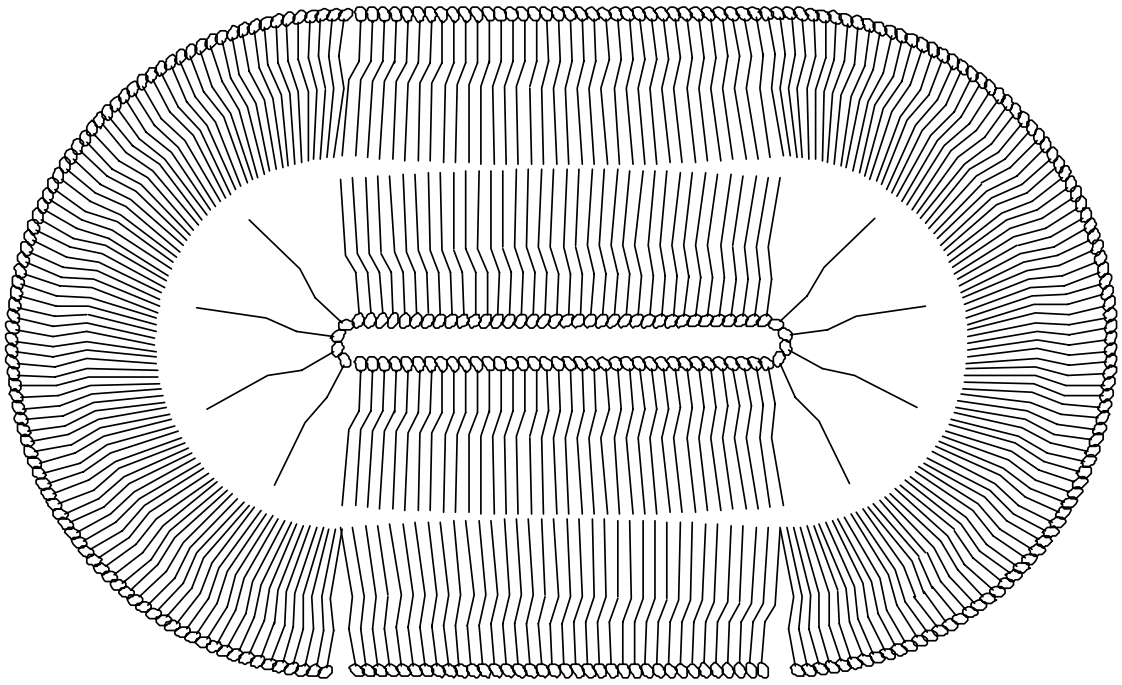

Figure 3.3 Cross-section of proposed tubelet structure. Note that it has a height of two bilayers, twice that of a simple bilayer. For clarity, each tail drawn actually represents two tails of the phospholipid.

Renditions of 3-dimensional objects in two dimensions can lead to gross exaggerations, e.g. "flat" representations of the earth all contain significant distortions. In this way, this Figure 3.3 dramatically over-emphasizes the packing defects that *must* occur at the tubelet's edges; we expect that molecules in the vicinities of the creases would tilt out of the plane and fill this space effectively. The principal idea of Figure 3.3 is to show the repeating vertical distance – created by the phospholipid multilayer – that would be consistent whether this fundamental building block were wound, twisted or remained flat.

3.2 Deposition Bed

Examination of the dried deposition bed shows it to be vertically stratified with ribbon-like structures appearing out of the crack face at some depth from the surface (~1 μm), seen in Figure 3.4. The lysozyme/tubule mixture forms an entangled fluid network whose structure is a consequence of gravity, electrostatic charge, and surface tension, and we surmise the cracking process that exposed the deposition bulk interior was gentle enough to not disturb this stratification. That is, the solvent evaporates slowly, causing the sample to form a gel, locking these components at their equilibrium electrostatic positions. As the evaporation continues, the gel steadily desiccates, decreasing the volume of the deposition bed and forming deep cracks perpendicular to the surface. The ribbons are usually pulled ~ 20 μm from the crack before breaking. It is apparent from the length and alignment of the ribbon-like structures that the contraction and splitting of the bed is a gentle process. These observations are coherent with accounts of sol-gel processes where the stratification is distinguished by electrostatic charge separation energy minimization.[5] Our studies suggest that stratification places tubules and cones only at the air/liquid surface of the deposition bed; they are not found at any distance away from the surface.

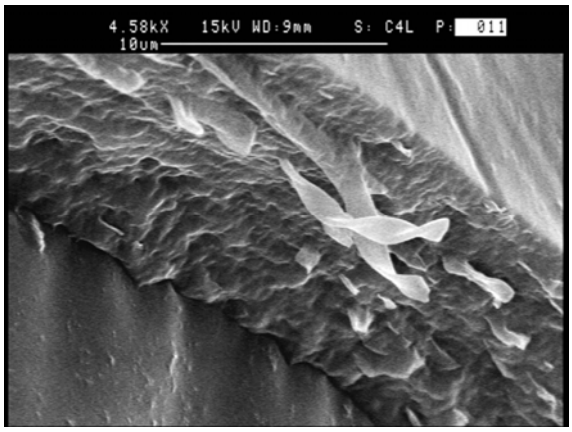

Figure 3.4 Scanning electron micrograph "edge-on" view of a DC(8,9)PC-lysozyme deposition bed crack, showing stratification and broken ribbon-like structures projecting into free space. Reprinted with permission from reference 2, Copyright (2005) *American Chemical Society.*

Since tubules and cones appear to be restricted to the bed surface, and tubelets are only observed within the deposition bed, surface characterization techniques such as SEM and AFM are unable to detect these tubelets under normal conditions. Tubelets also can not be distinguished by TEM; at the lipid concentrations required for these studies (and those resulting from air-drying required for TEM) tubelets simply cannot be differentiated in the tangled mass of self-assembled structures composing the gel. On rare occasion a flat, untwisted tubelet is located at the air/deposition cake surface and can be seen by surface probes, but until now, such structures were interpreted as partially submerged tubules. *For these reasons, the tubelet, which we interpret to be the principal tubule and cone precursor, remained unobserved until these experiments were conducted.*

3.3 Tubelets

We emphasize that the contrast between vacuum and the crack surface allow highly detailed examination of the deposition bed structure normal to the substrate surface, and

especially of tubelets projecting from the crack. Tubelets usually extend ~ 20 microns from the crack, but there are regions ranging from sub micrometer lengths to tubelets that emerge from one crack face, extend for over 100 μm until reentering the opposite crack face. Tubelets within a region are approximately the same length due to the environment within that region.

The cracks are not of uniform width along their length, and presumably did not widen at a uniform rate (or even time) throughout the deposition cake. Areas are observed where crack separation occurred rapidly, leaving only short tubelets projecting from the crack face, while in other areas, 100 μm long tubules are seen to emerge from one crack face and enter the opposing face; it is possible that such cracks widen slowly enough for "slippage" to occur as the tubule emerged from the drying gel.

It is difficult to determine tubelet total length, since at least one tubelet end is buried in the deposition bed. Tubelets entering the deposition bed close to the surface can be observed up to 30 μm in length using SEM before the tubelet becomes hidden. This gives a total observation length of approximately 50 μm and is consistent with the tubelets lengths on the order of 100 microns, which is expected for tubule formation.

Tubelets are always flattened in a (1) cylindrically wound state, type "A" curvature (termed by Oda et al.),[6] (2) axially twisted state, type "B" curvature, or an (3) untwisted, unwound state, although these are rarely seen, at least under our observation conditions.

3.3.1 Cylindrically Wound Tubelets

Although type "B" tubelets prevail, cylindrically wound type "A" tubelets are also observed winding like that of a ribbon to form a cylindrical structure seen in Figure 3.5. This type "A" formation is a precursor to tubule formation.

3.3.2 Axially Twisted Tubelets

The axially twisted tubelets, type "B", wind about the long axis of the fine structure shown in Figure 3.5. Under these conditions, this type "B" structure is most often seen.

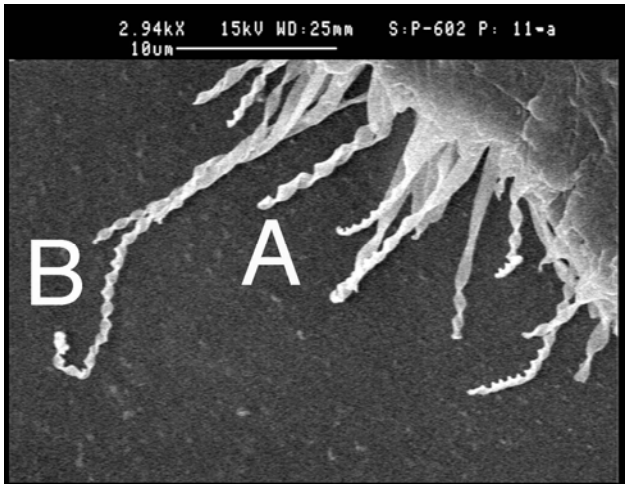

Figure 3.5 Scanning electron micrograph view of a crack face discontinuity from which structures possessing types of "A" and "B" windings are seen to project. Reprinted with permission from reference 2, Copyright (2005) *American Chemical Society.*

3.3.3 Flat Tubelets

Both wound and twisted tubelets have flat regions where they emerge from the crack, this may be due to the stretching that occurs when the material dries and the crack faces separate. Although very rare, there are areas where flat tubelets can be observed. Flat tubelets are often found in groups, as in Figure 3.6, which suggests the consistency of formation conditions at the time of separation (it is possible that the tubelets had not yet chiralized at the time of crack separation).

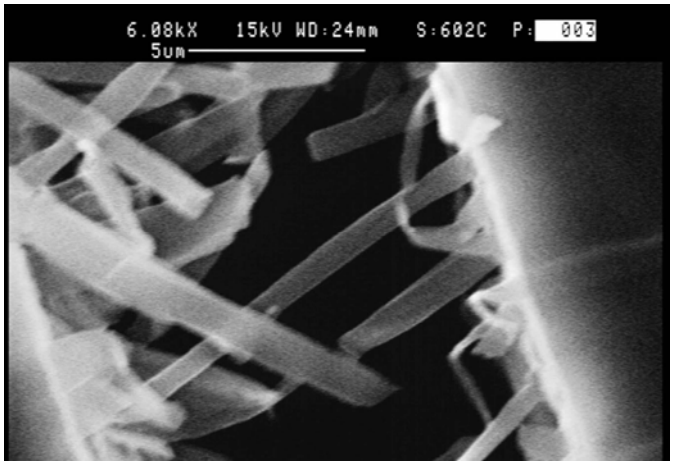

Figure 3.6 Scanning electron micrograph of unwound tubelets at a narrow crack interface. Reprinted with permission from reference 2, Copyright (2005) *American Chemical Society.*

3.3.4 Other Regions

Transitions between axial, cylindrical, and flat regions are frequently detected, as seen in Figure 3.7. The winding or twisting can change at flat/"A", flat/"B", or "A"/"B" connections. Another transition can be seen in Figure 3.7, where there is a kink in "B"/"B" and it is possible at these kinks for the twisting pattern to reverse. The cylindrical curvature and axially twisted phenomenon mentioned above has been observed in an unrelated gemini surfactant system.[6] (The cylindrical curvature is seen to form helical ribbons, while the twisted tubelets exhibit "Gaussian" curvature.) By studying charged gemini surfactants, the determination was made that long chain surfactants favor helical ribbons while short-chain surfactants favor twisted ribbons. The authors also developed a theory that for membranes in a fluid phase, a twisted ribbon has the lowest free energy, and that crystalline order is not compatible with this Gaussian curvature,[7] and that a helically-wound ribbon must be stabilized by crystalline order. Therefore,

they believe that twisted ribbons and helical ribbons result from fluid membranes and crystalline membranes, respectively.

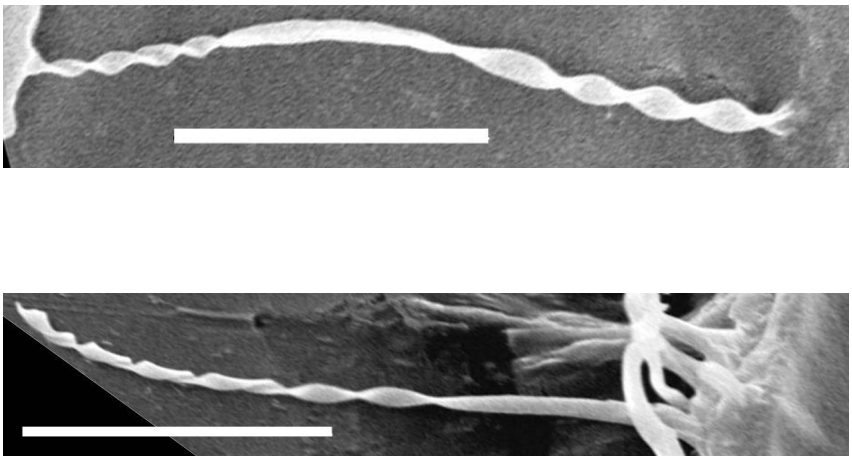

Figure 3.7 Scanning electron micrographs. (Top): A tubelet that emerges from a crack face with a right-handed type "B" winding, changes to flat configuration at its center, and resumes a right-handed type "B" winding before emerging at the opposing crack face discontinuity, (Bottom): A tubelet that undergoes a continuous transition from a type "A" winding at its left, to a type "B" winding at its center, and finally to a flat state as it enters the crack discontinuity. Both scale bars are 10 μm. Reprinted with permission from reference 2, Copyright (2005) *American Chemical Society.*

3.4 Tubelets as a Precursor

When tubules were first observed, deGennes suggested that they form as a result of a flat bilayer that winds to form tubules because of a ferroelectric charge separation resulting in the leading and trailing ribbon edges possessing slight amounts of opposing charge.[8] This theory was disproven by salt-screening experiments intended to interfere with this self-assembly mechanism.[9] Close examination of Figure 3.8 shows a topologically much more complicated structure - tubelets are not flat, but are actually hollow flattened tubes that wind up to form hollow cylindrical tubules.

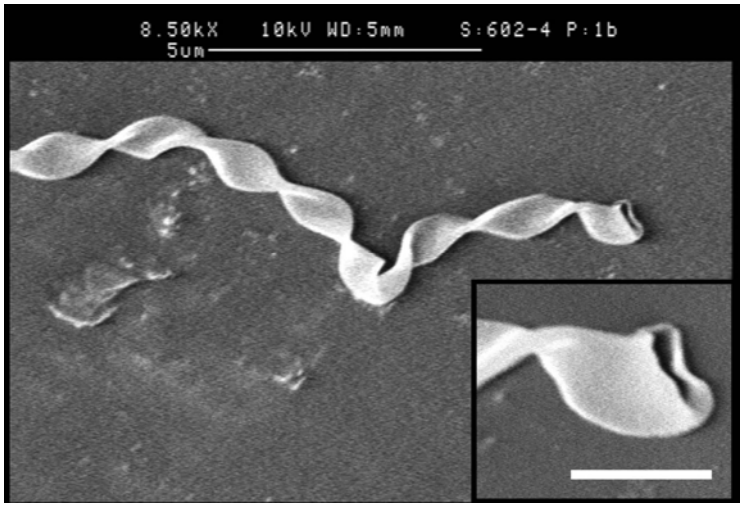

Figure 3.8 Scanning electron micrograph of an axially-twisted (type "B") tubelet, with characteristic 3 μm twist periodicity and a 90 degree kink where axial twist handedness sometimes, but not always, changes chiral sense. (This structure's left-handed twist does not change chiral sense at this junction.) (Inset): Magnification of the hollow tubelet's right end. The scale bar is 1 μm. Reprinted with permission from reference 2, Copyright (2005) *American Chemical Society.*

Our observations suggest the process shown in Figure 3.9: 1) A continuous hollow bilayer tube, the "tubelet," forms 2) the tubelet flattens spontaneously into either a cylindrical type "A" or axial type "B" curvature, or rarely, with no curvature. Our findings strongly suggest that DC(8,9)PC tubules and DC(8,9)PC/lysozyme cones are a result of the helical winding of these previously-unobserved tubelets. This model explains several of the problematic tubule features.

First, the unfavorable solvation energy along the edges of the ribbon before it winds to form a tubule is minimized. The sharp curvature occurs as a result of the tubelet becoming flattened, and membrane chiralization through spontaneous chiral symmetry breaking may play a significant role in the formation of creases and flattening of the initial, unflattened tubelets. Several papers have discussed the idea that chiral defects *must* form in adequately large chiral

domains.[6,10,11] We conjecture that as tubelets grow, increasing in length and perhaps diameter, such chiral defects occur and result in the twist (configuration "B"), or helical winding (configuration "A"). Our experimental discovery suggests profound re-evaluation of the ribbon edge/tubelet crease contributions to tubule energetics be undertaken.

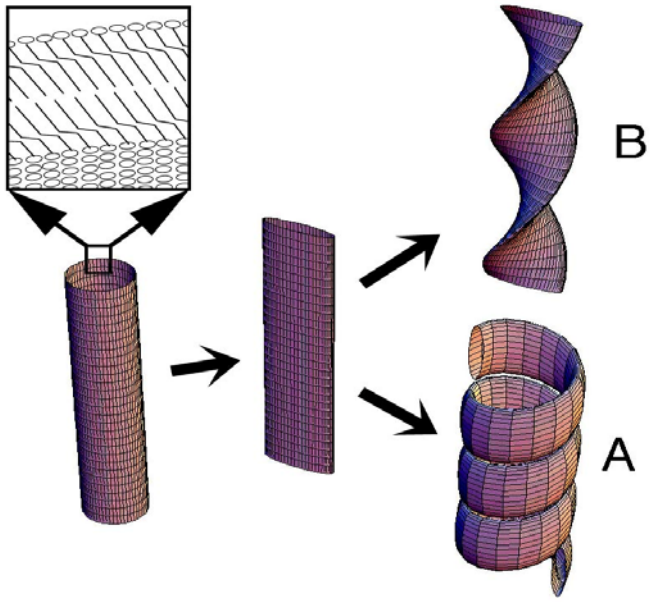

Figure 3.9 The formation of type "B" and "A" curvature structures appears to begin with the formation of the cylindrical tubelet (left), which spontaneously flattens (center). The tubelet occasionally remains flattened but far more likely assumes a type "B" curvature conformation (top right) or a cylindrical "A" curvature (bottom right). The inset drawing indicates the bilayer orientation of the amphiphilic molecules. Reprinted with permission from reference 2, Copyright (2005) *American Chemical Society.*

Second, the persistence of the "barber-pole" ridge on the surface of the tubule and the stability of propanol/DC(8,9)PC helices[12] and phosphonate DC(8,9)PC derivative helices[3,4] are made clear by this model. The ridges are not a result of two membranes meeting edge-to-edge

and fusing together but occur as two hydrophilic membranes form a junction. The "open" helices found in propanol/DC(8,9)PC and DC(8,9)PC phosphonate derivatives are thus seen to present hydrophilic headgroups along their edges, instead of exposed hydrocarbon tails under earlier tubule structure models.

A third tubule feature problem that is addressed by the discovery of tubelets is the tightly conserved interlamellar spacing found in tubules of different dimensions, compositions, and symmetry. SAXS and AFM show that phosphonate and DC(8,9)PC tubule walls are either two or four bilayers thick – odd number of bilayers are never observed. This is sensible if the bilayer "ribbon" is actually a collapsed bilayer tube. Using this model, the tubule in Figure 3.5 should have a wall thickness of two bilayers and the tubule wall thickness can be in increments of two bilayers, consistent with the SAXS and AFM determinations.

Are tubelets generated as a result of the introduction of protein into the system and not related to the formation of tubules? That is, does the protein deform existing cylindrical tubules into helically-wound tubelets? While the look and dimensions of the type "A" helical winding tubelet seen in Figure 3.5 and the bottom of Figure 3.7 provide a strong case for tubelets being a tubule precursor, they have only been detected in specimens containing protein. Nonetheless, we contend that tubelets are indeed tubule predecessors in protein free systems but can not be seen by SEM and TEM.

SEM and TEM investigation of the smooth regions of specimen containing protein reveal the coexistence of cones and tubules (seen in Figure 3.2), but neither technique detects tubelets in these uncracked regions. However, the crack of Figure 3.2 shows tubelets are there in large quantity. It appears SEM is unsuccessful in finding tubelets in the smooth regions because they are sufficiently far below the deposition bed surface to be detectable. On the other hand, TEM is

unable to resolve tubelets because of the closely packed structures within the ~ 12 μm deposition bed depth. At the protein-bearing specimen's deposition bed cracks, tubelets are seen in remarkable detail over large distances when they project from the crack face because there is no background obstruction of the specimen. These structures can only be found at distances of ~1 μm below the deposition bed surface. We believe that tubelets are also present in protein-free specimens, but are not detectable because they are within the specimen's interiors, and protein-free specimens do not crack to expose the inside of the deposition bed. If protein-free systems would form cracks, the beds' internal organization and intricate structures could be compared. Vertical slices made into these specimens with a razor blade do not reveal tubelet structures, however, the enormous artifacts that slicing makes in the sample, renders them completely uninterpretable. Extended efforts using conventional freeze-fracture techniques also failed to reveal these structures, in part because of the loss of orientational information, but largely due to the very limited sizes of regions that freeze-fracture would expose.

There similarities of cone and tubule structure seen not only in optical video microscopy but in SEM and SAXS studies of their internal structures strengthen the argument that cylinders and cones are more alike than dissimilar. The helical ridges on the both structures' exteriors, the remarkable conservation of interlamellar spacing, and the tubule wall thicknesses (always consisting of multiples of two bilayers) suggest strongly that tubule and cones are different manifestations of the tubelet precursor.

3.5 Conclusions

The interactions of gravity, electrostatic charge, and surface tension cause the structure of entangled protein-fortified fluid matrix to gel, crack, and expose the interior structure of the bulk droplet, revealing a previously-unobserved structure, the "tubelet". These tubelets appear to be

tubule precursors in protein-free systems and of tubules and cones in systems containing protein. The tubelet-as-precursor structure explains several important tubule characteristics and may signify a major shift in our understanding of their structure and how they form. The possibility of using tubules in applications such as biomedical encapsulation should be reassessed as well: rather than offering a simple 0.5 μm cylinder, from which encapsulated drugs would be expected to diffuse from so rapidly as to make the encapsulation pointless, tubules should now be regarded as a secondary winding of a smaller tube that may provide longer encapsulant retention times that are significantly longer than what would be expected from a simple hollow cylinder.

3.6 References

1. Mishra, B. K.; Thomas, B. N. Phospholipid/Protein Cones. *Journal of the American Chemical Society* **2002,** *124* (24), 6866-6871.

2. Mishra, B. K.; Garrett, C. C.; Thomas, B. N. Phospholipid Tubelets. *Journal of the American Chemical Society* **2005,** *127* (12), 4254-4259.

3. Thomas, B. N.; Corcoran, R. C.; Cotant, C. L.; Lindemann, C. M.; Kirsch, J. E.; Persichini, P. J. Phosphonate Lipid Tubules. 1. *Journal of the American Chemical Society* **1998,** *120* (47), 12178-12186.

4. Thomas, B. N.; Lindemann, C. M.; Corcoran, R. C.; Cotant, C. L.; Kirsch, J. E.; Persichini, P. J. Phosphonate Lipid Tubules II. *Journal of the American Chemical Society* **2002,** *124* (7), 1227-1233.

5. Ichinose, I.; Kuroiwa, K.; Lvov, Y.; Kunitake, T. Recent progress in the surface sol-gel process and protein multilayers. *Multilayer Thin Films* **2003,** 155-175.

6. Oda, R.; Huc, I.; Schmutz, M.; Candau, S. J.; MacKintosh, F. C. Tuning bilayer twist using chiral counterions. *Nature* **1999,** *399* (6736), 566-569.

7. Nelson, D. R.; Peliti, L. Fluctuations in membranes with crystalline and hexatic order. *Journal de Physique (Paris)* **1987,** *48* (7), 1085-1092.

8. Ambegaokar, V.; De Gennes, P. G.; Seguin-Tremblay, A. M. Antiferromagnetism and crystal field effects in superconducting copper oxides. *Comptes Rendus de l'Academie des Sciences, Serie II: Mecanique, Physique, Chimie, Sciences de la Terre et de l'Univers* **1987,** *305* (9), 757-760.

9. Zastavker, Y., V; Asherie, N.; Lomakin, A.; Pande, J.; Donovan, J. M.; Schnur, J. M.; Benedek, G. B. Self-assembly of helical ribbons. *Proc Natl Acad Sci U S A* **1999,** *96* (14), 7883-7887.

10. Kamien, R. D.; Selinger, J. V. Order and frustration in chiral liquid crystals. *Journal of Physics: Condensed Matter* **2001,** *13* (3), R1-R22.

11. Selinger, J. V.; MacKintosh, F. C.; Schnur, J. M. Theory of cylindrical tubules and helical ribbons of chiral lipid membranes. *Physical Review E: Statistical Physics, Plasmas, Fluids, and Related Interdisciplinary Topics* **1996,** *53* (4-B), 3804-3818.

12. Georger, J. H.; Singh, A.; Price, R. R.; Schnur, J. M.; Yager, P.; Schoen, P. E. Helical and tubular microstructures formed by polymerizable phosphatidylcholines. *Journal of the American Chemical Society* **1987,** *109* (20), 6169-6175.

Chapter 4

Encapsulation Studies with Chemotherapy Agents

4.1 Introduction

To determine whether or not tubules can be used as vehicles for medicines, it is first necessary to see whether or not they can even form in the presence of the drugs. This can be done in a straightforward fashion by optical microscopy, atomic force microscopy (AFM), and scanning electron microscopy (SEM). These probes will also allow us to see if structure of the tubule is the changed by the drugs.

If tubule formation persists in the presence of drugs, it must be in at least one of three places. The drug can stay in the bulk of solution, in the solution contained in the hollow tubule or tubelet composing the tubule, or become integrated into the tubule membrane. So long as either possibility (2) or (3) occurs, water-soluble and water-insoluble drugs can be considered for encapsulation: Water-soluble drugs will be encapsulated in the solution within the tubelet, or inside the larger tubule cavity, while water-insoluble drugs will partition within the membrane, i.e., with the hydrophobic tails of the phospholipid. AFM experiments will determine the effects that the drug has on tubule morphology, while energy dispersive spectroscopy (EDS EDAX) can help determine the location of the drug.

Tubule dimensions allow them to be aerosolized.[1] This property, along with the presumed biocompatibility of phospholipids with tissue membranes, suggests strongly that tubules can serve as benign drug carriers and be used in aerosol therapies. Aerosol therapy has two evident applications: medicines can be inhaled for application to respiratory tract tissue for treatment of asthma, epithelial cancer, or other illnesses of the lung. Interestingly, control of tubule diameter alone would permit regulation of their effective aerodynamic diameter, which in

turn would permit drug delivery to a specified distance along the respiratory tract.[2] Medicines can also be introduced into the circulatory system by inhalation for target sites outside of the lung. This delivery mode may enhance the efficacy of the medicine, for blood from the lungs is dispersed throughout the body before passing through the liver, where many drugs are processed for excretion. Not only could it enhance the efficacy, it could provide an alternative route for drug delivery of chemotherapy agents, which are currently administered intravenously. As cancer research is of very high interest, this can open many doors for these types of drugs.

Chemotherapy drugs are used to kill rapidly growing cancer cells. But, these drugs also kill healthy, rapidly growing cells such as stomach lining cells, red blood cells, platelets, and white blood cells. Being able to deliver the drug in a fashion that would minimize exposure to those tissues while targeting the cancer cells could prove more beneficial to treatment, as well as minimize the side effects. Although most chemotherapy drugs are delivered though an IV, some forms of chemo are delivered orally. If tubules can be used to encapsulate chemotherapy drugs, it may be possible to deliver these drugs though an inhaler. This could be a useful way to deliver any chemotherapy drug, if an adequate quantity can be delivered to the body. For the specific application of lung cancer, however, massive doses of the toxic drug can be delivered locally to the cancerous lesions, and because the dose is delivered to the desired point of action, the dose to the body overall can be quite small, sparing the stomach lining, blood cells, etc. By changing tubule diameter, we can manipulate the effective aerodynamic diameter of the tubule allowing us to determine which part of the lung the drug filled tubule would travel.[2] The larger the tubule diameter, the larger the aerodynamic radius, and the further down the bronchial tubes the tubule will travel. In this way, concentrating the toxic chemotherapeutic agents at the desired point can permit larger doses at the cancerous site and lower doses to the body *in toto*.

Another potential medical use does not involve aerosolization, but rather, direct implantation into the body, e.g., via subcutaneous injection. The anticipated advantage of this technique would be the slow release of encapsulated drugs directly "upstream" from the tumor, inflamed joint, etc., from which the tubules have been implanted. The slow, "point" source release could potentially deliver would be particularly promising for a number of the drugs. One should also consider that this "point" specificity may not matter for some drugs, but that tubules' potential long release time could nevertheless provide a substantial benefit, e.g., the continuous release of growth hormone over a period of weeks or even months.

4.2 Methotrexate Studies

Methotrexate (MTX), N-[4-[[(2,4-diamino-6-pteridinyl)methyl]-methylamino]benzoyl]-L-glutamic acid, whose chemical structure is shown in Figure 4.1, is used as a treatment for breast and lung cancers and autoimmune diseases, such as Crohn's disease and rheumatoid arthritis.[3] MTX is an antimetabolite; it is similar enough in structure to participate in normal biochemical reactions but different enough to interfere with normal division and function of cells. This is due to the fact that MTX is a folic acid analogue.[4,5] In 1947, aminopterin was synthesized by changing the 4-oxo moiety of folic acid to 4-NH_2.[6] This slight change in the folic acid caused the vitamin to become very toxic by the body's inability to differentiate it from the essential folic acid. It was used successfully in childhood leukemia but its toxicity inspired development of its 10-methyl congener, MTX, in the 1950s.[5] Since it also is a folic acid analogue, it is able to inhibit enzymatic pathways for biosynthesis of nucleic acids by substituting for folic acid. This inhibition interferes with the production and maintenance of DNA, allowing MTX to be used as a chemotherapy agent.[7] It is a yellow fluid that can be administered intravenously, through a central line, or into a PICC line or given as an IV drip.[3] It

can also be injected into the muscle, artery, or fluid surrounding the spinal cord. It can also be administered orally, if taken with plenty of water. The side effects include loss of blood cells, diarrhea, tiredness, sore mouth and taste change, skin changes, inflammation of the cornea, blurred vision, hair loss, sensitivity to sun, changes to lung tissue, and kidney and liver damage.[3] Delivery of this potent drug to the desired point of action could minimize these serious side effects.

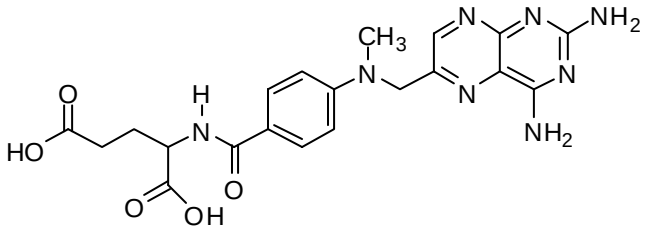

Figure 4.1 Chemical structure of methotrexate.

A sample was prepared by adding methotrexate to the standard 1 mg lipid / ml stock solution, where the percentage of drug in the sample was very high, 28 weight%. The sample was subjected to the canonical DC(8,9)PC tubule formation process, that is, heating to 45^{o}C, where, as with pure DC(8,9)PC specimens, the solution became clear. The sample was then allowed to cool slowly back to room temperature where it became a cloudy yellow solution, indicating that tubules had formed. Optical microscopy was performed in order to confirm the presence of tubules. At this very high drug concentration, the number of tubules seen is significantly lower than in the pure DC(8,9)PC sample, but it was somewhat surprising to find that tubules form at all at such high MTX concentrations. Some new features are introduced in this specimen, shown in the AFM shown in Figure 4.2. The image shows some branch-like structures (resembling crystallization) and some very high structures that look like clumps

(possibly the drug's effect on the lipid, or the drug itself) around the tubules that have not been observed previously. Control experiments performed with MTX do not exhibit these features either; the AFM scans of MTX under the same conditions (in ethanol/water solution and taken through the thermal cycle), remain featureless. These tall structures make AFM difficult because their height exceeds the ≈ 6 μm height maximum of the AFM, compromising several of the raster scan lines during the AFM scan.

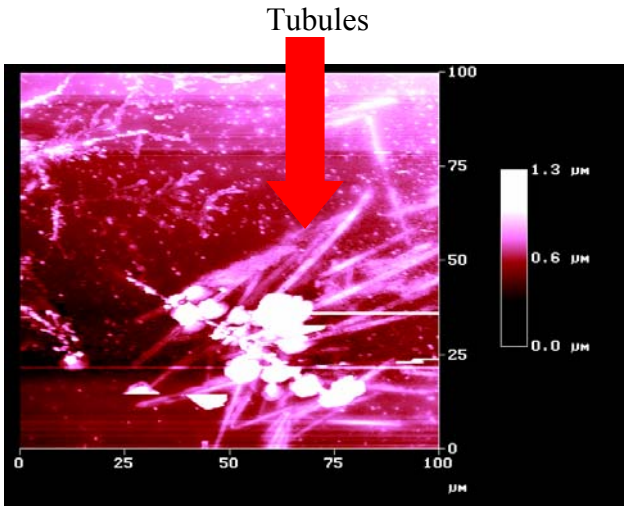

Figure 4.2 100 μm x 100 μm contact mode atomic force micrograph of DC(8,9)PC doped with 28% methotrexate.

It is possible, however to take a closer look at a clean area – one free of these tall structures -- once the large-area scan has been captured by using the zoom feature when working up data. Such an area is shown in Figure 4.3.

Given the positive outcome of tubule formation at this high MTX concentration, other samples were made at lower MTX concentrations to see if the drug's influence – apparent changes in tubule structure and possible MTX co-precipitation - will continue at these lower

MTX concentrations. Methotrexate was added to the lipid stock solution where the percentage of drug was 8%. The sample was taken through the normal tubule formation process and once again showed the presence of tubules by optical microscopy. The AFM of Figure 4.4 shows that tubules are much more plentiful as expected due to the higher relative lipid concentration, but still not as numerous as in pure DC(8,9)PC samples. Their diameter is larger in comparison to that of MTX-free DC(8,9)PC tubules' 0.5 μm diameter, indicating a significant interaction between the drug and lipid has occurred. A closer look at the scan reveals that tubule diameter has increased to about 1.25 μm, seen in Figure 4.5. One possibility is that the drug is filling the inside of the tubule causing it to swell, thus increasing the diameter. Another possibility is that the MTX/lipid membrane interaction has reduced the membrane's intrinsic curvature, resulting in larger-diameter structures. Further studies must be performed to determine the location of methotrexate in the samples and the modified membrane's bending moduli.

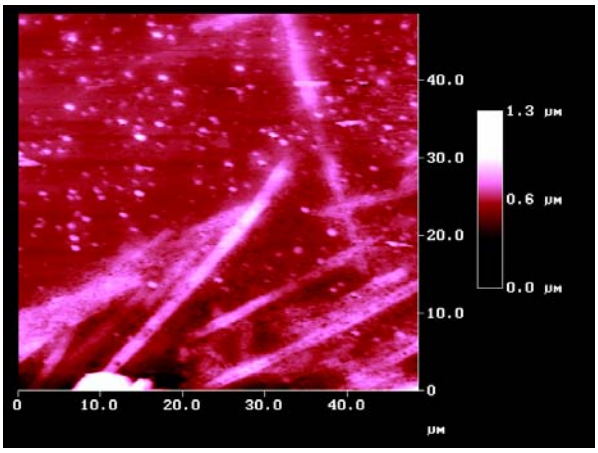

Figure 4.3 50 μm x 50 μm contact mode atomic force micrograph of DC(8,9)PC doped with 28% methotrexate.

A. B.

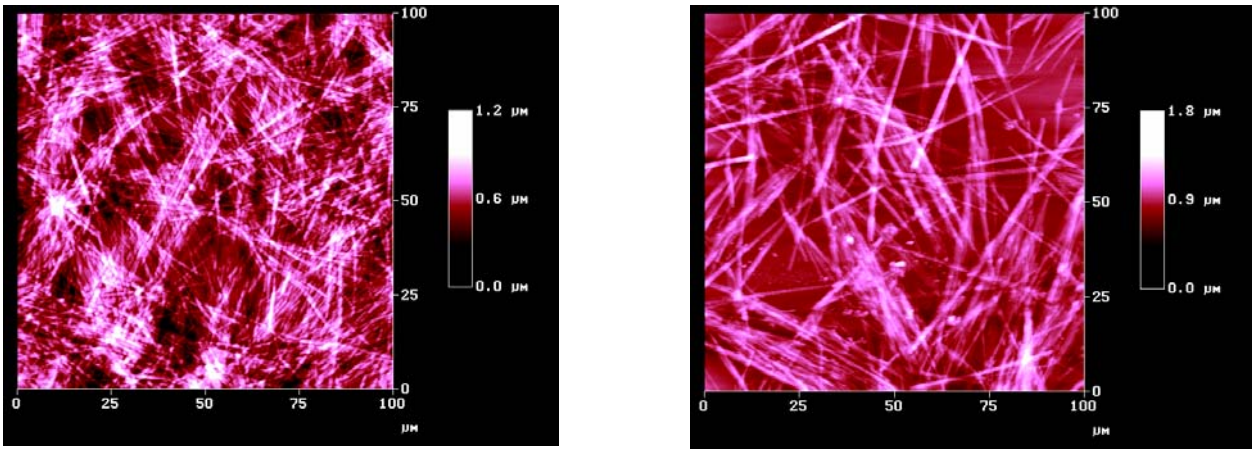

Figure 4.4 100 µm x 100 µm contact mode atomic force micrographs of A. DC(8,9)PC tubules (shown for comparison) and B. DC(8,9)PC tubules doped with 8% methotrexate.

A. B.

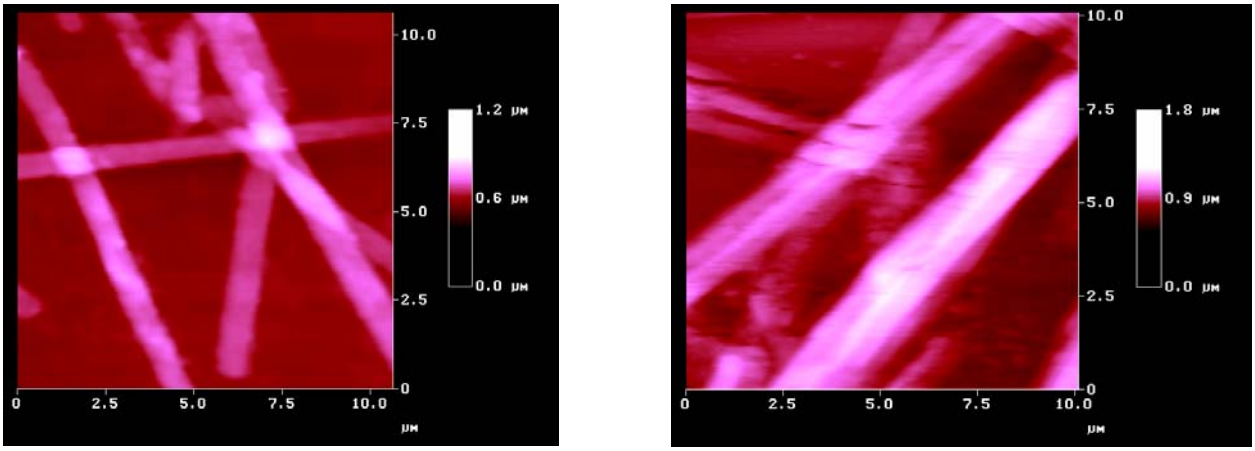

Figure 4.5 10 µm x 10 µm contact mode atomic force micrographs of A. DC(8,9)PC tubules (shown for comparison and B. DC(8,9)PC tubules doped with 8% methotrexate.

4.3 Mitoxantrone Studies

Mitoxantrone, 1,4-dihydroxy-5,8-bis[[2-[(2-hydroxyethyl)amino]ethyl]amino]-9,10-anthracenedione dihydrochloride, shown in Figure 4.6, is another chemotherapy agent used primarily to treat breast cancer, myeloid leukemia, and non-Hodgkin lymphoma.[8] It is also used for treatment of multiple sclerosis (MS).[8] It can not cure MS, but it can lengthen the time between relapses. Mitoxantrone is an antineoplastic or "antitumor antibiotic", which is able to interfere with the growth of cancer cells by blocking an enzyme, topoisomerase II, which is required for cell division.[9,10] When this enzyme is blocked, cells are unable to divide and grow into new cells. Antineoplastics also generate free radicals that damage DNA and cell membranes. Mitoxantrone is a dark blue fluid that can be injected into the vein for 5 to 20 minutes a day for 3 consecutive days or once every 3 weeks.[8] Some of the side effects include changes in liver function, sore mouth, reduction in platelet production leading to bruising or bleeding, anemia, nausea, and weakness.[8]

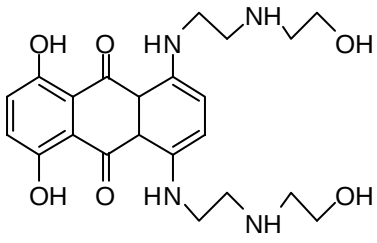

Figure 4.6 Chemical structure of mitoxantrone.

A sample was prepared using mitoxantrone at the very high concentration of 28 weight%. Mitoxantrone was added to the previously-prepared lipid stock solution and heating to 50 ^{o}C, where the solution was a clear dark blue. As the solution cooled back down to room temperature, it was hard to determine if a precipitate had formed due to the darkness of the solution. Optical microscopy and AFM were conducted on the sample, and because tubules were

hard to locate, we conclude that the high concentration of mitoxantrone inhibited, but did not completely prevent tubule formation. Some tubules were present, as seen in Figure 4.7.

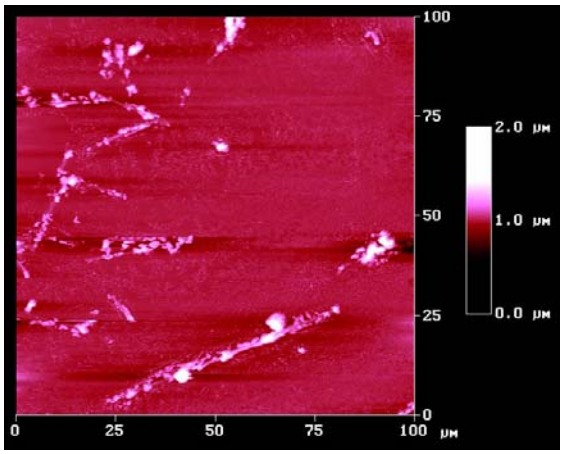

Figure 4.7 100 μm x 100 μm contact mode atomic force micrograph of DC(8,9)PC doped with 28% mitoxantrone.

When the concentration of mitoxantrone was reduced to 8%, tubules were, as with MTX, much more numerous, but again, their number is still not quite as large as that of pure DC(8,9)PC stock solution run through the thermal cycle without addition of mitoxantrone. Again, as in the methotrexate sample seen in Figure 4.2, there is a presence of high structures that interfere with the scan. This again, could be the result of the presence of drug in the sample. Even though, the drug is added at 8%, much lower than the original sample with 28%, it obviously has an effect on tubule morphology. Tubules can definitely form after being doped with mitoxantrone, but their morphology is altered and the number of tubules is significantly lower, as seen in Figure 4.8. A closer look at the tubules formed indicates that their morphology has been altered to yield tubules of much larger diameters, as seen in the isolated tubule of Figure 4.9, showing the dramatic increase in tubule diameter from 0.5 μm to 2.5 μm.

A. B.

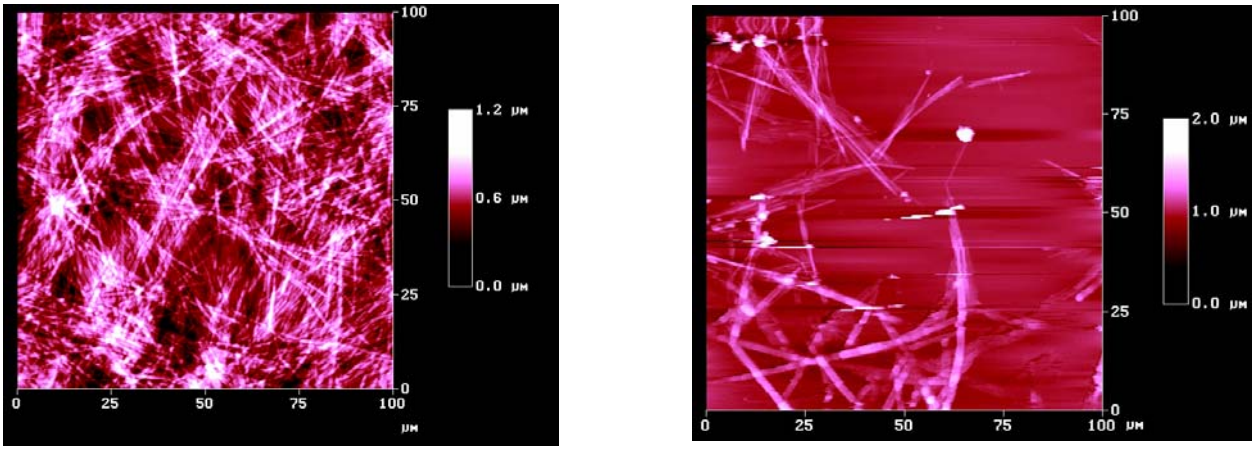

Figure 4.8 100 μm x 100 μm atomic force micrographs of A. DC(8,9)PC tubules (shown for comparison) and B. DC(8,9)PC tubules doped with 8% mitoxantrone.

A. B.

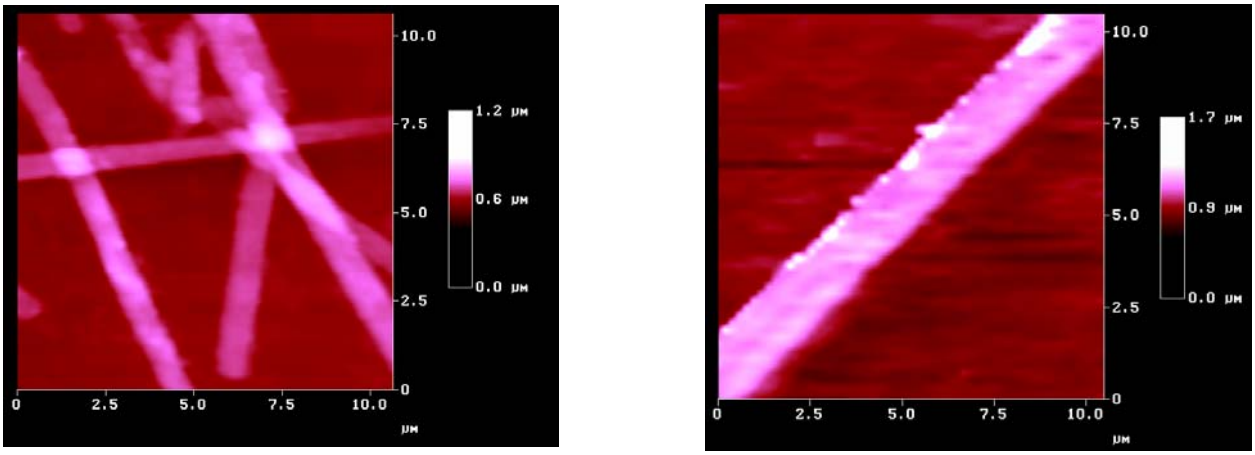

Figure 4.9 10 μm x 10 μm atomic force micrographs of A. DC(8,9)PC tubules (shown for comparison) and B. DC(8,9)PC tubules doped with 8% mitoxantrone.

4.4 Carboplatin Studies

Carboplatin [*cis*-diamine (1, 1-cyclobutane-dicarboxylato) platinum (II)], shown in Figure 4.10, is another chemotherapy drug that is used to treat a wide variety of cancers, including ovarian and lung cancer.[11] Platinum-containing compounds are often used as chemotherapy agents.[12-14] Carboplatin was derived from cisplatin, which was discovered in the 1970s for the treatment of cancer, in an attempt to reduce toxicity.[15,16] It is an alkylating agent, as it transfers alkyl groups to other molecules, and stops tumor growth by cross-linking guanine nucleobases in DNA strands, preventing cell division and leading to eventual cell death.[17-19] It is a clear fluid that is currently administered as an infusion drip into the vein through a cannula, a tube inserted into the vein, or through a central line that is inserted under the skin into a vein near the collar bone.[11] As with most chemotherapy drugs, the side effects are numerous. Some of these include loss of blood cells, nausea, vomiting, diarrhea, fatigue, loss of appetite and taste, changes in hearing, numbness in hands and feet, and loss of hair.[11] Carboplatin also has side effects that may not occur for months or years after the treatment has been stopped. Ironically, one delayed effect is the induction of another cancer, leukemia. These side effects can possibly be minimized if the drug could be administered in another fashion, via an inhaler, or if the drug could be targeted to the site of the cancer via injection, minimizing exposure of the whole body to the drug.

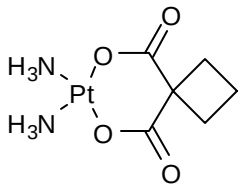

Figure 4.10 Chemical structure of carboplatin.

A sample was prepared by adding carboplatin in to the lipid stock solution, where the percentage of drug in the sample was 28 weight%. The sample was heated to 55 degrees Celsius where the solution became clear. The sample was then allowed to cool slowly back to room temperature where it became a cloudy solution, indicating that tubules had formed, which was confirmed by optical microscopy. At this high drug concentration, AFM results were generally poor because of the presence of tall structures that had been seen in samples where MTX was added. We tentatively conclude, as control studies with carboplatin under these same conditions (in ethanol/water and taken through the thermal cycle) remain relatively featureless, that these tall structures are carboplatin/lipid co-precipitate. There is some evidence of cones in our sample; one gently-tapered structure is shown in Figure 4.11.

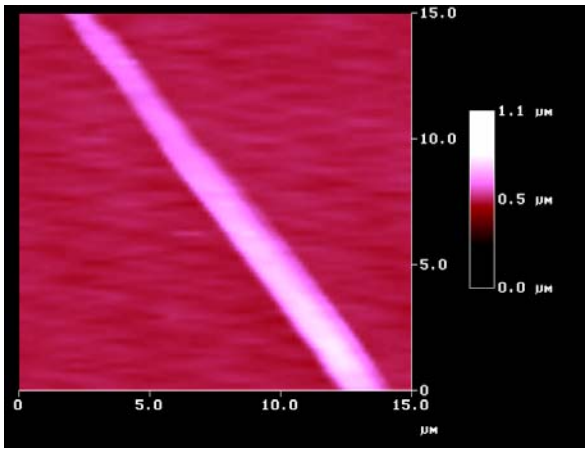

Figure 4.11 15 μm x 15 μm atomic force micrograph of DC(8,9)PC tubules doped with 28% carboplatin. This seems to be cone-shaped.

As with the previous drugs, another sample was again made with carboplatin at a concentration of 8%. As before tubules became much more abundant, and again they had significantly larger diameters than tubules made from drug-free DC(8,9)PC stock solution (as seen in Figure 4.12). A smaller scan area (that is, at higher magnification) shows tubules with a

diameter of approximately 2 μm (see Figure 4.13) much larger of those made from pure DC(8,9)PC.

A. B.

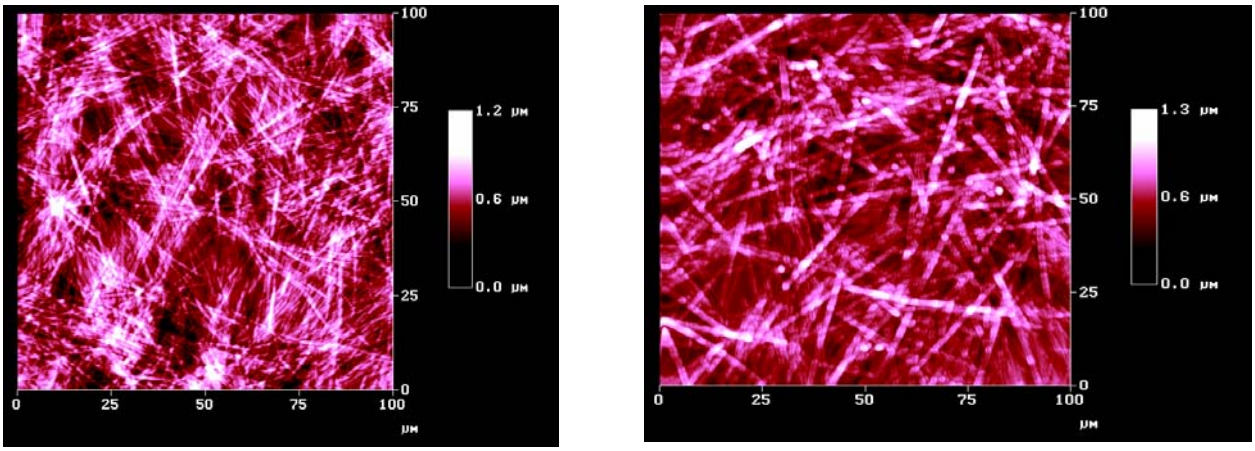

Figure 4.12 100 μm x 100 μm contact mode atomic force micrographs of A. DC(8,9)PC tubules (shown for comparison) and B. DC(8,9)PC tubules doped with 8% carboplatin.

A. B.

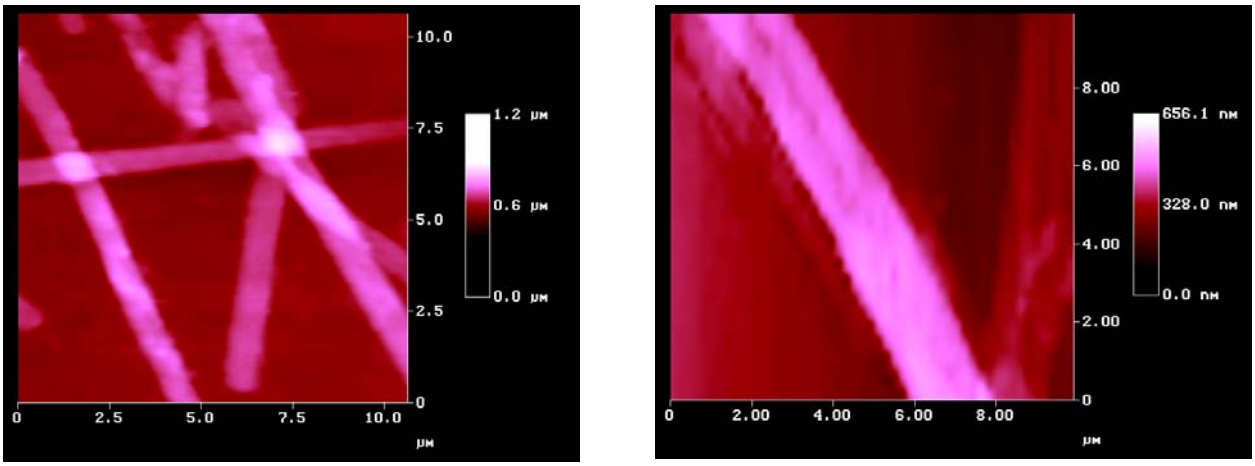

Figure 4.13 10 μm x 10 μm contact mode atomic force micrographs of A. DC(8,9)PC tubules (shown for comparison) and B. DC(8,9)PC tubules doped with 8% carboplatin.

Carboplatin presents an unusual study opportunity because it contains the high-Z element, platinum. Platinum's *K*, *L*, and *M* fluorescence is easily differentiated not only from the carbon, hydrogen, oxygen, nitrogen and phosphorus contained by DC(8,9)PC, but from any metals such as copper, iron, etc. that might compose the electron microscopy grid the specimen lies upon. That is, carboplatin is intrinsically "labeled" for EDS EDAX probes.

The second, less carboplatin-rich sample was examined using EDS EDAX where we were able to locate the carboplatin in the sample. Figure 4.14 shows EDAX emanating from the tubule; fluorescence yield data indicates that the tubule is 4.5 weight % platinum, a surprisingly high value. This finding is underscored by the fact that Pt was not detected anywhere else on the deposited specimen surface except on, or within 0.5 μm of the tubules. The area on the tubule exterior (Figure 4.15), revealed platinum present in concentrations of 24.1 weight %, suggesting the carboplatin either adheres to the tubule exterior, or is integrated into the tubule's membrane. Figure 4.16 shows that there was absolutely no detectable platinum on the areas of the substrate where tubules were not present. These results indicate that carboplatin adheres to tubule exteriors, or incorporates into the membranes, and does so voraciously. This result is the most promising so far with our encapsulation studies. It is possible that our interpretation that carboplatin adheres to the tubule exterior is an artifact resulting from the fact that the sample is air dried before it is examined: If the tubule dries flat, then it is possible that if the carboplatin was captured inside the tubule in solution, it may be released upon drying, producing a high concentration near the tubule. But, spatial resolution with EDAXS can be limited by secondary electron scattering within the substrate, and the 0.5 μm distance from the tubule edge where Pt is found may be an artifact of this "blossoming." Whether carboplatin resides *in* or *on* the tubule, it is apparent that tubule's potential utility as encapsulation agents merit further research.

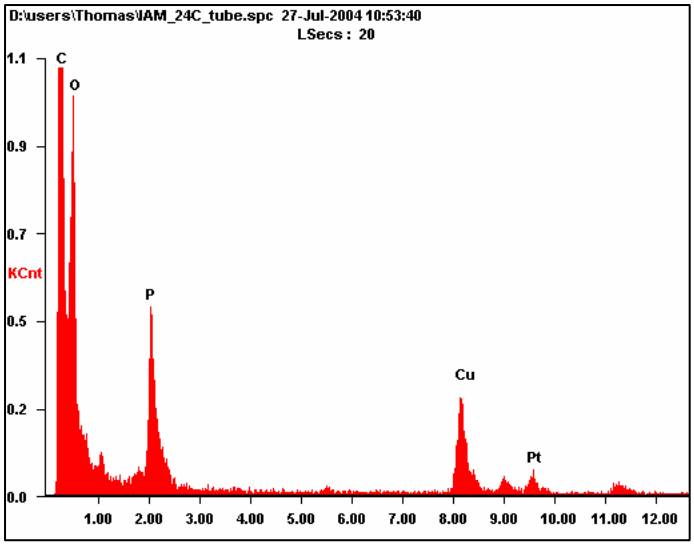

Elemental Analysis:

CK – 75.9 weight % / 87.8 atomic %

OK – 10.5 weight % / 9.1 atomic %

PK – 3.5 weight % / 1.6 atomic %

CuK – 5.7 weight% / 1.2 atomic %

PtL – 4.5 weight % / 0.3 atomic %

Figure 4.14 Energy dispersive spectroscopy results of the tubule itself.

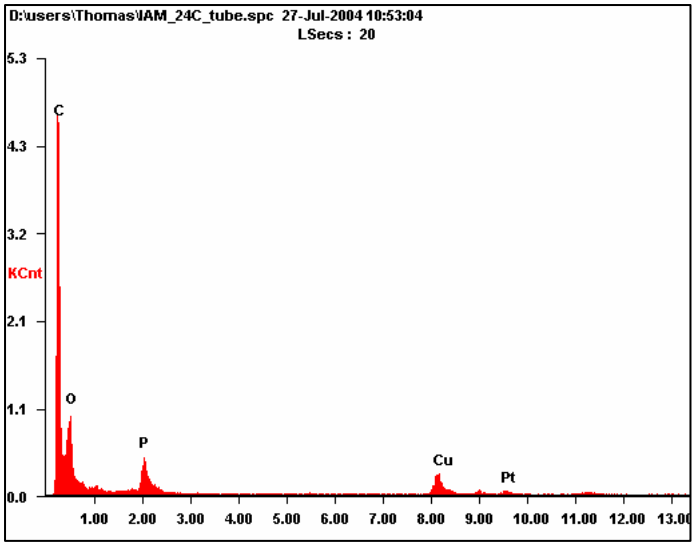

Elemental Analysis:

CK/OK – 39.2 weight % / 72.0 atomic %

PK – 15.4 weight % / 14.6 atomic %

CuK – 21.3 weight% / 9.8 atomic %

PtL – 24.1 weight % / 3.6 atomic %

Figure 4.15 Energy dispersive spectroscopy results at the perimeter of the tubule.

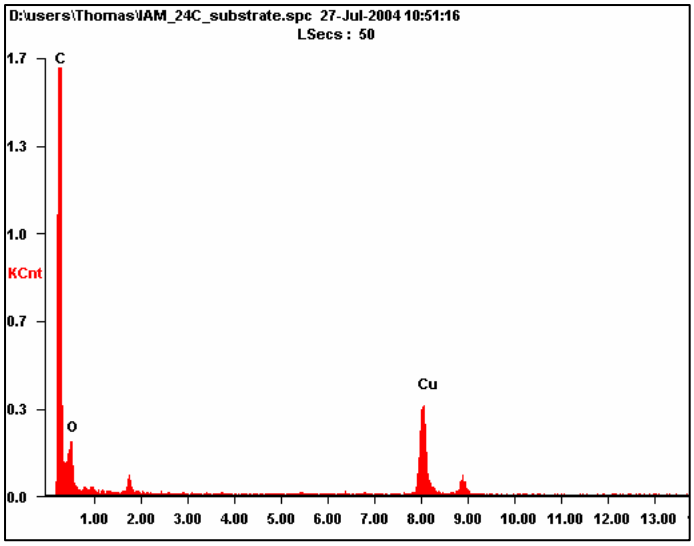

Elemental Analysis:

CK – 83.0 weight % / 94.3 atomic %

OK – 3.3 weight % / 2.8 atomic %

CuK – 13.7 weight % / 2.9 atomic %

Figure 4.16 Energy dispersive spectroscopy results of the substrate area without tubules present.

4.5 Conclusion

The encapsulation studies prove that it is possible to form tubules in the presence of a drug. The chemotherapy drugs do, however, have a couple of effects on the tubule morphology. First, when chemotherapy agents are added at 28%, tubules are not as plentiful and there seems to be an existence of high structures in the AFM scans, which are tentatively interpreted as being the drug itself co-precipitating alongside the tubules. Alternatively, these high drug concentrations may interfere with tubules formation, creating regions of non-tubule, drug-containing "bulk" lipid. The drugs all increase the diameter of the tubules as well. This effect persists when the drugs are added to attain 8% concentrations. EDS results show that carboplatin is centered around the tubule and apparently no carboplatin at all is left in the solution after tubules have formed. More experiments need to be performed in order to gain a better understanding of what is happening when the tubules are drying and becoming flattened (or

releasing the carboplatin). Also further studies need to be examined with methotrexate and mitoxantrone to determine where it is located throughout the tubule.

4.6 References

1. Johnson, D. L.; Polikandritou-Lambros, M.; Martonen, T. B. Drug encapsulation and aerodynamic behavior of a lipid microtubule aerosol. *Drug Delivery* **1996,** *3* (1), 9-15.

2. Johnson, D. L.; Esmen, N. A.; Carlson, K. D.; Pearce, T. A.; Thomas, B. N. Aerodynamic behavior of lipid microtubule aerosols. *Journal of Aerosol Science* **1999,** *31* (2), 181-188.

3. Methotrexate Sodium (for injection) . Xanodyne Pharmacal, Inc. Patient Package Insert. 2003. Ref Type: Pamphlet

4. Martinelli, J. E.; Chaykovsky, M.; Kisliuk, R. L.; Gaumont, Y. Synthesis of aza homologues of folic acid. *J Med Chem* **1979,** *22* (7), 874-877.

5. McGuire, J. J. Anticancer antifolates: Current status and future directions. *Current Pharmaceutical Design* **2003,** *9* (31), 2593-2613.

6. Seeger, D. R.; Cosulich, D. B.; Smith, J. M., Jr.; Hultquist, M. E. Analogs of pteroylglutamic acid. III. 4-Amino derivatives. *Journal of the American Chemical Society* **1949,** *71*, 1753-1758.

7. Werkheiser, W. C. Specific binding of 4-amino folic acid analogs by folic acid reductase. *Journal of Biological Chemistry* **1961,** *236*, 888-893.

8. Novantrone (mitoxantrone for injection concentrate) . OSI Pharmaceuticals, Inc. Patient Package Insert. 2005. Ref Type: Pamphlet

9. Ehninger, G.; Schuler, U.; Proksch, B.; Zeller, K. P.; Blanz, J. Pharmacokinetics and metabolism of mitoxantrone: a review. *Clinical Pharmacokinetics* **1990,** *18* (5), 365-380.

10. Niang, M.; Melka, M.; Stoklasova, A.; Cerman, J.; Tomsik, P. Evaluation of the antineoplastic activity of mitoxantrone-L-carnitine combination therapy on an experimental solid form of ehrlich tumour in mice. *Pharmacological Research* **2006,** *54* (6), 447-451.

11. Paraplatin (carboplatin aqueous solution) . Bristol-Myers Squibb Company, Patient Package Insert. 2004. Ref Type: Pamphlet

12. Abrams, M. J.; Murrer, B. A. Metal compounds in therapy and diagnosis. *Science* **1993,** *261* (5122), 725-730.

13. Lepre, C. A.; Lippard, S. J. Interaction of platinum antitumor compounds with DNA. *Nucleic Acids and Molecular Biology* **1990,** *4*, 9-38.

14. Sundquist, W. I.; Lippard, S. J. The coordination chemistry of platinum anticancer drugs and related compounds with DNA. *Coordination Chemistry Reviews* **1990,** *100*, 293-322.

15. Ozols, R. F.; Behrens, B. C.; Ostchega, Y.; Young, R. C. High dose cisplatin and high dose carboplatin in refractory ovarian cancer. *Cancer Treatment Reviews* **1985,** *12* (Suppl. A), 59-65.

16. Ozols, R. F.; Bundy, B. N.; Greer, B. E.; Fowler, J. M.; Clarke-Pearson, D.; Burger, R. A.; Mannel, R. S.; de Geest, K.; Hartenbach, E. M.; Baergen, R. Phase III trial of carboplatin and paclitaxel compared with cisplatin and paclitaxel in patients with optimally resected stage III ovarian cancer: a Gynecologic Oncology Group Study. *Journal of Clinical Oncology* **2003,** *21* (17), 3194-3200.

17. Admiraal, G.; Van der Veer, J. L.; De Graaff, R. A. G.; Den Hartog, J. H. J.; Reedijk, J. Intrastrand bis(guanine) chelation of trinucleoside diphosphate d(CpGpG) to cis-platinum: an x-ray single-crystal structure analysis. *Journal of the American Chemical Society* **1987,** *109* (2), 592-594.

18. Peyratout, C. S.; Aldridge, T. K.; Crites, D. K.; McMillin, D. R. DNA-Binding Studies of a Bifunctional Platinum Complex That Is a Luminescent Intercalator. *Inorganic Chemistry* **1995,** *34* (17), 4484-4489.

19. Sherman, S. E.; Gibson, D.; Wang, A. H. J.; Lippard, S. J. Crystal and molecular structure of cis-[Pt(NH3)2[d(pGpG)]], the principal adduct formed by cis-diamminedichloroplatinum(II) with DNA. *Journal of the American Chemical Society* **1988,** *110* (22), 7368-7381.

Chapter 5

Optimization of Phospholipid Tubule Morphology

5.1 Introduction

It is important to understand the significance of optimizing tubule morphology for drug encapsulation applications. Tubule drug-loading capacity presumably scales with tubule size, that is, a larger tubule should deliver a larger dose. Because the amount of drug administered to the body is adjusted simply by regulating the number of drug-bearing tubules that are delivered, the question of why it is important to control tubule size occurs naturally. The answer is two-fold: 1) The *drug release rate* and the *duration of its release* are certain to depend upon tubule length and diameter; and 2) In aerosol-delivery respiratory therapy modalities, the deposition location in the respiratory tract is almost solely a function of tubule diameter.[1]

There are two ways to regulate tubule diameter. The first is to modify the tubule-forming molecule, e.g., the doubling of tubule diameter by using phosphonate DC(8,9)PC derivatives rather than DC(8,9)PC.[2,3] This requires considerable (and expensive) synthetic effort and the result is "quantized" in the sense that a given molecule tends to produce tubules of a given, and possibly off-optimum diameter and length. The second approach is to add co-surfactants, or so-called "spacer" lipids that modify whatever processes lead to membrane chiralization and winding, or polymers or proteins that exert similar effects, presumably by similar mechanism(s).[4] This latter approach could prove useful for a number of applications, for tubule diameter is presumably continuously adjustable by this approach, and the co-surfactant or polymer could be an inexpensive, stable material. Optimizing tubule dimensions for a particular application by the addition of co-surfactant or large molecules may result in non-cylindrical morphologies that may affect their performance (for better or worse), e.g. the protein lysozyme added to the cooling

spherical DC(8,9)PC vesicles produces gently-tapered hollow cones, rather than the cylinders formed in protein-free systems.[5] Whether or not the conical transformation caused by the large lysozyme molecule is desirable remains a question for further study.

In this chapter, two molecules, semi-saturated DC(8,9)PC analog 1,2-dioleoyl-*sn*-glycero-3-phosphoethanolamine, (DOPE) and cholesterol, are investigated in order to regulate tubule morphology.

5.2 DOPE Studies

The semi-saturated DC(8,9)PC analog 1,2-dioleoyl-*sn*-glycero-3-phosphoethanolamine (DOPE) shown in Figure 5.1 was selected as a co-surfactant for its similarity to DC(8,9)PC and its unusual tendency to form inverted hexagonal phases above 10 degrees Celsius.[6,7] DOPE was added in various weight ratios and taken through the thermal tubule formation process to determine if tubule formation persisted in view of DOPE's ability to form inverted hexagonal phases, and if so, what changes might be seen in tubule structure.

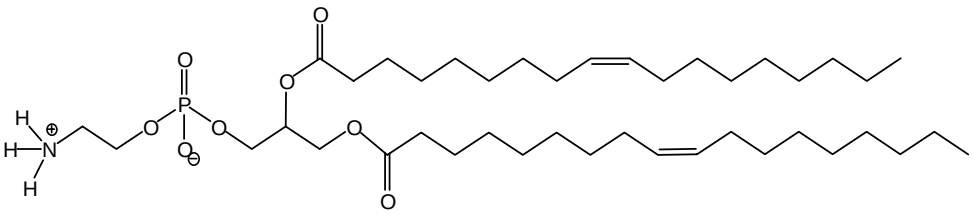

Figure 5.1 Structure of 1,2-dioleoyl-*sn*-glycero-3-phosphoethanolamine, (DOPE).

DOPE was first added to existing 1 mg lipid / ml EtOH/H_2O stock solution to obtain a 1:1 DOPE:DC(8,9)PC weight ratio or 1.2 mole%. At this very high ratio, tubule formation was seen to persist, as seen in Figure 5.2, and tubule diameters increased from 0.5 μm to ~1-2 μm

upon this introduction of DOPE. So, at this concentration, DOPE did not prevent tubule formation, and exerted only a small change upon tubule structure.

A. B.

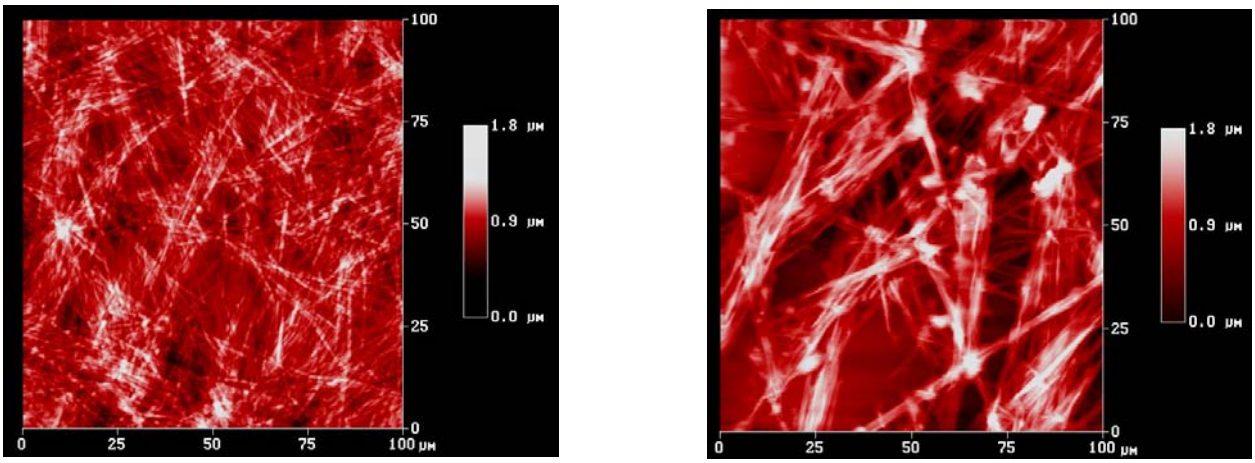

Figure 5.2 100 μm x 100 μm contact mode atomic force micrograph of A. DC(8,9)PC tubules (shown for comparison) and B. DOPE:DC(8,9)PC [1:1] tubules, showing an increase in diameter.

Given this somewhat surprising outcome, samples were prepared at a 2:1 DOPE:DC(8,9)PC weight ratio or 2.5 mole%. Figure 5.3 shows that tubule formation still persists at the 2:1 DOPE:DC(8,9)PC weight ratio, but now tubule diameters are found to range from 1 μm to 6 μm. These results are consistent with those of Singh et al.; simpler "spacer lipids", short-chain saturated phospholipids, were used to tune the diameter of DC(8,9)PC tubules.[4] When chain lengths are long enough, these spacer lipids can penetrate the membrane to the depth of the DC(8,9)PC diacetylene groups, thus interfering with diyne/diyne interactions. This interference causes an increase in tubule diameter above the otherwise narrowly disperse 0.5 μm diameter; and DOPE's chain length is just long enough to "mask" the diacetylene group interactions and cause an increase in diameter. So, in conclusion, the presence of DOPE does

not cause a change in phase or a disruption in the lamellar phase out of which tubules form, even at preponderant concentrations of 4:1 DOPE:DC(8,9)PC (4.9 mole%).

A. B.

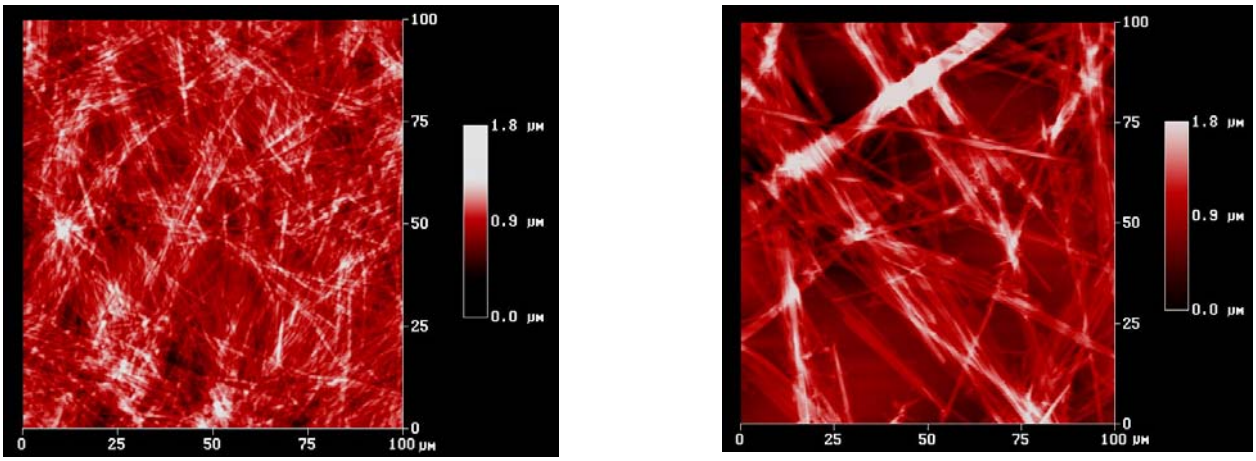

Figure 5.3 100 μm x 100 μm contact mode atomic force micrograph of A. DC(8,9)PC tubules (shown for comparison) and B. DOPE:DC(8,9)PC [2:1] tubules, showing an increase in diameter.

5.3 Cholesterol Studies

Cholesterol, shown in Figure 5.4, is a rigid ring system with a short branched hydrocarbon tail. It is largely hydrophobic due to its possessing only one hydrophilic moiety, a hydroxyl group. Even so, the distal position of the hydroxyl group makes this hydrocarbon amphipathic. Cholesterol is known to insert itself into bilayer membranes with the hydroxyl group forming a H-bond with the polar headgroups of the phospholipid and the short branched hydrocarbon tail aligning with that of the hydrophobic region of the phospholipid hydrocarbon tail.[8] By inserting itself into the membrane in this fashion, cholesterol is able to decrease the

mobility of the phospholipid tails and cause them to expand or straighten, resulting in an increase of bilayer thickness.[9-11]

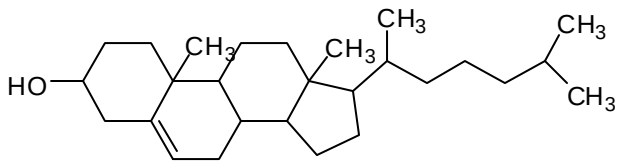

Figure 5.4 Chemical structure of cholesterol

As cholesterol is known to generally increase lipid chain order and bilayer thickness in membranes, it was added to the standard DC(8,9)PC thermal cycling mixture to study its effects upon tubule formation, which result from a highly unusual DC(8,9)PC membrane.

Another reason for choosing cholesterol is that it can serve as an indication of how other molecules having the same characteristics might act in the membrane. If cholesterol can be successfully incorporated into the membrane, other steroids such as sex hormones, anti-inflammatory agents such as prednisone, etc. may act in a similar fashion. There has been much interest in recent years on the delivery of steroid hormones such as estradiol, progesterone, and testosterone. Because these molecules' structures are derived from cholesterol, cholesterol is an excellent model for these other compounds.

Cholesterol was added to a solution of previously-formed tubules at various mole% ratios and taken through the tubule formation thermal cycle, i.e., heating the suspension to clarity and cooling slowly. Surprisingly at 11 mole% cholesterol, no detectable change was seen in tubule morphology, as seen in the SEM image Figure 5.5. Tubule diameter and morphology remained unchanged at lower cholesterol concentrations as well.

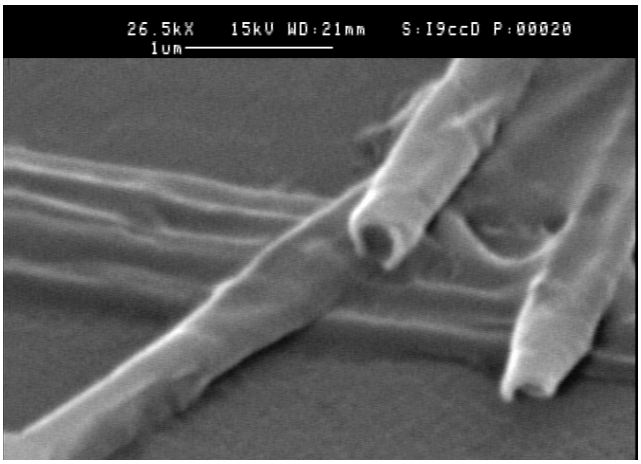

Figure 5.5 Scanning electron micrograph of DC(8,9)PC tubules with 11 mole% cholesterol, showing tubule morphology is consistent with that of pure DC(8,9)PC.

When DC(8,9)PC is doped with higher amounts of cholesterol significant changes in the morphology can be observed. Figure 5.6 shows an atomic force micrograph of DC(8,9)PC tubules with 40 mole% cholesterol, showing an increase in diameter. Upon the addition of 30 and 40 mole% cholesterol, tubule diameter increases because of the addition of cholesterol, as shown in Figure 5.7. The trend discerned is that as the amount of cholesterol increases, so does tubule diameter, which is interpreted as the expected increase in bilayer thickness.

In order to determine whether or not this presumed bilayer thickness was occurring, AFM section analysis was performed on the samples. AFM cross-sections of DC(8,9)PC and phosphonates are observed to be trapezoidal and not the expected semi-circular shape that an unflattened tubule would generate.[2] As the AFM tip is rastered across the sample in a horizontal fashion, the vertical displacement is translated as the sample height. When the tip reaches the cylinder's edge, it is unable to reach under the segment of the cylinder whose portion is tangent is normal to the substrate surface. The section analysis tool can give information on the height of the tubules, which can reveal information about the thickness of the bilayers, because it is known

A. B.

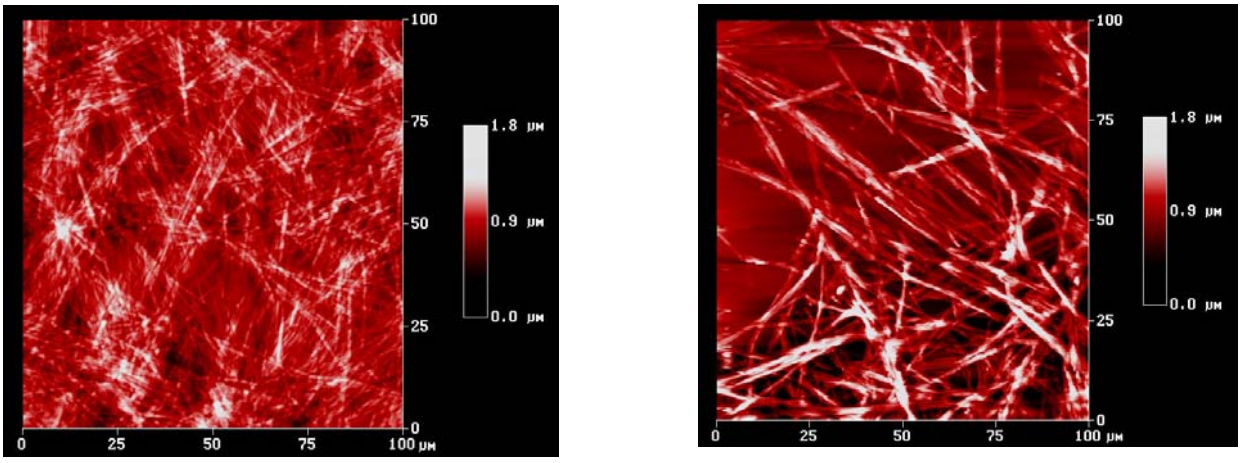

Figure 5.6 100 μm x 100 μm contact mode atomic force micrograph: A. DC(8,9)PC tubules (shown for comparison) and B. DC(8,9)PC tubules with 40 mole% cholesterol, showing a change in tubule morphology.

A. B.

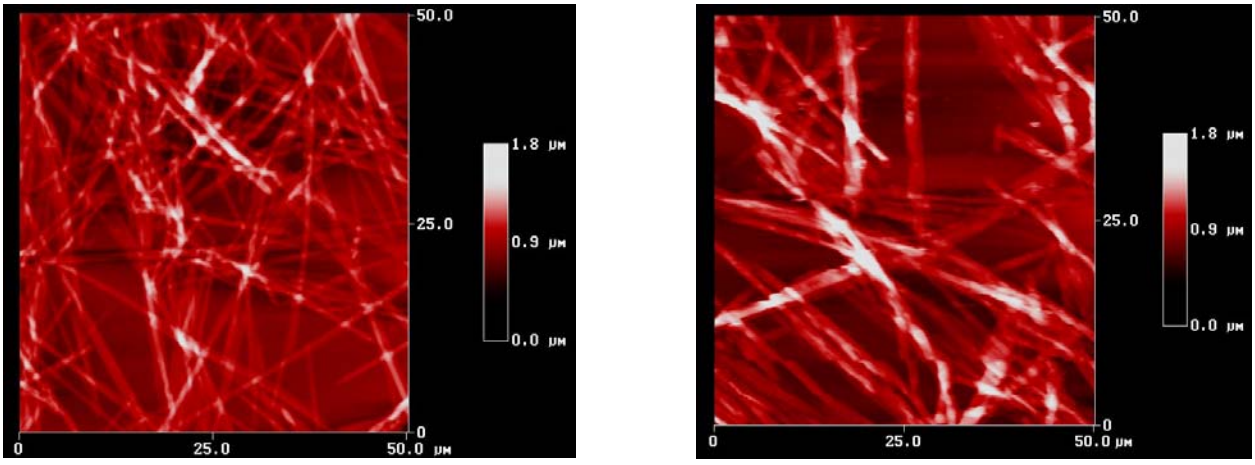

Figure 5.7 50 μm x 50 μm contact mode atomic force micrograph: A. DC(8,9)PC tubules with 30 mole% cholesterol and B. DC(8,9)PC tubules with 40 mole% cholesterol

that tubules' circular cross section flattens upon drying. A height measurement thereby yields information about bilayer thicknesses. All measurements were made under the same conditions in order to make our comparisons as accurate and consistent as possible. The pure DC(8,9)PC height profile, shown in Figure 5.8, reveals that tubule heights are ~100 nm, while 30 mole% cholesterol/DC(8,9)PC specimens gave tubule heights of ~200 nm, as seen in the height profile in Figure 5.9. Tubule height for 40 mole% cholesterol/DC(8,9)PC increases to ~30 nm, as shown in Figure 5.10. Tubule wall thickness appears to depend upon the cholesterol content. So, AFM section analysis reveals that above a certain mole% threshold (somewhere above 11%) tubule wall thickness increases in an apparently linear fashion upon the addition of cholesterol.

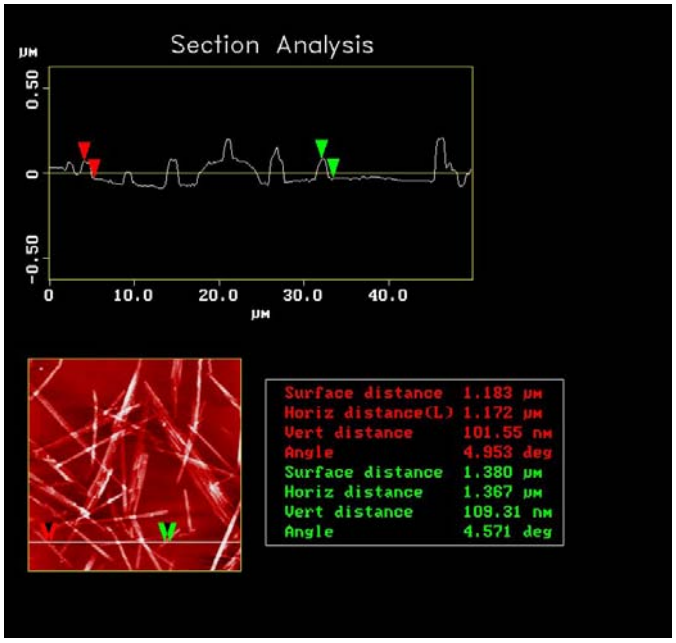

Figure 5.8 Atomic force microscopy section analysis yielding DC(8,9)PC tubule height profile. Tubule height ~100 nm.

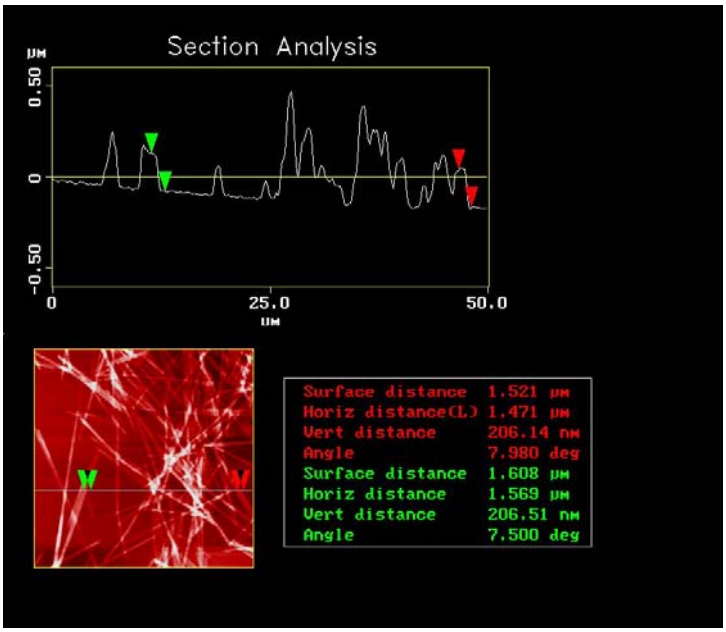

Figure 5.9 Atomic force microscopy section analysis yielding DC(8,9)PC tubules with 30 mole% cholesterol tubule height profile. Tubule height ~200 nm.

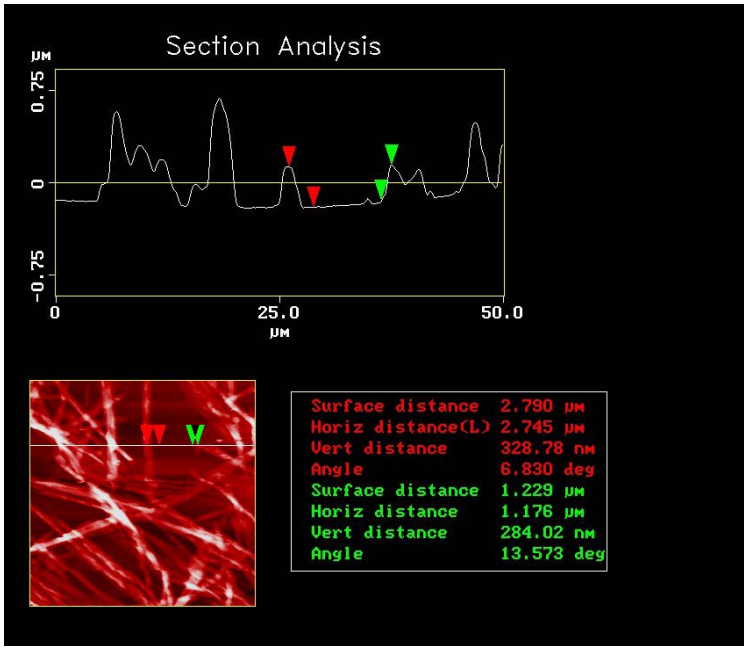

Figure 5.10 Atomic force microscopy section analysis yielding DC(8,9)PC tubules with 40 mole% cholesterol tubule height profile. Tubule height ~300 nm.

5.4 Conclusions

Tubule formation persists in the presence of both DOPE and cholesterol, but the morphology of the tubules is altered by the presence of these molecules. DOPE did not cause a change in phase or apparently otherwise disrupt the DC(8,9)PC lamellar phase from which tubules form, even at concentrations as high as 4:1 DOPE:DC(8,9)PC. But DOPE is able to significantly alter the tubule diameter up to sizes of ~6 μm. Cholesterol is also able to alter tubule morphology with concentrations above a certain mole% threshold (11 mole%). Above this mole% threshold, tubule wall thickness increases in an apparently linear fashion with respect to cholesterol concentration.

5.5 References

1. Johnson, D. L.; Esmen, N. A.; Carlson, K. D.; Pearce, T. A.; Thomas, B. N. Aerodynamic behavior of lipid microtubule aerosols. *Journal of Aerosol Science* **1999,** *31* (2), 181-188.

2. Thomas, B. N.; Corcoran, R. C.; Cotant, C. L.; Lindemann, C. M.; Kirsch, J. E.; Persichini, P. J. Phosphonate Lipid Tubules. 1. *Journal of the American Chemical Society* **1998,** *120* (47), 12178-12186.

3. Thomas, B. N.; Lindemann, C. M.; Corcoran, R. C.; Cotant, C. L.; Kirsch, J. E.; Persichini, P. J. Phosphonate Lipid Tubules II. *Journal of the American Chemical Society* **2002,** *124* (7), 1227-1233.

4. Singh, A.; Wong, E. M.; Schnur, J. M. Toward the rational control of nanoscale structures using chiral self-assembly: Diacetylenic phosphocholines. *Langmuir* **2003,** *19* (5), 1888-1898.

5. Mishra, B. K.; Thomas, B. N. Phospholipid/Protein Cones. *Journal of the American Chemical Society* **2002,** *124* (24), 6866-6871.

6. Cullis, P. R.; De Kruijff, B. The polymorphic phase behavior of phosphatidylethanolamines of natural and synthetic origin. A phosphorus-31 NMR study. *Biochimica et Biophysica Acta, Biomembranes* **1978,** *513* (1), 31-42.

7. Rand, R. P.; Fuller, N. L. Structural dimensions and their changes in a reentrant hexagonal-lamellar transition of phospholipids. *Biophysical Journal* **1994,** *66* (6), 2127-2138.

8. Alberts, B.; Johnson, A.; Lewis, J.; Raff, M.; Roberts, K.; Walter, P. *Molecular Biology of the Cell;* 3rd ed.; Garland Publishing, N.Y.: 1994.

9. Hui, S. W.; He, N. B. Molecular organization in cholesterol-lecithin bilayers by X-ray and electron diffraction measurements. *Biochemistry* **1983,** *22* (5), 1159-1164.

10. Nezil, F. A.; Bloom, M. Combined influence of cholesterol and synthetic amphiphillic peptides upon bilayer thickness in model membranes. *Biophys J* **1992,** *61* (5), 1176-1183.

11. Smondyrev, A. M.; Berkowitz, M. L. Structure of dipalmitoylphosphatidylcholine/cholesterol bilayer at low and high cholesterol concentrations: molecular dynamics simulation. *Biophysical Journal* **1999,** *77* (4), 2075-2089.

Chapter 6

Modifying DC(8,9)PC to Create New Tubule-forming Molecules

6.1 Introduction

Given the striking correspondence between DC(8,9)PC chirality and the helical sense of handedness (helicity) of the tubule exterior, molecular chirality was understandably at the center in the development of tubule theory.[1-6] But as described in Chapter 1, Thomas et al. developed two results inconsistent with these "chiral packing" theories: 1) tubules' inner cylinder's helicity is random,[7] and more strikingly, 2) that molecular chirality is *not* essential for membrane chiralization to occur[8]. Armed with these new discoveries, we embarked upon developing a series of compounds to determine what DC(8,9)PC molecular features enable tubule formation. Since it is now known tubules can form from achiral DC(8,9)PC analogs, it is clear that the diynes are the enabling feature, and their contribution must be investigated.

Inspiration is drawn from recent results in liquid crystal physics, namely the so-called achiral "banana" or "bow"-shaped molecules that spontaneously form locally-chiral phases, by way of a chiral symmetry-breaking transition.[9,10] We speculate the tubule forming molecule, DC(8,9)PC, may enter such a "bow" conformation by rotations of tail segments about the diyne and form chiral mesoscale structures by the same mechanism as the "bow"-shape liquid crystals do, shown in Figure 6.1.

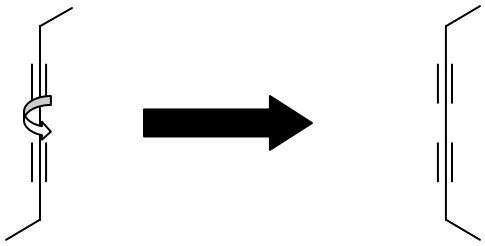

Figure 6.1 Represents the tails of the phospholipid rotating about the diyne to enter the "bow" confirmation.

This hypothesis was tested by synthesizing compounds in which the diynes in the DC(8,9)PC tails are replaced by either a cis- or trans- "ene" bond. When cis ene bonds lie in the tails, the hydrocarbon tails are forced into a "bow" shape, but trans ene bonds exclude that conformation, and essentially result in a more-or-less straight hydrocarbon tail. Oleic acid, linoleic acid, and γ-linolenic acid (Figure 6.2) were selected as sources for the hydrocarbon tails of the phospholipid because of their number of cis bonds. Oleic acid has one cis bond, while linoleic and γ-linolenic acids have two and three, respectively. This range in the number of cis bonds can possibly force a "bow" confirmation to varying degrees as seen in Figure 6.2, if they were constrained to lie in a plane, as forced to draw them. One of three outcomes can be expected: 1) The cis- AND trans compounds form tubules; 2) Neither cis- and trans compound forms tubules; 3) Only one compound forms tubules. The cis compounds were selected as a starting point, for tubule formation from these compounds would confirm our conjecture, but in order to fully understand and confirm this theory, the trans-"ene" bond must be synthesized. That is to say, if our "bow" chiral symmetry-breaking model speculation is correct, we expect outcome #3, specifically, that the cis compound will form tubules, and that the trans compound will not. However, given the primitive state of understanding of tubule formation, outcomes #1 and #2 and even #3 with the trans compound would be groundbreaking.

6.2 Synthetic Steps

6.2.1 Acetonide Protection of Glycerol

The first step in the synthesis of the DC(8,9)PC derivatives requires protection of the 1,2 diol on the glycerol backbone shown in Scheme 6.1. The protected glycerol is made by adding an acetonide group and is frequently used for the protection of 1,2 and 1,3 diols.[11] Literature

provides verification that the 1,2-acetonide is preferred over the 1,3-derivative; however, it is structure-dependent.[12]

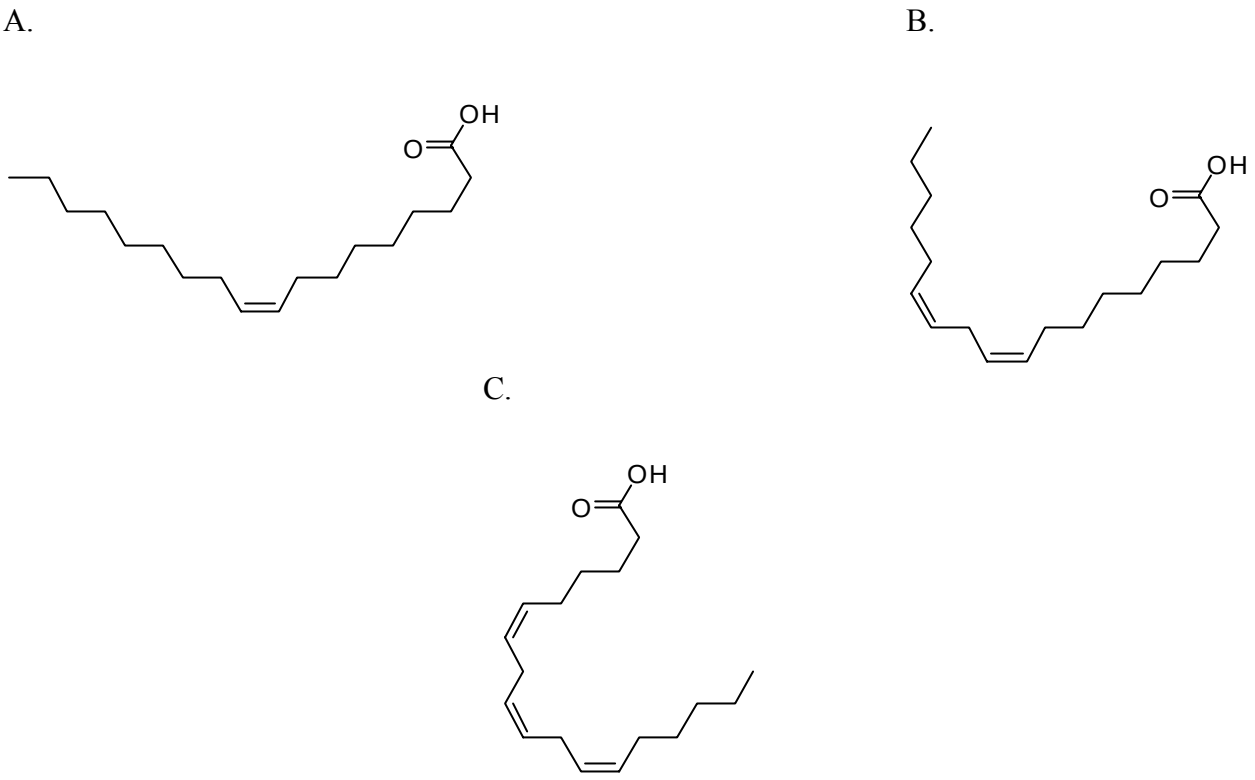

Figure 6.2 Structures of A. oleic acid, B. linoleic acid, and C. γ-linolenic acid.

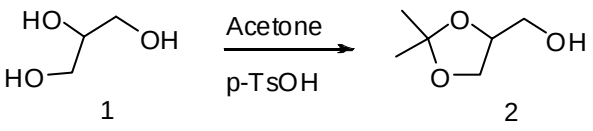

Scheme 6.1 Acetonide protection of glycerol.

6.2.2 Addition of Diethylchlorophosphate

Phospholipids are synthesized by esterification (Scheme 6.2) of an alcohol to the phosphate of phosphatidic acid (1,2-diacylglycerol 3-phosphate). The third oxygen on glycerol is bonded to phosphoric acid through a phosphate ester bond.[13,14]

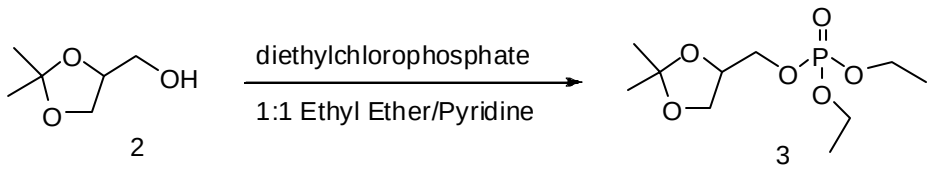

Scheme 6.2 Addition of diethylchlorophosphate.

6.2.3 Deprotection

Deprotection of the glycerol backbone, shown in Scheme 6.3, will be achieved through hydrolysis of the acetonide, using p-TsOH and ethanol (Scheme 4).[11,14]

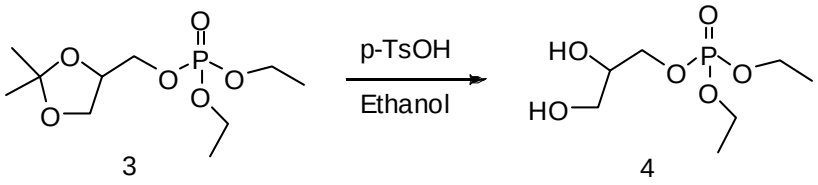

Scheme 6.3 Deprotection of glycerol backbone.

6.2.4 Addition of Fatty Acid Tails

The addition of long chain acids (oleic, linoleic, and γ-linolenic) to glycerol will be accomplished via an ester linkage (Scheme 6.4).[13,14]

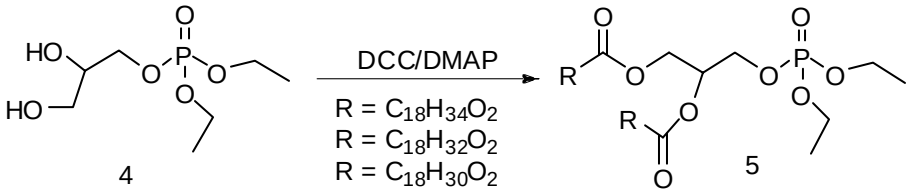

Scheme 6.4 Addition of fatty acid tails.

6.3 Equipment

^{1}H-NMR (400MHz) and ^{13}C-NMR (100MHz) data was acquired on a JOEL JNM-ECP400 FT-NMR spectrometer, using $CDCl_3$ as the solvent.

6.4 Synthesis

6.4.1 Acetonide Protection

Glycerol (47.6 g, 51.6 mmol), acetone (90 ml), chloroform (200 ml), and p-TSOH (8.9 g, 5.2 mmol) were added to a round bottom flask attached to a Dean-Stark apparatus and refluxed for 10 hours. The reaction mixture was allowed to cool to room temperature and neutralized by stirring with potassium carbonate (3.0 g) for 1 hour. The reaction mixture was vacuum distilled to obtain 3.10 g of 1,2-O-isopropylidene glycerol (**2**) (74%)**.** ^{1}H-NMR ($CDCl_3$) δ 1.36 (s,3H), 1.45 (s, 3H), 3.60 (dd, 1H), 3.62 (dd, 1H), 3.97 (dd, 1H), 4.15 (m, 1H). ^{13}C-NMR ($CDCl_3$) δ 25.3, 26.8, 63.1, 65.8, 76.3, 109.5.

6.4.2 Addition of Diethylchlorophosphate

A solution of (**2**) (6.0 g, 4.5 mmol) in anhydrous ether/pyridine (12.5 m, 1:1 v/v) was stirred under nitrogen for ~20 minutes at 0^{o} C before adding diethylchlorophosphate (13.19 ml, 9.1 mmol). The reaction immediately formed a white precipitate and was stirred for 30 minutes. The reaction mixture was poured over 125 g of ice and reached room temperature as the ice melted. An extraction was carried out with 100 ml ether followed by a wash with copper sulfate.

The mixture was washed with water, saturated brine, dried with Na_2SO_4, and filtered. The sample was concentrated under reduced pressure to obtain 5.96 g of phosphate. The phosphate compound (**3**) was used without further purification. ^{1}H-NMR ($CDCl_3$) δ 1.21-1.52 (m, 12H), 2.07-2.33 (m, 2H), 3.67 (dd, 1H), 4.15 (m, 5H), 4.30 (m, 1H).

6.4.3 Deprotection

A mixture of (**3**) (2.96 g, 11 mmol) and p-toluenesulfonic acid (326 mg, 1.6 mmol) in ethanol (85 ml), was refluxed for 14 hours under Nitrogen at room temperature. Sodium bicarbonate was added to the reaction to neutralize the acid. The mixture was filtered and placed on the rotovap. The residue was re-dissolved in chloroform (50 ml) and filtered through Celite before concentrating under reduced pressure, yielding 1.99 g (79%). The material was used without further purification (**4**). ^{1}H-NMR ($CDCl_3$) δ 1.25 (dd, 6H), 2.12 (m, 2H) 3.40 (dd, 1H), 3.68 (dd, 2H), 4.10 (m, 5H), 4.20 (m, 1H). ^{13}C-NMR ($CDCl_3$) δ 16.3, 61.1, 66.5, 69.8, 75.3.

6.4.4 Addition of Fatty Acid Tails

6.4.4.1 (9Z,9`Z)-3-(diethoxyphosphoryloxy)propane-1,2-diyl dioctadec-9-enoate

A solution of deprotected starting material (**4**) (1.99 g, 9.5 mmol) and 1,3-dicyclohexylcarbodiimide (4.31 g, 21.0 mmol) in methylene chloride (7 ml) was stirred before adding pyridine (0.14 g, 1.7 mmol), oleic acid (5.64 g, 19 mmol), and more methylene chloride (35 ml). The mixture was stirred under Nitrogen for 48 hours at room temperature. After reaction was complete, the mixture was filtered over Celite and placed on the rotovap. The concentrated material was then re-dissolved in hexane, filtered again over Celite, and evaporated to yield 5.09 g (71%) of yellow oil (**5**). The purification of the oil was carried out by flash chromatography on silica gel using hexane/ethyl acetate (10:1)**.** ^{1}H-NMR ($CDCl_3$) δ 0.86 (t,

5H), 1.23-1.97 (m, 58H), 2.28-2.37 (m, 10H), 4.06-4.13 (m, 6H), 5.31 (m, 8H) ^{13}C-NMR ($CDCl_3$) δ 14.2, 22.7, 24.8, 25.4, 26.5, 29.5, 31.2, 32.0, 76.8, 77.1, 77.4, 128.1, 130.2, 155.2.

6.4.4.2 (9Z,9'Z,12Z,12'Z)-3-(diethoxyphosphoryloxy)propane-1,2-diyl dioctadeca-9,12-dienoate

A solution of deprotected starting material (**4**) (1.70 g, 8.1 mmol) and 1,3-dicyclohexylcarbodiimide (3.69 g, 17.9 mmol)) in methylene chloride (7 ml) was stirred before adding pyridine (0.14 g, 1.7 mmol), linoleic acid (4.8 g, 17.1 mmol), and more methylene chloride (35 ml). The mixture was stirred under Nitrogen for 48 hours at room temperature. After reaction was complete, the mixture was filtered over Celite and placed on the rotovap. The concentrated material was then re-dissolved in hexane, filtered again over Celite, and evaporated to yield 4.12 g (65%) of yellow oil (**5**), which was used without further purification for tubule studies. ^{1}H-NMR ($CDCl_3$) δ 0.90 (t, 6H), 1.11-1.84 (m, 53H), 2.01-2.29 (m, 8H), 4.09 (m, 6H), 4.21 (dd, 2H), 5.3 (m, 8H). ^{13}C-NMR ($CDCl_3$) δ.14.2, 22.7, 24.8, 25.7, 27.3, 29.4, 30.9, 49.8, 76.8, 77.3, 128.1, 130.3, 154.2.

6.4.4.3 (6Z,6`Z,9Z,9'Z,12Z,12'Z)-3-(diethoxyphosphoryloxy)propane-1,2-diyl dioctadeca-6,9,12-trienoate

A solution of deprotected starting material (**4**) (0.272 g, 1.3 mmol) and 1,3-dicyclohexylcarbodiimide (0.621 g, 3 mmol) in methylene chloride (7 ml) was stirred before adding pyridine (21.5 mg, 0.03 mmol), γ-linolenic acid ((0.80 g, 2.9 mmol) 4.8 g, 17.1mmol), and more methylene chloride (35 ml). The mixture was stirred under Nitrogen for 48 hours at room temperature. After reaction was complete, the mixture was filtered over Celite and placed on the rotovap. The concentrated material was then re-dissolved in hexane, filtered again over Celite, and evaporated to yield 1.14 g (51%) of yellow oil (**5**), which was used without further purification for tubule studies. ^{1}H-NMR ($CDCl_3$) δ 0.91 (t, 6H), 1.08-1.89 (m, 43H), 2.00-2.43

(m, 10H), 3.92 (m, 6H), 4.12 (dd, 2H), 5.31 (m, 12H). ^{13}C-NMR ($CDCl_3$) δ 14.1, 22.7, 23.9, 25.7, 27.2, 29.4, 30.9, 32.9, 77.5, 128.2, 129.7, 130.5, 172.1.

6.5 Results

The oleic acid tail compound (containing one cis moiety per tail), (9Z,9`Z)-3-(diethoxyphosphoryloxy)propane-1,2-diyl dioctadec-9-enoate, was studied first to test if tubules could form from molecules forced to be in the "bow" shape. Originally, the new compound was treated as DC(8,9)PC, adding 1 mg/ml of solution (ethanol:water, 75:25). Upon this preparation, the solution was immediately clear, revealing that the material was completely dissolved, even before heating. Since DC(8,9)PC tubules are present at room temperature, this result was not very promising. The sample was then titrated with water, in order to make the compound less soluble in the solution. A total of 1835 μl was added before the material became cloudy, practically reversing the solvent ratio (ethanol:water 26:74), at room temperature. As the mixture was heated to 45^{o}C, it turned cloudier. (Upon heating the comparable DC(8,9)PC solution to this temperature, it becomes clear). The oleic-acid-based compound mixture finally turned clear at ~70 ^{o}C, indicating that the compound was now in solution. Upon returning back to room temperature, the solution remained clear, indicating that the material was still in solution and no tubules had precipitated. As a last measure, the mixture was put in the freezer (~5^{o}C) for ~1 hour in order to induce the phase transition to tubules. Indeed, the solution became cloudy and was examined by optical microscopy, where a small number of tubules (Figure 6.3) and some other irregular structures (Figure 6.4) were seen. While this is not the robust DC(8,9)PC outcome, tubules are indeed present, strongly supporting the notion that the "bow" conformation is necessary for tubule formation.

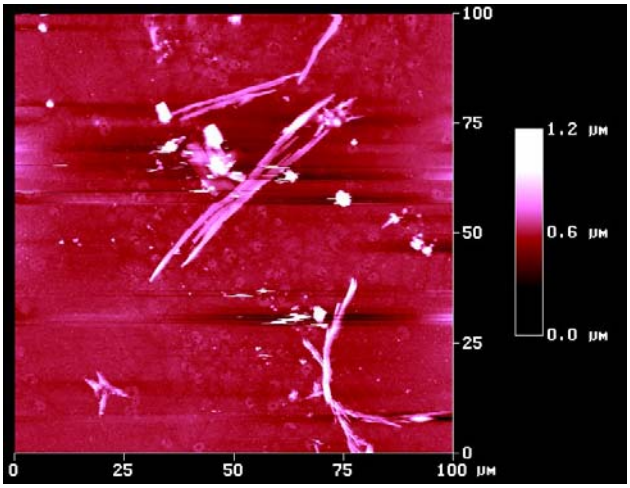

Figure 6.3 100 μm x 100 μm atomic force micrograph of new tubule-forming compound, showing that some tubules are present.

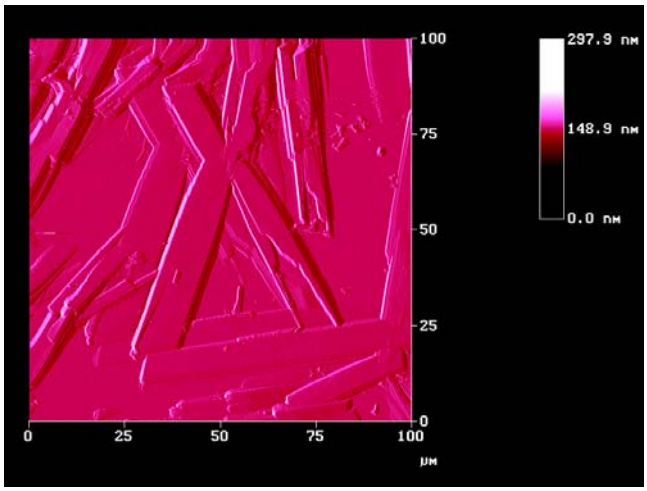

Figure 6.4 100 μm x 100 μm atomic force micrograph of new tubule-forming compound, showing rigid, sheet-like structures.

It is not clear if this lower phase transition temperature is a kinetics effect or a consequence of using a solvent system that happens to be far from optimal for this new

molecule; it is possible that both are in play. Supporting the idea that this molecule's tubule formation kinetics are slow is the observation that once formed, the tubules did not melt at room temperature, and that going far below the L_{α}-to-$L_{\beta'}$ transition temperature simply sped up the L_{α}-to-$L_{\beta'}$ phase transition. As far as the notion that solvent composition may require optimization is the observation that methanolic and propanolic DC(8,9)PC solutions produce somewhat different self-assembly structures than ethanolic ones; it is natural to assume that this new molecule's optimum solvent composition might be different from that of DC(8,9)PC.

The 10-15 μm diameter tubules that are present are much larger than the traditional 0.5 μm DC(8,9)PC tubule. Figure 6.4 shows some objects that are not completely understood at this point in time. They appear to be sheets similar to those formed by DC(8,9)PC shown in Figure 1.4, from which tubules form, but we cannot exclude the possibility this is merely bulk crystal. It is possible for sheets to exist and tubules not to form, but in this case, it seems that both the sheets and tubules are present.

Several combinations of ethanol/ water and varying the amount of lipid were investigated in order to discover the optimum conditions for normal tubule precipitation to occur with this new compound. Figure 6.5A and 6.5B and show the well-known "starburst" pattern left after an L_{α} spherical vesicle has radiated from a center (the spherical vesicle) and been completely converted to tubules. Several of these clusters can be seen in Figure 6.5A. Both Figures 6.5A and 6.5B scans are representative of the entire sample as indicated by the two completely different areas that are showing this starburst phenomenon. Another critical structure in these micrographs is the presence of a faint, thin but large sheet in the midst of these clusters. This structure is tentatively interpreted to be the flat sheet from which tubules can form, as discussed in Section 1.1.3.3.

A. B.

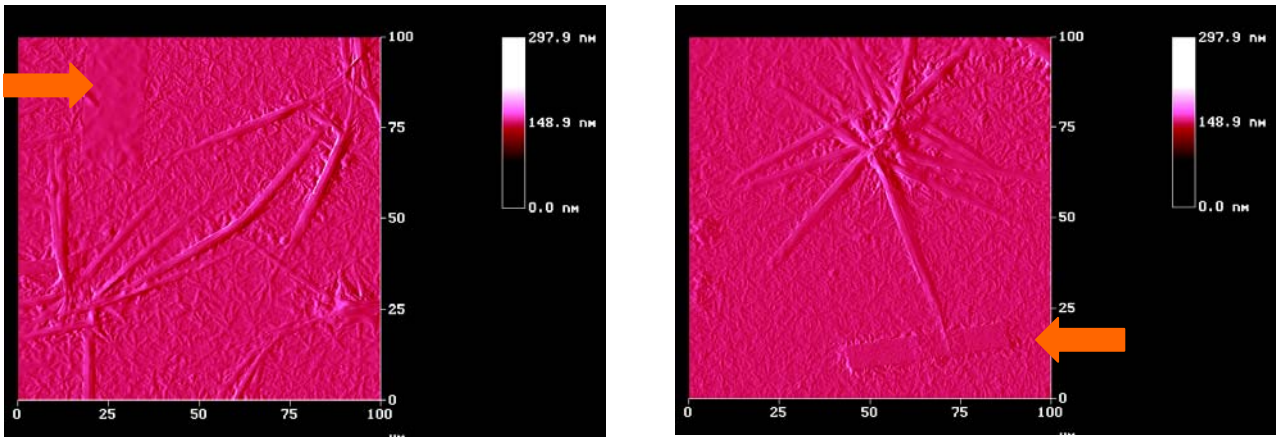

Figure 6.5 A. and B. 100 μm x 100 μm atomic force micrograph of new tubule-forming molecule, arrows are pointing to sheets.

6.6 Conclusions

In conclusion, the new compound containing oleic acid tails formed tubules. The conditions for this initial study are certain to not be optimized, but this early success with this compound indicates that triple bonds are not necessary for tubule formation, and suggest powerfully that the hydrocarbon tail segments attached to the triple bonds present tails in a "bow" configuration, and that the chiral symmetry-breaking theory developed for "banana" liquid crystals may now be the best starting point for developing a general tubule structure and formation theory. As seen in the images above, tubules can be obtained without diynes in the tails, but instead with a cis ene bond present that forces the molecule into a "bow" shape.

Another important factor to point out is that this new tubule-forming phospholipid has an ester headgroup, instead of a choline headgroup as in DC(8,9)PC, proving further that the headgroup has little, if any effect whether tubule formation is possible. It is likely that the shape

and charge distribution of the choline headgroup may further enhance the packing of the phospholipids, and it may possibly yield tubules in greater numbers. There is still much to be studied about these compounds, including investigation of the linoleic and γ-linolenic acid tails, along with synthesizing the expected counter-example trans-"ene" compounds that cannot access "bow" configurations.

6.7 References

1. Schnur, J. M.; Ratna, B. R.; Selinger, J. V.; Singh, A.; Jyothi, G.; Easwaran, K. R. K. Diacetylenic lipid tubules: experimental evidence for a chiral molecular architecture. *Science (Washington, DC, United States)* **1994,** *264* (5161), 945-947.

2. Selinger, J. V.; MacKintosh, F. C.; Schnur, J. M. Theory of cylindrical tubules and helical ribbons of chiral lipid membranes. *Physical Review E: Statistical Physics, Plasmas, Fluids, and Related Interdisciplinary Topics* **1996,** *53* (4-B), 3804-3818.

3. Selinger, J. V.; Schnur, J. M. Theory of chiral lipid tubules. *Physical Review Letters* **1993,** *71* (24), 4091-4094.

4. Selinger, J. V.; Spector, M. S.; Schnur, J. M. Theory of Self-Assembled Tubules and Helical Ribbons. *Journal of Physical Chemistry B* **2001,** *105* (30), 7157-7169.

5. Selinger, R. L. B.; Selinger, J. V.; Malanoski, A. P.; Schnur, J. M. Visualizing chiral self-assembly. *Chaos* **2004,** *14* (4), S3.

6. Spector, M. S.; Easwaran, K. R.; Jyothi, G.; Selinger, J., V; Singh, A.; Schnur, J. M. Chiral molecular self-assembly of phospholipid tubules: a circular dichroism study. *Proc Natl Acad Sci U S A* **1996,** *93* (23), 12943-12946.

7. Thomas, B. N.; Lindemann, C. M.; Clark, N. A. Left- and right-handed helical tubule intermediates from a pure chiral phospholipid. *Physical Review E: Statistical Physics, Plasmas, Fluids, and Related Interdisciplinary Topics* **1999,** *59* (3-A), 3040-3047.

8. Pakhomov, S.; Hammer, R. P.; Mishra, B. K.; Thomas, B. N. Chiral tubule self-assembly from an achiral diynoic lipid. *Proc Natl Acad Sci U S A* **2003,** *100* (6), 3040-3042.

9. Maclennan, J. E.; Clark, N. A.; Walba, D. M. Biaxial model of the surface anchoring of bent-core smectic liquid crystals. *Physical Review E: Statistical, Nonlinear, and Soft Matter Physics* **2001,** *64* (3-1), 031706-1-031706/6.

10. Walba, D. M.; Korblova, E.; Shao, R.; Maclennan, J. E.; Link, D. R.; Glaser, M. A.; Clark, N. A. A ferroelectric liquid crystal conglomerate composed of racemic molecules. *Science (Washington, D. C.)* **2000,** *288* (5474), 2181-2184.

11. Yu, C. C.; Lee, Y. S.; Cheon, B. S.; Lee, S. H. Synthesis of glycerol monostearate with high purity. *Bulletin of the Korean Chemical Society* **2003,** *24* (8), 1229-1231.

12. Greene, T. W.; Wuts, P. G. M. *Protective Groups in Organic Synthesis. 2nd Ed;* 1991.

13. Thomas, B. N.; Corcoran, R. C.; Cotant, C. L.; Lindemann, C. M.; Kirsch, J. E.; Persichini, P. J. Phosphonate Lipid Tubules. 1. *Journal of the American Chemical Society* **1998,** *120* (47), 12178-12186.

14. Thomas, B. N.; Lindemann, C. M.; Corcoran, R. C.; Cotant, C. L.; Kirsch, J. E.; Persichini, P. J. Phosphonate Lipid Tubules II. *Journal of the American Chemical Society* **2002,** *124* (7), 1227-1233.

Chapter 7

Conclusions and Future Work

7.1 Conclusions

7.1.1 A New Tubule Formation Intermediate: The Tubelet

Perhaps the most important result reported in this dissertation, both in terms of theory and application, is the discovery of the structure we call the "tubelet," a previously-unobserved structure, apparently the precursor to the tubule.[1] This structure was serendipitously discovered through the addition of lysozyme at approximately 1 mg protein / ml DC(8,9)PC stock solution during the standard tubule formation thermal cycling. Lysozyme's presence unexpectedly promoted crack formation in the drying droplet of sample placed atop a carbon electron microscopy stem. Probing these cracks in the deposition bed with scanning electron microscopy allowed unprecedented detailed examination of the liquid specimen's interior, which was exposed at the crack interface in a manner similar to conventional freeze-fracture techniques. The slow and gentle surface-cracking behavior exposes these structures for extended lengths into free space – completely eliminating the background of the dried specimen and the dense thicket of other structures it contains. This remarkable stroke of luck allows clear and unambiguous characterization of these previously unobserved tubelets over lengths up to approximately 50 microns.

This discovery shows that tubules are not comprised of a helically-wound flat bilayer membrane at all,[2] but are instead formed by flattened tubelets, whose structure is topologically much more complex than a phospholipids bilayer ribbon. The tubelet may be thought of as a flattened firehose, where the firehose wall is composed of a phospholipids bilayer. Such a structure explains a number of otherwise difficult-to-justify tubule features, such as the

extraordinarily high aspect ratio of the tubule precursor. That is, the simple phospholipids bilayer ribbon has hydrocarbon tails exposed to the aqueous environment along its enormous perimeter, while the tubelet is edge-free (except perhaps for the circular cross-sections at the tubelet's ends). Another behavior that is well-explained by the tubelet as a tubule precursor is the tightly-conserved interlamellar spacing found in tubules whose diameters may differ by a factor of 5, or by tubules made by DC(8,9)PC derivatives:[3,4] the interlamellar spacing is a reflection of the collapsed firehose spacing, and not of independent, coaxial phospholipids bilayer ribbons.

The tubelet structure also provides critical new insights regarding the use of tubules as drug delivery vehicles. This is so because the ~0.5 μm diameter DC(8,9)PC tubule could easily be dismissed as encapsulation agents because their diameter is too great to provide significant drug retention time. But, the secondary winding of a smaller tube (that is, the tubelet), and the more convoluted exit pathway an encapsulant must traverse are expected to greatly enhance retention times over that expected from a simple cylinder.

7.1.2 Encapsulation Studies with Chemotherapy Agents

The encapsulation studies reported in this dissertation demonstrate that it is possible to form tubules in the presence of a variety of chemotherapy agents, and do so at clinically-relevant concentrations. Methotrexate, mitoxantrone, and carboplatin did not significantly hinder tubule formation, but in all three cases, the drugs did exert significant effects upon tubule morphology. This implies significant drug/tubule interaction, and as discussed, in the carboplatin case, EDS unambiguously shows this interaction is indeed encapsulation, or at the very least, strong association with the tubule surface.

When any of these 3 chemotherapy agents are present at concentrations of approximately 28 weight%, tubule yield drops precipitously and non-tubule structures appear that are not seen in drug-free DC(8,9)PC samples or drug-containing samples at lower concentrations. These structures are presumably co-precipitated lipid, drug, or some mixture of the two. It is found that tubule diameter increases upon the addition of any of these drugs over the concentration range studied; this outcome strongly suggests that the drugs decrease the membrane's intrinsic curvature, the hallmark feature of tubule formation. In turn, this diameter increase is most easily interpreted as interference with the tubule formation mechanism, most likely by incorporation of the drug into the membrane, but the possibility of strong association between the drug and the membrane's headgroups cannot be dismissed from our data.

As mentioned, carboplatin presents a special opportunity, for it contains platinum, and energy dispersive spectroscopy (EDS) can be used to easily locate the carboplatin without the possibility of confusing it with other metals present in the electron microscopy grid. The carboplatin was found to be in (or, as we must permit, possibly on), the tubules or within the region around the tubule that is defined by the EDS spatial resolution. A centrally important fact from the EDS spectroscopy is that there is essentially no platinum found away from the tubule. This absence of Pt in specimen regions lying between tubules merits special comment.

We know that tubules fall to the bottom of the droplet within minutes after its deposition on the electron microscopy stem, and the droplet dries over the course of time. As the droplet dries, the solution, which contains DC(8,9)PC "monomer" and carboplatin in equilibrium with the DC(8,9)PC/carboplatin tubules forms a round, waxy disk, with the tubules lying at the bottom of the disk. That is to say, these inter-tubule regions represent significant amounts of the solution, considering that the droplet is initially about 1 mm in height (compared to the 0.5 μm

DC(8,9)PC tubule diameter). That EDS spectroscopy failed to detect Pt in these regions suggests that tubules are voraciously effective as carboplatin encapsulants.

Although the three drugs mentioned above permitted tubule formation at clinical concentrations, an example of a drug that was a powerful inhibitor of tubule formation is bleomycin, a mixture of cytotoxic glycopeptide antibiotics, which is isolated from a strand of bacteria found in soil and dying vegetation, Streptomyces verticillus.[5] Given that tubules were merely distorted into cones by lysozyme, it is important to understand why this bleomycin is so potent an inhibitor of tubule formation.

7.1.3 Optimization of Phospholipid Tubule Morphology

Optimizing tubule properties, such as their dimension, for a particular application by adding a co-surfactant or other small molecule, could be necessary in drug delivery, either to counter the drug's own effects upon tubule morphology, or perhaps to enhance these effects.

1,2-dioleoyl-*sn*-glycero-3-phosphoethanolamine (DOPE) was selected as a co-surfactant in order to determine how it might affect tubule morphology. This choice was made because DOPE is known to induce an inverse hexagonal phase.[6,7] Interestingly, DOPE did <u>not</u> affect tubule formation, even at the very high [DOPE:DC(8,9)PC] concentrations of 4:1. DOPE did, however, cause a dramatic increase in tubule diameter, ranging from 0.5 μm to some 6 μm, within a single sample. These larger tubules could possibly increase the drug loading capacity of a given tubule; dosage to the patient would accordingly be adjusted by decreasing the number of tubules dispensed.

Another molecule known to modify membrane structure, cholesterol, was used to determine if it would have an effect on tubule formation. Cholesterol is known to increase bilayer thickness in phospholipids and increase membrane fluidity.[8-11] As discussed in Chapter

5, AFM section analysis shows directly that it was able to do so with DC(8,9)PC, and the tubules did exhibit an in increase in bilayer thickness from 100 nm up to 200 and 300 nm upon the addition of 30 and 40 mole% respectively.

7.1.4 Modifying DC(8,9)PC to Create New Tubule-forming Molecules

A completely different, but far more labor-intensive approach to regulating tubule structure is to modify the tubule-forming molecule. For example, Thomas et al. demonstrated that changing the headgroup was successful in altering tubule morphology, creating tubules with larger diameters.[3,4]

We chose to synthesize a class of compounds whose design was inspired by results from liquid crystal physics. The new compounds were designed to test whether the tails' diynes are the feature that enables tubule formation. Specifically, the reason that the diynes enable tubule formation may be that they enable DC(8,9)PC tails to enter into the "bow" confirmation described by Clark et al.[12,13]

Three compounds were made with at least one cis bond in their tails, in order to force a "bow" confirmation; the counter-example would be the corresponding trans compounds which cannot enter a "bow" configuration. Studies of the first compound, with oleic acid tails (9Z,9`Z)-3-(diethoxyphosphoryloxy)propane-1,2-diyl dioctadec-9-enoate, indicate that tubule formation is possible from these "ene" compounds, and that the "bow" chiral symmetry-breaking mechanism described by Clark is the mechanism that chiralizes the tubule-forming membrane. Interestingly, tubules produced by this compound are significantly larger (~10-15 μm range). Another feature of great interest seen in the sample are large sheets, which we tentatively interpret as being the sheets from which ribbons separate edge-wise from the sheet's long edge. It is important to note that our compound does not have a polar headgroup, as in the case of

DC(8,9)PC, which further illustrates that the "bow" confirmation in the tails is what allows tubule formation.

7.2 Future Work

There is still much to be learned about tubule formation and morphology in order to efficiently develop tubules for potential applications. Although the chemotherapy agents were able to increase tubule diameter, leading us to believe that the drug is possibly entering the membrane or interfering with the membrane chiralization, thereby increasing tubule diameter. To optimize tubule morphology for drug encapsulation, it will be important to locate exactly where the drug resides. EDS was used in the case of carboplatin, but other methods (such as small angle x-ray scattering) could also be used to confirm this result and determine the location of the other drugs, methotrexate and mitoxantrone. SAXS can give information about membrane spacing and the extent over which this spacing is conserved. This information would allow us to infer where the drug is located. NMR can also be used to determine if encapsulation has been successful. A sample can be prepared with the drug, thoroughly washed with water to ensure that any drug that remained in the solution will no longer be present, centrifuged to get a pellet, and then examined with standard liquid NMR techniques. Because tubules are crystalline, and are very large and hence stationary, the encapsulated drug should not be able to tumble freely, and this anisotropic condition should result in essentially no detectable NMR signal. Such a sample can then either be titrated with ethanol in order to dissolve the tubule, or simply heated above the spherical vesicle formation temperature, releasing any drug located in the membrane into solution. In either case, if drug is released from the solid tubule phase into solution, it will show up on the NMR spectra. Subtler questions regarding the location, orientation and conformation of the drug can be answered using MAS or solid-state NMR, but the use of simple,

conventional liquid NMR techniques as described to find if there is any drug in the membrane is a sensible first step.

The successful incorporation of cholesterol into the membrane of DC(8,9)PC serves as a model for the incorporation of other important, closely-related compounds. For instance, hormones having similar structures to that of cholesterol (testosterone, progesterone, etc.), should be studied in order to determine if tubules can be used as vehicles for these types of amphipathic compounds. Also, the fact that cholesterol was able to increase bilayer thickness may prove useful for expanding the hydrophobic regions in the tubule, thus creating a larger space for hydrophobic drugs to reside. After the addition of cholesterol, water insoluble drugs should be added to determine if drug loading can be increased.

We have shown tubules form from a compound that is structurally significantly different from DC(8,9)PC. The oleic acid tail compound should be investigated further to determine its optimal conditions for tubule formation. Along with these studies, the other two compounds with linoleic acid and γ-linolenic acid, must be investigated. In order to fully prove the "bow" conformation theory of tubule formation, the trans compounds must be made. While the expected outcome is no tubule formation, this "null" result must be demonstrated under a wide range of conditions before we can be confident it is in fact correct.

7.3 References

1. Mishra, B. K.; Garrett, C. C.; Thomas, B. N. Phospholipid Tubelets. *Journal of the American Chemical Society* **2005,** *127* (12), 4254-4259.

2. Schnur, J. M.; Ratna, B. R.; Selinger, J. V.; Singh, A.; Jyothi, G.; Easwaran, K. R. K. Diacetylenic lipid tubules: experimental evidence for a chiral molecular architecture. *Science (Washington, DC, United States)* **1994,** *264* (5161), 945-947.

3. Thomas, B. N.; Corcoran, R. C.; Cotant, C. L.; Lindemann, C. M.; Kirsch, J. E.; Persichini, P. J. Phosphonate Lipid Tubules. 1. *Journal of the American Chemical Society* **1998,** *120* (47), 12178-12186.

4. Thomas, B. N.; Lindemann, C. M.; Corcoran, R. C.; Cotant, C. L.; Kirsch, J. E.; Persichini, P. J. Phosphonate Lipid Tubules II. *Journal of the American Chemical Society* **2002,** *124* (7), 1227-1233.

5. Blenoxane (bleomycin sulfate for injection) . Bristol-Myers Squibb. 2005. Ref Type: Pamphlet

6. Cullis, P. R.; De Kruijff, B. The polymorphic phase behavior of phosphatidylethanolamines of natural and synthetic origin. A phosphorus-31 NMR study. *Biochimica et Biophysica Acta, Biomembranes* **1978,** *513* (1), 31-42.

7. Rand, R. P.; Fuller, N. L. Structural dimensions and their changes in a reentrant hexagonal-lamellar transition of phospholipids. *Biophysical Journal* **1994,** *66* (6), 2127-2138.

8. Alberts, B.; Johnson, A.; Lewis, J.; Raff, M.; Roberts, K.; Walter, P. *Molecular Biology of the Cell;* 3rd ed.; Garland Publishing, N.Y.: 1994.

9. Hui, S. W.; He, N. B. Molecular organization in cholesterol-lecithin bilayers by X-ray and electron diffraction measurements. *Biochemistry* **1983,** *22* (5), 1159-1164.

10. Nezil, F. A.; Bloom, M. Combined influence of cholesterol and synthetic amphiphillic peptides upon bilayer thickness in model membranes. *Biophys J* **1992,** *61* (5), 1176-1183.

11. Smondyrev, A. M.; Berkowitz, M. L. Structure of dipalmitoylphosphatidylcholine/cholesterol bilayer at low and high cholesterol concentrations: molecular dynamics simulation. *Biophysical Journal* **1999,** *77* (4), 2075-2089.

12. Maclennan, J. E.; Clark, N. A.; Walba, D. M. Biaxial model of the surface anchoring of bent-core smectic liquid crystals. *Physical Review E: Statistical, Nonlinear, and Soft Matter Physics* **2001,** *64* (3-1), 031706-1-031706/6.

13. Walba, D. M.; Korblova, E.; Shao, R.; Maclennan, J. E.; Link, D. R.; Glaser, M. A.; Clark, N. A. A ferroelectric liquid crystal conglomerate composed of racemic molecules. *Science (Washington, D. C.)* **2000,** *288* (5474), 2181-2184.

Appendix A

Supplemental NMR Data

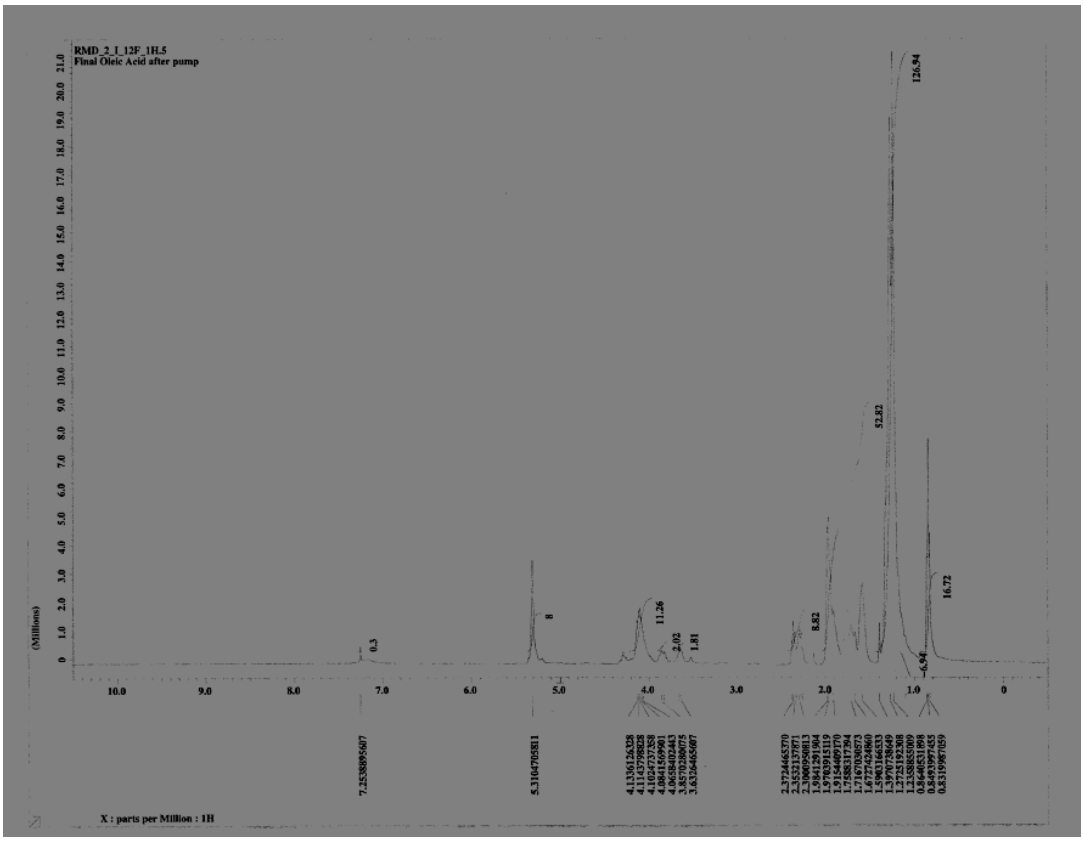

Figure A.1 ^{1}H-NMR of 6.4.4.1.

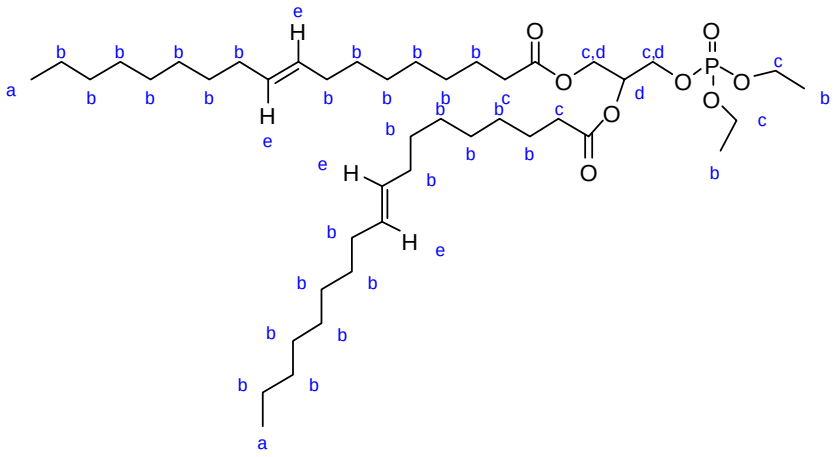

a-0.86; b-1.23-1.97; c-2.28-3.37; d-4.06-4.13; e-5.31

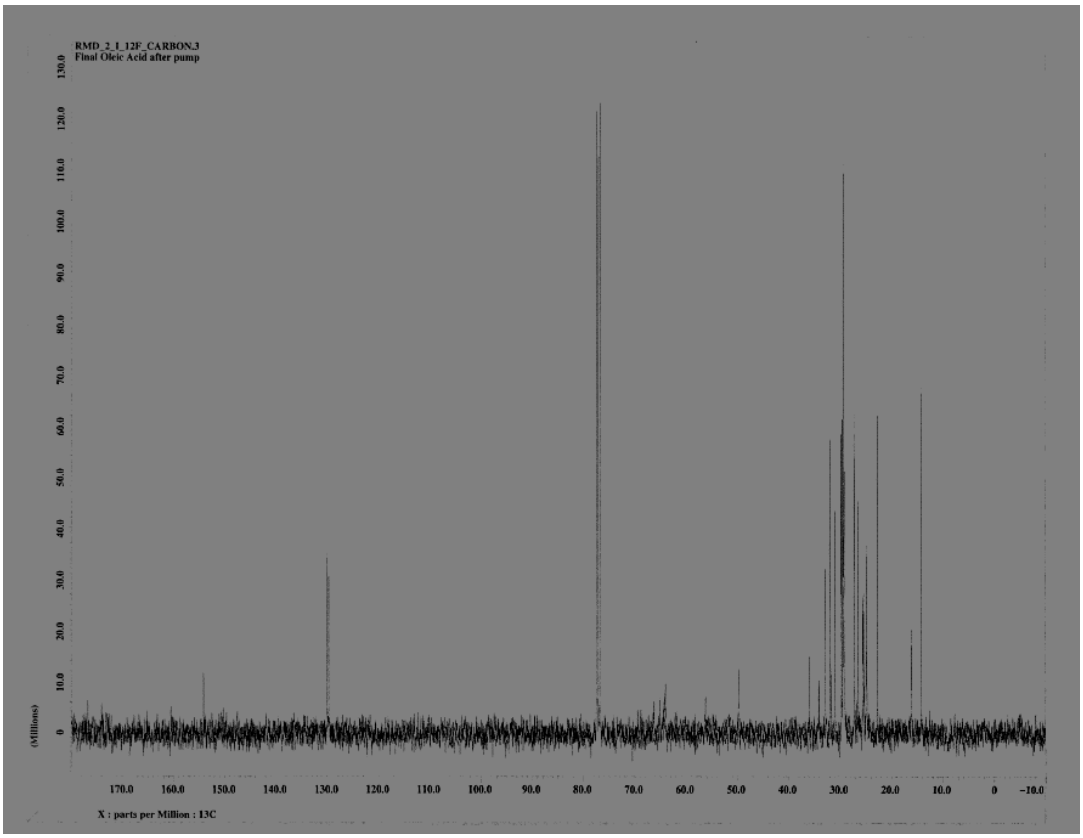

Figure A.2 ^{13}C-NMR of 6.4.4.1.

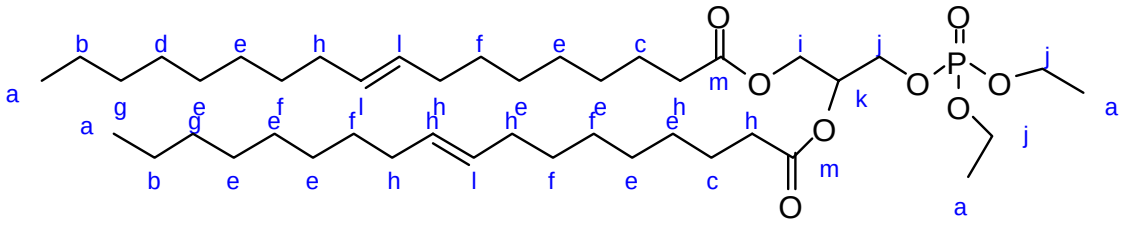

a-14.2; b-22.7; c-24.8; d-25.4; e-26.5; f-29.5; g-31.2; h-32.0; i-76.8; j-77.1; k-77.4; l-130.2; m-155.2

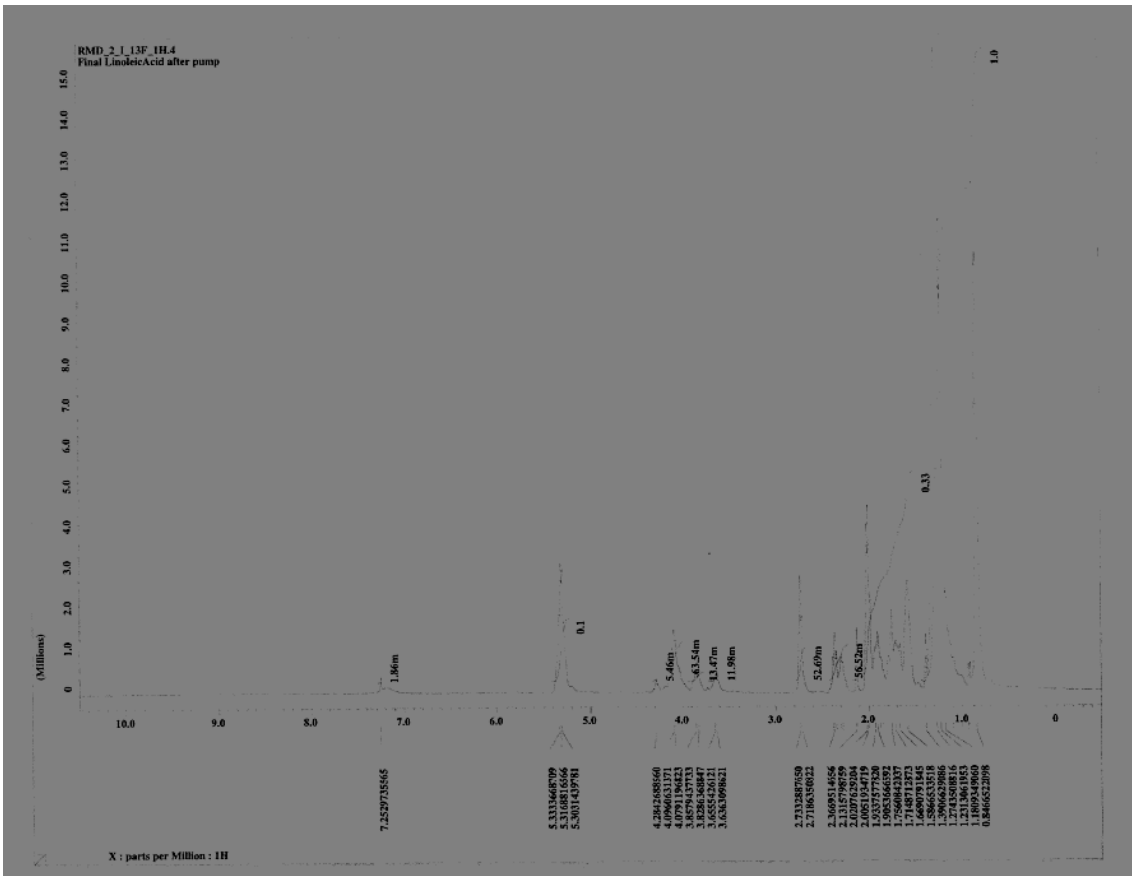

Figure A.3 ^{1}H-NMR of 6.4.4.2.

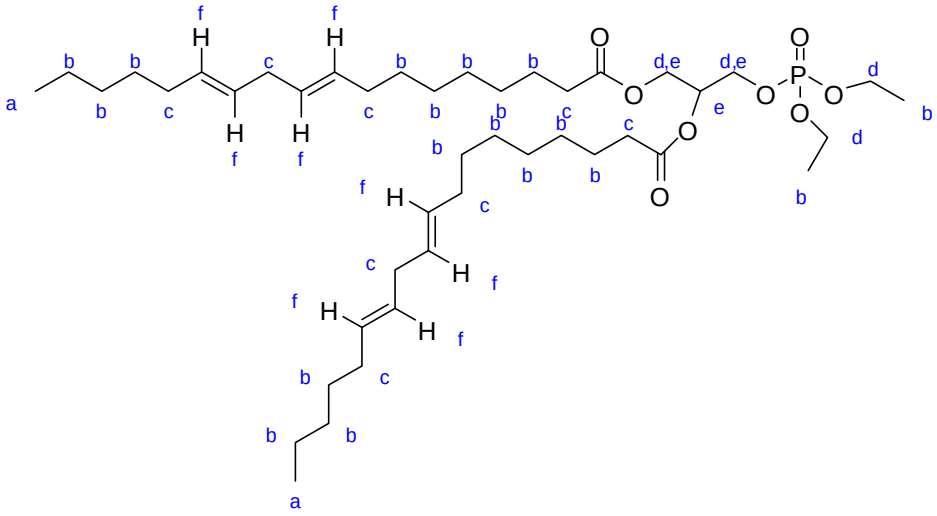

a-0.90; b-1.11-1.84; c-2.01-2.29; d-4.09; e-4.21; f-5.3

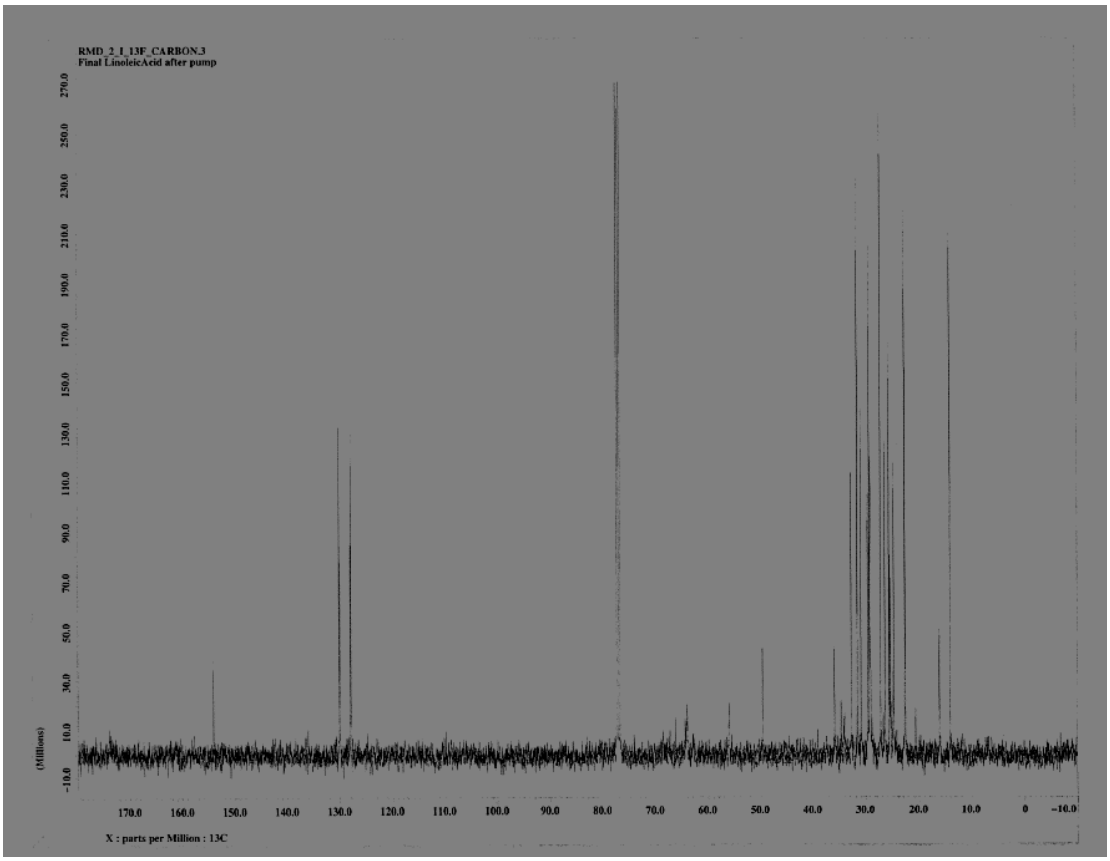

Figure A.4 ^{13}C-NMR of 6.4.4.2.

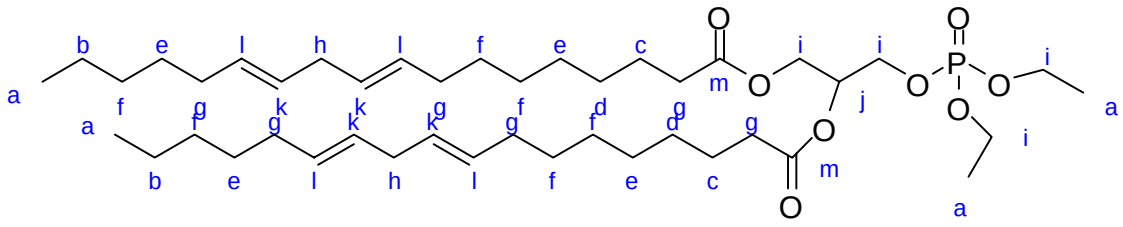

a-14.2; b-22.7; c-24.8; d-25.7; e-27.3; f-29.4; g-30.9; h-49.8; i-76.8; j-77.3; k-128.1; l-130.3; m-154.2

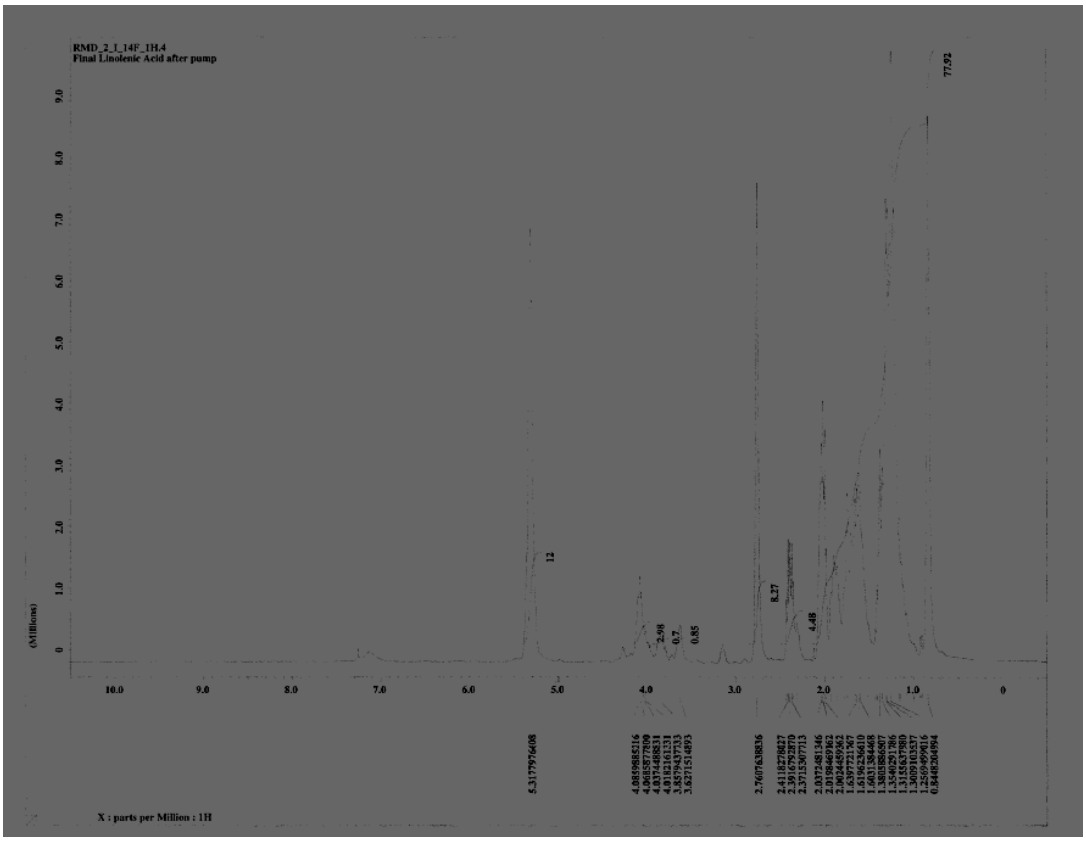

A.5 ^{1}H-NMR of 6.4.4.3.

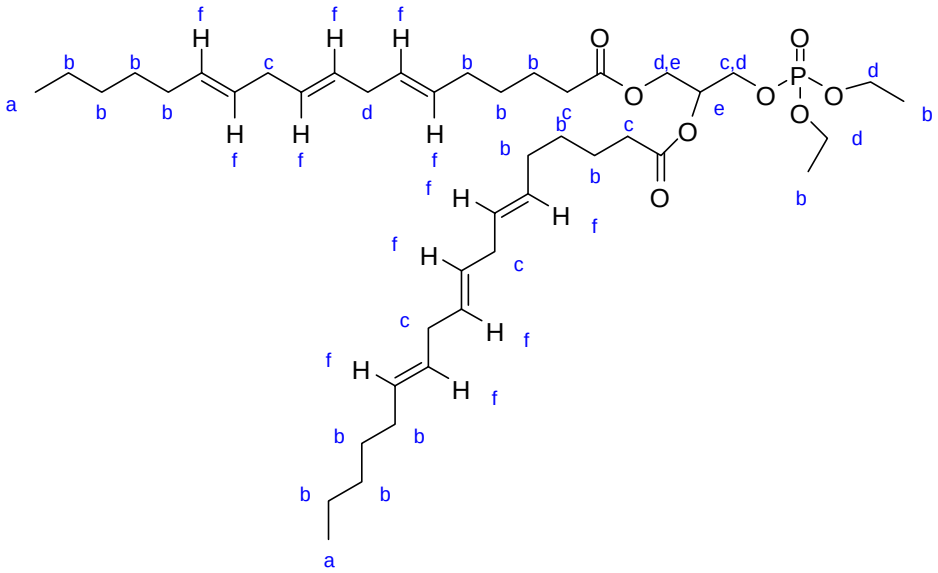

a-0.91; b-1.08-1.89; c-2.0-2.43; d-3.92; e-4.12; f-5.31

Appendix B

Permission to Reprint

Karen Buehler

From: Colleen Colson [ccolso2@lsu.edu]
Sent: Friday, January 12, 2007 1:38 PM
To: Copyright
Subject: copyright permission

To whom it may concern:

I am a graduate student in the Department of Chemistry at Louisiana State University. I am currently writing my dissertation and would like to request permission to use Figures 1-9 from a JACS paper where I am second author in my dissertation. The article citation follows:

Mishra, Bijaya K.; Garrett, Colleen C.; Thomas, Britt N. **Phospholipid Tubelets.** Journal of the American Chemical Society (2005), 127(12), 4254-4259.

My contact information:

Colleen C. Garrett
Louisiana State University
232 Choppin Hall
Baton Rouge, LA 70803
Phone:225-578-3355
Fax:225-578-3458

Thank you for your consideration.

Colleen C. Garrett

PERMISSION TO REPRINT IS GRANTED BY THE AMERICAN CHEMICAL SOCIETY

ACS CREDIT LINE REQUIRED. Please follow this sample: Reprinted with permission from (reference citation). Copyright (year) American Chemical Society.

APPROVED BY: *C. Arleen Courtney* 1/12/07
ACS Copyright Office

☐ If box is checked, author permission is also required. See original article for address.

VITA

Colleen Colson Garrett was born December 15, 1980, in New Orleans, Louisiana, to Kenny and Susan Colson. She graduated from Mount Carmel Academy high school in 1998, and then attended the University of Southern Mississippi, where she conducted undergraduate research on lyotropic liquid crystals under the guidance of Dr. C. Allan Guymon. As an undergraduate she was selected for an internship at Massachusetts Institute of Technology under the supervision of Prof. Michael F. Rubner, which extended her experience to the study of polyelectrolyte multilayers. She graduated from USM with a Bachelor of Science degree in polymer science in 2002, and began graduate research at Louisiana State University in the research group of Dr. Britt Thomas, where she investigated the morphology of phospholipid tubules and their use in drug delivery. In 2004 she married Gentry Garrett. While at LSU, she performed collaborative research in the laboratories of Noel A. Clark of the University of Colorado Condensed Matter Physics Laboratory and Philip J. Persichini of the Allegheny College Department of Chemistry to conduct highly-sophisticated optical probes of tubules, and synthesize new tubule-forming molecules, respectively. In the summer of 2006 she was awarded a highly competitive internship at Abbott Laboratories, which resulted in a permanent employment offer. She is currently completing the requirements for her Ph. D. in chemistry.